Departement Fysica, Faculteit Wetenschappen, Universiteit Antwerpen

Binary Polariton Fluids

Auteur:

Mathias Van Regemortel

Promotor:

Prof Dr. Michiel Wouters

Proefschrift ter verkrijging van de graad van Master in de Fysica

2012-2013

Abstract

Polaritons are quasiparticles that rise from a strong coupling between photons and a dipole excitation in matter. When a quantum well is placed inside a planar microcavity, this strong coupling occurs between the incident light and the quantum well excitons, giving rise to a two-dimensional gas of polaritons. Thanks to their photonic component, these polaritons have a small effective mass, whereas the excitonic component mediates interactions.

Since polaritons are unstable particles because the photons can escape from the microcavity, a constant injection of coherent photons is necessary to balance the losses. Therefore a polariton gas is inherently a non-equilibrium system, which involves a wide variety of interesting new physics. Since polaritons are excited coherently in the systems that are studied in this work, they form a coherent quantum fluid that can be regarded as a *non-equilibrium* Bose-Einstein condensate. In this work we will study polariton fluids that have two spin components. The main goal is to generalize and unify the already established theories for, on one side, single-spin polariton fluids, and on the other, two-spin Bose-Einstein condensates, which will also be the two fundamental theories on which we base this work. As such the generalized physics for describing a *two-spin non-equilibrium* quantum fluid will be examined in the view of these two, already profoundly studied systems.

First of all we will generalize the concept of Bose-Einstein condensation for non-equilibrium systems and derive the appropriate wave equation, the non-equilibrium Gross-Pitaevskii equation, to start our work from. From there on the spectrum of excitations of the binary polariton fluid will be examined, as well as its superfluid properties and the drag force exerted when flowing along a defect. During this progress we will take the limit back to the equivalent results of both the one-spin polariton fluid and the two-spin Bose-Einstein condensate, in order to understand how this generalization comes into play.

One of the main results that will be presented, is a phase diagram for excitation spectra that allows us to move from one of the limiting cases to the other continuously in parameter space, hence providing a full generalized theory in which the two earlier established limits can be recovered.

The other main result is the occurance of an exotic *negative* drag force under certain conditions. This means that in these circumstances the polariton fluid is *driven* forward, rather than *slowed down* when passing a defect.

Voorwoord

Deze uiteenzetting is het resultaat van zowel een onderzoeksstage aan de Universidad Autnoma de Madrid (UAM), onder begeleiding van Francesca Maria Marchetti, als onderzoekswerk verricht aan de Universiteit Antwerpen geleid door Michiel Wouters. Vandaar zou ik graag beide personen intens willen bedanken voor al hun zorgen, al hun onvoorwaardelijk geduld en alle informatie waar ze mij op een bijzonder boeiende en interactieve manier mee hebben laten kennismaken. Ik kan alleen maar zeggen dat ik oprecht genoten heb van de werkwijze waarop deze thesis tot stand gekomen is, en zonder deze twee personen zou het onmogelijk geweest zijn om met dit werk in zijn geheel als resultaat naar buiten te komen.
Verder zijn er uiteraard nog een hele hoop andere personen aan wie ik een woord van dank verschuldigd ben. Om te beginnen zijn er natuurlijk mijn ouders, die mij gedurende mijn volledige, vijf-jaar-durende studie zowel op persoonlijk als op financieel vlak gesteund en gemotiveerd hebben, alsook tijdens de slopende, en soms zware maanden van het thesisschrijven. Daarnaast zijn er ook nog mijn kotgenoten, mijn vrienden en alle anderen die mij van tijd tot tijd van de nodige ontspanning hebben voorzien, welke eveneens van fundamenteel belang was om dit werk succesvol te beëindigen.

Nederlandstalige samenvatting

In dit werk zal de niet-evenwichtsfysica van binaire polaritonfluïda bestudeerd en geanalyseerd worden. Polaritonen zijn quasideeltjes die ontstaan uit een coherente superpositie tussen fotonen en een dipolaire excitatie in materie. Specifiek zullen wij ons toelichten of tweedimensionale microcaviteiten waarin exciton-polaritonen geëxciteerd worden door een laser. Op deze manier ontstaat een tweedimensionaal gas van polaritonendeeltjes met merkwaardige eigenschappen. Zo verkrijgen de deeltjes een kleine effectieve massa door hun fotonische component, wat een typisch gevolg is van de opsluiting van fotonen in een microcaviteit, maar daarnaast ontstaan ook effectieve interacties door hun materiecomponent, het exciton. Hierdoor is een polaritongas in zekere zin fysisch equivalent aan een gas van *interagerende* fotonen, wat ongekend is onder normale omstandigheden. Vandaar wordt volop onderzoek gedaan naar deze systemen, met als uiteindelijk doel om deze niet-lineaire optische eigenschappen ten volle te benutten en te implementeren in allerhande optische toestellen, zoals bijvoorbeeld polaritonlasers of optische schakelaars.

Vanwege de coherente excitatie door een laser, vormen de polaritonen een coherent gas van deeltjes dat vele eigenschappen heeft van een Bose-Einstein condensaat. Paradoxaal genoeg zijn het juist de niet-evenwichtseigenschappen die een heel gamma aan nieuwe, bijzonder interessante fysica opleveren, maar tevens een herziening vereisen van de welbekende fenomenen die gepaard gaan met Bose-Einstein condensatie in koude atomen (macroscopische bezetting toestand, superfluïditeit...). Vandaar zal een uitvoerige uiteenzetting voorzien worden waarin uitgelegd wordt hoe deze fenomenen geplaatst en begrepen moeten worden in de context van niet-evenwichtsfysica.

Dit werk concentreert zich rond de studie van de fysica van *binaire* polaritonfluïda; zijnde polaritonsystemen met een extra spinvrijheidsgraad. Als dusdanig zal worden onderzocht hoe deze vrijheidsgraad de niet-evenwichtsfysica beïnvloedt en welke interessante effecten dit met zich meebrengt. De rode draad doorheen het werk is de unificatie van twee reeds uitvoerig in de literatuur beschreven fysische systemen: het één-spin-polaritoncondensaat en het binaire Bose-Einsteincondensaat. Het eerste bevat alle essentiële ingrediënten om niet-evenwichtskwantumvloeistoffen te beschrijven, terwijl het laatste de nodige fysica bevat voor een kwantumfluïdum met spinvrijheidsgraadsgraad. Het hoofddoel van deze thesis is dus om de niet-evenwichtseigenschappen en de spinvrijheidsgraad samen te voegen en een brug te slaan tussen beide, tot op heden afzonderlijke onderwerpen.

Het eerste deel van het werk bestaat uit de afleiding en uitgebreide toelichting van de centrale vergelijking in dit werk: de niet-evenwichts-Gross-Pitaevskii-vergelijking met spinvrijheidsgraad. Vanaf daar zal in het volgende hoofdstuk het excitatiespectrum afgeleid en besproken worden. Het centrale resultaat hiervan is een fasediagram in functie van twee fundamentele dimensieloze parameters, één kwantificeert de spinvrijheidsgraad en de andere geeft een maat voor het niet-evenwicht, waarop de verschillende berekende excitatiespectra zijn geclassificeerd. Via deze weergave is het duidelijk dat zowel de spin- als de niet-evenwichtseigenschappen geïncorporeerd zijn in een algemene theorie en dat, bovenal, beide bovengenoemde limieten duidelijk teruggevonden kunnen worden.

Vanuit dit resultaat zal dan in het laatste hoofdstuk de verstrooiingsfysica van het fluïdum onderzocht worden. Hiertoe zullen eerst de golfachtige dichtheidsprofielen van de vloeistof als gevolg van verstrooiing aan een defect berekend en besproken worden, waarna superfluïde eigenschappen en de wrijvingskracht aan bod komen. Als meest opmerkelijke resultaat uit dit deel noteren we dat onder bepaalde omstandigheden de wrijvingskracht *negatief* kan worden. Hieruit blijkt dus dat in deze omstandigheden de kwantumvloeistof *voortgestuwd* wordt wanneer het langs een defect passeert. Bijgevolg wordt er dus geen energie gedissipeerd door wrijving, zoals we gewoon zijn, maar blijkt er een mechanisme in te treden dat energie *absorbeert* uit de omgeving. Het zal blijken dat dit exotisch fenomeen rechtstreeks gerelateerd is aan de niet-evenwichtseigenschappen van de vloeistof.

Dit werk is het resultaat van zowel een onderzoeksstage aan de Universidad Autónoma de Madrid (UAM) als rechtstreeks thesiswerk verricht aan de Universiteit van Antwerpen (UA). Daar de strikte scheiding tussen beide is uitgevaagd doorheen de tijd, omvat dit verslag een samenvatting van de belangrijkste resultaten die gedurende het volledig onderzoek bekomen werden. Gelieve er dus rekening mee te houden dat dit werk in principe telt voor 42 ECTS (30 voor de masterthesis en 12 voor de onderzoeksstage), waavan er 12 reeds beoordeeld zijn aan de UAM op basis van een tussentijds verslag.
Omwille van praktische redenen is de thesis dan ook geschreven in het Engels, dit om de communicatie te vergemakkelijken en de transparantie naar beide partijen toe te verhogen.

Contents

Chapter 1

Polaritons in Microcavities

1.1 Introduction

Polaritons are quasiparticles resulting from strong coupling between light and a dipole excitation in matter. Originally they were predicted theoretically by Hopfield in [1] and by Pekar [**?**]. The origin of this excitation might come from various physical properties of a material, but the most common are couplings to phonons, plasmons or excitons. The physics of the resulting system is similar for all these types of excitations. Apart from the presence of a strong coupling, polariton systems give rise to a number of non-linear optical effects, that make them particularly interesting for implementation in many optical devices. Known and thoroughly investigated examples include, among others, the construction of optical switches, parametrical amplification of light and promising new laser devices. The particular interest of polariton systems lies in the fact that they introduce an effective coupling between photons themselves, an effect which is extremely weak in vacuum. Next to that, the photons acquire an effective mass and are therefore subject to a completely different type of physics, opening up a new world in the context of optics. In this work we will concentrate specifically on semiconducter exciton-polariton systems and present them in the context of microcavity physics.

Excitons are bound hydrogen-like states of an electron-hole pair in a semiconductor that can be created by absorption of a photon. Typically these states are metastable because the electron-hole pair recombines again by emitting a photon with a frequency related to the binding energy of the exciton. As this photon can excite another exciton with a certain cross-section, and so on, this process results in the creation of a new system of effective quasiparticles, known as exciton-polaritons, that are a manifestation of a quantum mechanical superposition of a photon and an exciton state.
In an ideal system where the photons are perfectly locked up in a cavity, this would give rise to a stable interacting system of polaritons, in which the interactions are governed by the excitonic component, whereas the photonic component induces the usual optical effects of light. In this way, such a system can be regarded as, and is in a certain sense physically equivalent to, a system of interacting photons. In reality however, such systems are always subject to a continuous loss rate of photons, since it is impossible to construct perfect mirrors to lock them up perfectly. Therefore the system should be pumped continuously by a photon source to make up for this, resulting in an inherent non-equilibrium system. The apparent drawback of the necessity to form a non-equilibrium system, actually turns out to involve a large number of fascinating properties, that are far from accessible in equilibrium systems. These effects lie in the realm of non-equilibrium quantum fluids and will be presented and explained thoroughly throughout this work. They represent the most interesting part of polariton systems, and moreover open up a whole gamma of unique physics.

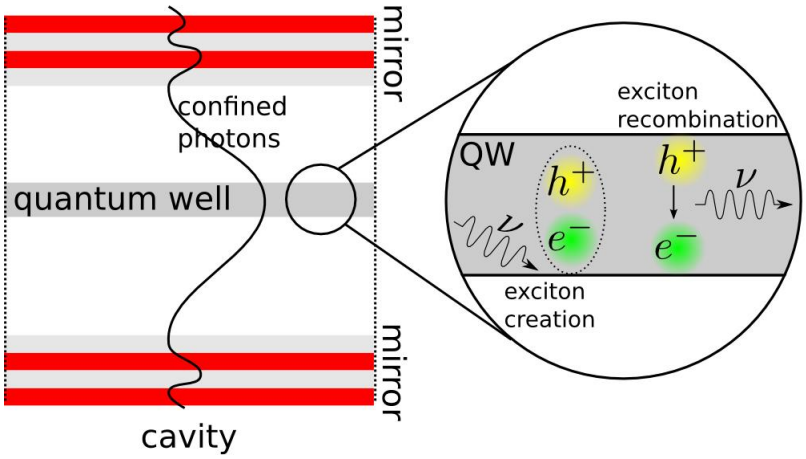

Figure 1.1: A schematic image of a polariton microcavity. An electron-hole pair is combined by absorbing a photon and decays again by emitting one. Picture taken form [10]

1.2 The Polariton Model

In this section, an introductory summary on exciton-polariton physics will be outlined, based on [9], [10], [11]. In order to present a complete and comprehensive approach, we will consecutively go through excitons in semiconductors, microcavity physics of confined light and eventually the combination of these two to present polaritons.

1.2.1 Photons in Microcavities

In order to create polaritons, the excitons should interact with a light mode to obtain the necessary strong coupling. A microcavity will be used to confine photons and realize this, whereas the provided light source is a laser.

Structure of a Microcavity

The microcavities used to design polariton systems are semiconductor microcavities, constructed from distributed Bragg reflectors. In reality, we usually deal with two-dimensional planar devices, in which polaritons are confined in the direction perpendicular to the plane. There are also examples of 0D (quantum dots) and 1D systems, but in this work we will only focus on planar semiconductor microcavities.

The microcavity itself consists of alternating layers of materials with different refractive index, optimized to confine photons inside the cavity and exciting excitons. The two Bragg reflectors consist of a number of quarter wavelength thick layers, with a varying refractive index. In this way, a standing wave pattern is created inside the microcavity, in order to maximize the radiation intensity. As the Bragg reflectors are not perfect mirrors, there is always a certain loss rate of photons and a pumping on the sample by a laser is needed to balance this. Furthermore the mirrors are usually designed with a wedge, meaning that the distance between the mirrors varies in space. In this way the resonance frequency of the standing wave, ω_0, is space-dependent and in a certain region this frequency corresponds to the exciting energy of the exciton, realizing optimal coupling. At the antinodes of the standing wave, planar quantum wells are placed in which the excitons are confined, so that the coupling between the incident radiation and the excitons is maximized in these planes. The materials that are used to excite excitons are usually III-V materials, such as GaAs or AlGaAs [11]. The first realizations of microcavity polaritons were performed in 1992 and are presented in [3]. See figure 1.1 for a schematic representation of a typical microcavity.

Energy of the Confined Photons

By changing the angle of incidence of the laser beam with respect to the planar microcavity, the in-plane momentum of the photons can be adapted, because this is directly related to their momentum projected on the cavity plane. The momentum of photons inside a cavity is thus quantized in the direction perpendicular to the plane, whereas the parallel component is not.
For a cavity with length w and a refractive index n the energy of confined photons with in-plane momentum $\mathbf{k}$ can then be written as:

$$\omega(\mathbf{k}) = \frac{c}{n}\sqrt{k^2 + \left(\frac{2\pi N}{w}\right)^2} \approx \omega_0 + \frac{k^2}{2m} \tag{1.1}$$

Where we defined the effective photon pseudomass $m = \frac{2\pi n N}{cw}$ and N as the index of the transverse mode of the photons inside the cavity.
Notice that by considering a two-dimensional system, it follows naturally that the photons should obtain an effective mass. This is an important feature which will come into play again when setting up the general polariton theory. Notice that we have set $\hbar = 1$, as will be done throughout the whole work.
As in typical systems $m/M \sim 10^{-4}$, one usually considers the exciton energy as a dispersionless constant with respect to the photon energy, and therefore $\varepsilon_{\mathbf{k}} \approx \varepsilon_0 = \varepsilon_{ex} - \varepsilon_b$. Furthermore, we define the detuning δ as the gap between the photon and exciton energy for zero momentum, i.e $\delta = \omega_0 - \varepsilon_0$.

The Photon Spin

Out of fundamental quantum field theory, it follows that photons can have two linearly independent polarization states and that they have to be oriented perpendicular to the motion of the photon, as a consequence of gauge redundancy.
Formally every photon can thus be represented in spin space as:

$$|\Psi\rangle \equiv \alpha_x |\Psi_x\rangle + \alpha_y |\Psi_y\rangle$$

With $|\alpha_x|^2 + |\alpha_y|^2 = 1$ to normalize the state.
The two spin states $|\Psi_{x,y}\rangle$ represent in the semiclassical view a photon oscillating in x- or y-direction, when its motion is along the z-direction. In our case, for a laser beam incident on a planar microcavity, we can rotate this basis in such a way that one of these directions corresponds to oscillations parallel to the plane and the other to perpendicular oscillations. As is common in optics, these two states are referred to as the *transverse electric* (TE) and the *transverse magnetic* (TM) state, originating from whether the electric or the magnetic field is oscillating transversal to the plane. When the laser beam is positioned perpendicular to the plane, these states are clearly degenerate, since both the magnetic and the electric field are then oriented parallel to the plane.

We can rotate this linear basis to obtain a different one, given by:

$$\begin{aligned} |\Psi_+\rangle &\equiv \frac{|\Psi_x\rangle + i\,|\Psi_y\rangle}{\sqrt{2}} \\ |\Psi_-\rangle &\equiv \frac{|\Psi_x\rangle - i\,|\Psi_y\rangle}{\sqrt{2}} \end{aligned}$$

These eigenkets now represent the circularly polarized states of the photon.
For the purposes of this work, it will soon become clear that this basis is the most representative to do calculations. The coherent photons coming from the laser beam will therefore be represented as a coherent superposition of a so-called *spin-up* and *spin-down* component.

The Photon Field

We have argued that two independent quantum numbers are of importance and should be incorporated in a theory of the photons, the spin and the in-plane momentum $\mathbf{k}$. All these quantum states should be included in a Hamiltonian representing the energy of a photon field:

$$\hat{H}_{cav} = \int \frac{d^2k}{(2\pi)^2} \sum_{\sigma=+,-} \omega(\mathbf{k}) \hat{\psi}^\dagger_{\mathbf{k},\sigma} \hat{\psi}_{\mathbf{k},\sigma} \tag{1.2}$$

Where the quantum operators $\hat{\psi}^\dagger_{\mathbf{k},\sigma}$ and $\hat{\psi}_{\mathbf{k},\sigma}$ respectively represent the operators creating and anihilating a photon with momentum $\mathbf{k}$ and spin σ inside the cavity.
As the photons are bosonic particles, they should satisfy the bosonic commutation relations:

$$\begin{aligned} \left[\hat{\psi}_{\mathbf{k},\sigma}, \hat{\psi}^\dagger_{\mathbf{k}',\sigma'}\right] &= (2\pi)^2 \delta_{\mathbf{k},\mathbf{k}'} \delta_{\sigma,\sigma'} \\ \left[\hat{\psi}_{\mathbf{k},\sigma}, \hat{\psi}_{\mathbf{k}',\sigma'}\right] &= \left[\hat{\psi}^\dagger_{\mathbf{k},\sigma}, \hat{\psi}^\dagger_{\mathbf{k}',\sigma'}\right] = 0 \end{aligned}$$

Notice that we implicitely assumed the photon energy to be degenerate, since the same energy is associated with each of the two possible spin states. In reality this might not be entirely correct, since the reflectance of the Bragg mirrors is in general different for the TE and TM linear polarization states. However, we will neglect the spin-dependent frequency shift during this work for the sake of simplicity. Actually the TE and TM eigenstates determine the mass basis, in which the free photons are diagonal, whereas the interactions are diagonal in the spin basis. This is analog to the standard model where a rotation via the so-called *CKM matrix* is needed to transform fermions from their mass basis to the basis of the weak interactions.
The TE/TM splitting can be observed experimentally in the emitted polariton spectra, but the effect can also be reduced by the design of the Bragg mirrors. [21]

1.2.2 Excitons

Excitons are quasiparticles that arise from bound electron-hole pairs in semiconductors. An excited electron with sufficient energy hops from the valence band to the conduction band and is free to start moving inside the lattice. Because of the missing electron, a positively charged hole remains in the lattice and this can be considered as a positively charged particle that is free to propagate as well. Both the electron and the hole have their specific energy-momentum relation, depending on the specific topology of the atoms building up the lattice, and this is known as the electronic band structure of a solid.
Instead of hopping from the valence band completely to the conduction band, a number of intermediate metastable energy levels can exist that correspond to the formation of bound electron-hole pairs. In this case the excited electron and the hole bind by the attractive Coulomb interaction to a new quasiparticle that is known as an exciton. Thanks to the dipolar transition, excitons couple to light. By confining excitons in quantum wells, the binding energy can be increased so that the excitons can be considered as polarized bosonic particles, as their internal fermionic structure can be neglected within good approximation at sufficiently low densities.
The binding length of the exciton is larger than the typical lattice constant in semiconductors. This justifies the approximation of considering the excitons as independent quasiparticles, since quantum lattice effects are averaged out over the typical length scales that are dealt with. Furthermore this large length scale corresponds to momenta close to the center of the Brillouin zone, where the dispersion of the electron and hole are quadratic within good approximation.

Band Energy

Excitons are considered as independent massive quasiparticles propagating in the solid. For small momenta the energy relation of these particles is therefore the usual quadratic relation:

$$\varepsilon_{\mathbf{k}} = \varepsilon_{ex} - \varepsilon_b + \frac{k^2}{2M} \tag{1.3}$$

ε_{ex} is the energy of the exciton level and ε_b the intrinsic binding energy of the exciton through the Coulomb interaction.
In analogy with the hydrogen atom, which also originates from the Coulomb interaction, the energy levels are given by:

$$\varepsilon_{b,n} = \left(\frac{\mu}{\varepsilon^2 m_0}\right)\frac{E_R}{n^2}$$

With μ the reduced electron band mass, m_0 electron rest mass and ε the dielectric permittivity.
Here we encounter the importance of considering the lattice as a smooth background, as this permits us to describe exciton physics in a medium with an altered permittivity ε to make up for all lattice effects. Since in general $\varepsilon \gg \varepsilon_0$, the permittivity of the vacuum, the binding energy in an exciton is typically much smaller than in a hydrogen atom, as well resulting in a larger Bohr radius. In GaAs we find that $\varepsilon/\varepsilon_0 \approx 10$, thus leading to factor 10^2 difference in binding energy and 10 in bohr radius with respect to a hydrogen atom.

The resulting zero-point energy ω_0 is the difference between the exciton band energy level ε_{ex} and the binding energy ε_b; this result is important, as it will come into play again when coupling the excitons to light.
Furthermore the excitons acquire an effective mass M, which is the sum of the electron and the hole band mass.

Angular Momentum and Spin

The spin of an exciton as a composite particle depends on the represention of the product of the groups describing the spin space of the electron and the hole, their angular momenta inside the cristal and the angular momentum of the electron-hole pair.
We consider a GaAs lattice grown in the (100) direction, for which the relevant planar symmetry is given by D_2. For these types of cristals the lower conduction band is s-like and therefore the contributing angular momentum coming from the electron is only determined by its spin: $J_e = S_e = 1/2$ and $j_e = \pm 1/2$. The upper valence band has $J_h = 3/2$ and splits up for small momenta into a *heavy*- and a *light*-hole band, respectively with $j_{hh} = \pm 3/2$ and $j_{lh} = \pm 1/2$. Since the typical energy splitting of these two bands is larger than the binding energy of the exciton, only the heavy hole will significantly contribute to the formation of excitons. [7]

The angular momentum of the bound electron-hole pair depends on its orbital quantum state, in analogy with the hydrogen atom: $1s$, $2s$, $2p\ldots$. We will assume excitons with maximum binding energy, as this is the lowest energy state, which are in the $1s$ orbital with $L = 0$.
The spin space of the considered excitons is then given by the different product spaces of

$\left|J_e, j_e\right\rangle \otimes \left|J_h, j_{hh}\right\rangle$:

$$\begin{aligned}
\left|\frac{1}{2}, +\frac{1}{2}\right\rangle \otimes \left|\frac{3}{2}, +\frac{3}{2}\right\rangle &\equiv \left|2, +2\right\rangle \\
\left|\frac{1}{2}, -\frac{1}{2}\right\rangle \otimes \left|\frac{3}{2}, +\frac{3}{2}\right\rangle &\equiv \frac{1}{2}\left|2, +1\right\rangle + \frac{\sqrt{3}}{2}\left|1, +1\right\rangle \\
\left|\frac{1}{2}, +\frac{1}{2}\right\rangle \otimes \left|\frac{3}{2}, -\frac{3}{2}\right\rangle &\equiv \frac{1}{2}\left|2, -1\right\rangle - \frac{\sqrt{3}}{2}\left|1, -1\right\rangle \\
\left|\frac{1}{2}, -\frac{1}{2}\right\rangle \otimes \left|\frac{3}{2}, -\frac{3}{2}\right\rangle &\equiv \left|2, -2\right\rangle
\end{aligned}$$

In order to achieve a polariton condensate, a strong coupling with the incident light should be realized. Since light only has the $|1, +1\rangle \equiv |+\rangle$ and the $|1, -1\rangle \equiv |-\rangle$ spin states, a coupling can only exist with excitons having either of these two spins. As a consequence of this, excitons with angular momentum $J = 2$ states are also called *dark* excitons, since they do not couple to photons. Therefore the excitons that we consider for the purposes of our work, will only be the ones having $s_{ex} = \pm 1$ and we will neglect contributions coming from the other spin states.

Interactions

We have already argued that within good approximation the excitons can be considered as composite particles by neglecting their internal structure. The next step is to determine how effective interactions are mediated via these particles. Obviously the interaction between two excitons with the same spin state is different from the interaction between two with opposite spins.

- Two excitons in the same spin are indistinguishable and due to their quantum nature the interaction potential is given by the sum of the *direct* and the *exchange* interaction: $V = V_{\text{dir}} + V_{\text{exch}}$. Since the particles are not electrically charged, only higher orders of the direct interaction will contribute. The main contribution to the interaction potential is therefore given by the exchange interaction, which is a consequence of the two-particle wave function being symmetric under the exchange of the two particles. Since excitons are bosonic particles, this results in an *repulsive* interaction between excitons with the same spin.

- Two excitons with opposite spin have a different quantum number and are therefore not indistinguishable. The main contribution to the interactions will now come from the dipole moment of the excitons. Therefore the interaction between two opposite-spin excitons is *attractive* and usually about one order of magnitude smaller than the one between two equal-spin particles.

It is important to stress out the fundamental difference between the interactions of two equal-spin and two opposite-spin excitons, as it will be one of the keypoints throughout this work.

Because of the attractive interaction between two opposite-spin excitons, an energy minimum will be present in the potential. This is important since it implicates the existence of bound exciton pairs with opposite spin, the so-called *biexcitons*. When the kinetic energy of the excitons is nearing the binding energy of these bound states, a resonance will occur that changes the nature of the interaction, known as a *Feshbach* resonance. More specifically, this resonance affects the interaction strength between the two particles and is therefore of great practical importance, since it allows us to tune the interaction parameter. However, since during this process metastable bound states with a finite lifetime are formed, also an imaginary part is contributing to the interaction potential that should be taken into account. Actually this imaginary contribution implicates that there is a certain loss rate of excitons, due the formation of

molecular-like bound states.
Experiments to verify and measure this tuning possibility have been carried out in Lausanne recently, but the data are still being analysed at this moment.

The Exciton Field

After pointing out all necessary ingredients that should be included in a theory describing the dynamics of excitons, it is time to start constructing an appropriate field theory from an electron-hole Hamiltonian that will be coupled to an effective exciton Hamiltonian.
We will start from the free electron-hole Hamiltonian:

$$\hat{H}_0 = \sum_{\sigma=\pm 1/2} \sum_{\mathbf{k}} \varepsilon_c(\mathbf{k}) \hat{c}^\dagger_{\mathbf{k},\sigma} \hat{c}_{\mathbf{k},\sigma} + \sum_{\sigma=\pm 3/2} \sum_{\mathbf{k}} \varepsilon_h(\mathbf{k}) \hat{v}^\dagger_{\mathbf{k},\sigma} \hat{v}_{\mathbf{k},\sigma} \tag{1.4}$$

The operator $\hat{c}^\dagger_{\mathbf{k},\sigma}$ creates an electron in the conduction band with spin σ and band energy $\varepsilon_c(\mathbf{k})$ and $\hat{v}^\dagger_{\mathbf{k},\sigma}$ creates a heavy hole with spin σ in the valence band with band energy $\varepsilon_h(\mathbf{k})$. Remember that we are constructing an effecctive field theory that only takes into account physically relevant parameters. That is why we start here with neglecting the light hole contributions: we argued that their influence is negligible.
The next thing to do is to add interactions between electrons and holes:

$$\begin{aligned} \hat{H}_{int} \quad = \quad & \frac{1}{2} \sum_{\mathbf{k},\mathbf{k}'} \sum_{\mathbf{q}} V_{coul}(\mathbf{q}) \Bigg(\sum_{\text{spins}} \hat{c}^\dagger_{\mathbf{k}'+\mathbf{q},\sigma'} \hat{c}^\dagger_{\mathbf{k}-\mathbf{q},\sigma} \hat{c}_{\mathbf{k}',\sigma'} \hat{c}_{\mathbf{k},\sigma} \\ & + \sum_{\text{spins}} \hat{v}^\dagger_{\mathbf{k}'+\mathbf{q},\sigma'} \hat{v}^\dagger_{\mathbf{k}-\mathbf{q},\sigma} \hat{v}_{\mathbf{k}',\sigma'} \hat{v}_{\mathbf{k},\sigma} \\ & - 2 \sum_{\text{spins}} \hat{v}^\dagger_{\mathbf{k}'+\mathbf{q},\sigma'} \hat{c}^\dagger_{\mathbf{k}-\mathbf{q},\sigma} \hat{v}_{\mathbf{k}',\sigma'} \hat{c}_{\mathbf{k},\sigma} \Bigg) \end{aligned}$$

The three different terms describe respectively the $e^- - e^-$, the $h - h$ and the $e^- - h$ interactions. The former two are repulsive, whereas the latter is attractive.
The Coulomb interaction strength is given by:

$$V_{coul}(\mathbf{q}) = \frac{e^2}{2\varepsilon |\mathbf{q}|}$$

The next step is to introduce bosonic particles that are composed of an electron and a hole, orbiting around each other:

$$\begin{aligned} \hat{a}^\dagger_{\mathbf{k},+} \quad &= \quad \sum_{\mathbf{q}} f(\mathbf{q}) \hat{c}^\dagger_{\mathbf{k}+\mathbf{q},-1/2} \hat{v}_{\mathbf{k}-\mathbf{q},+3/2} \\ \hat{a}^\dagger_{\mathbf{k},-} \quad &= \quad \sum_{\mathbf{q}} f(\mathbf{q}) \hat{c}^\dagger_{\mathbf{k}+\mathbf{q},+1/2} \hat{v}_{\mathbf{k}-\mathbf{q},-3/2} \end{aligned}$$

It is easily seen that these operators satisfy the bosonic commutation relations:

$$\begin{aligned} \left[\hat{a}^\dagger_{\mathbf{k}}, \hat{a}^\dagger_{\mathbf{k}'}\right] = [\hat{a}_{\mathbf{k}}, \hat{a}_{\mathbf{k}'}] \quad &= \quad 0 \\ \left[\hat{a}_{\mathbf{k}}, \hat{a}^\dagger_{\mathbf{k}'}\right] \quad &= \quad \delta_{\mathbf{k},\mathbf{k}'} \end{aligned}$$

The next step is to transform the original fermmionic Hamiltonian to the new bosonic basis, which can be achieved via a so-called Usui transformation. The complete derivation of this process rather long and technical and is beyond the scope of this work. We refer the interested reader to [17] for a

detailed explanation. After a diagonalization procedure of the bosonic Hamiltonian obtained after the Usui transform, the Hamiltonian in the exciton basis is established.
The free Hamiltonian is then given by

$$\hat{H}_0 = \sum_{\sigma=\pm} \sum_{\mathbf{k}} \left(\varepsilon_{\mathbf{k}} \hat{D}^\dagger_{\mathbf{k},\sigma} \hat{D}_{\mathbf{k},\sigma} \right), \tag{1.5}$$

with the correct energy dispersion $\varepsilon_{\mathbf{k}}$, given by (1.3).
And the interaction Hamiltonian

$$\hat{H}_{int} = \frac{1}{2} \sum_{\mathbf{k},\mathbf{k}'} \sum_{\mathbf{q}} \left(V_1(\mathbf{q}) \sum_{\sigma=\pm} \left(\hat{D}^\dagger_{\mathbf{k}'+\mathbf{q},\sigma} \hat{D}^\dagger_{\mathbf{k}-\mathbf{q},\sigma} \hat{D}_{\mathbf{k}',\sigma} \hat{D}_{\mathbf{k},\sigma} \right) - 2V_2(\mathbf{q}) \hat{D}^\dagger_{\mathbf{k}'+\mathbf{q},-} \hat{D}^\dagger_{\mathbf{k}-\mathbf{q},+} \hat{D}_{\mathbf{k}',-} \hat{D}_{\mathbf{k},+} \right) \tag{1.6}$$

The interaction functions in momentum space $V_1(\mathbf{q})$ and $V_2(\mathbf{q})$ can be derived out of this theory up to any given order, but we prefer leaving them in this way for now, since we will approximate them later on anyway.
Worth noticing though is that $V_1(\mathbf{q})$ describes a repulsive interaction for two excitons with the same spin, whereas $V_2(\mathbf{q})$ denotes an attractive interaction for two particles with opposite spins. As we pointed out earlier on mere intuitive grounds, it can be derived from the Usui theory that the first leading order of $V_1(\mathbf{q})$ is determined by the exchange interaction, while $V_2(\mathbf{q})$ is a dipole-dipole interaction. Therefore holds that $|V_1(\mathbf{q})| \gg |V_2(\mathbf{q})|$ under normal circumstances. However, remember also that we mentioned the existence of bound molecular-like states of two excitons with opposite spin, the biexcitons, which allows us to tune $V_2(\mathbf{q})$ for energy scales close to these resonances. Under these circumstances it will be possible to reach regimes in energy-momentum space where $|V_1(\mathbf{q})| \approx |V_2(\mathbf{q})|$ or where an effective repulsive opposite-spin interaction takes place. Some complications arise as well, however, since in these regimes bound states are formed, which corresponds to a net loss rate of particles.

1.2.3 Microcavity Exciton-polaritons

We have established two field theories describing both the microcavity photon field and the interacting exciton gas. The next step is to introduce strong couplings between these two in order to construct new effective fields that describe the polariton fields required for the continuing of this work.

Free Hamiltonian

The most straightforward fashion of setting up a polariton field theory is by introducing a coupling between the photon and exciton field. In this way we describe effective interactions that allow a photon to transform in an exciton and vice versa, correspondig to the operators $\hat{D}^\dagger \hat{\psi}$ and $\hat{\psi}^\dagger \hat{D}$ respectively. Due to hermiticity these processes have to occur with the same transmission amplitude. Furthermore we imply that the quantum numbers spin and momentum must be conserved.
Out of this considerations follows that the free Hamiltonian in its most general form can be written as:

$$\hat{H}_0 = \sum_{\mathbf{k},\sigma} \left(\hat{\psi}^\dagger_{\mathbf{k},\sigma}, \hat{D}^\dagger_{\mathbf{k},\sigma} \right) \begin{pmatrix} \omega_{\mathbf{k}} & \Omega/2 \\ \Omega/2 & \varepsilon_{\mathbf{k}} \end{pmatrix} \begin{pmatrix} \hat{\psi}_{\mathbf{k},\sigma} \\ \hat{D}_{\mathbf{k},\sigma} \end{pmatrix} \tag{1.7}$$

Where we used $\omega_{\mathbf{k}}$ and $\varepsilon_{\mathbf{k}}$, defined by (1.1) and (1.3), and defined Ω as the Rabi-splitting, the coupling strength between the photon and the exciton.
The diagonalisation of the Hamiltonian and plugging in the original expressions for the energies, leads us to the different energy levels of the polariton system:

$$E^{\pm}_{\mathbf{k}} = \frac{1}{2} \left(\delta + \frac{k^2}{2m} \pm \sqrt{\left(\delta - \frac{k^2}{2m} \right)^2 + \Omega^2} \right) \tag{1.8}$$

As is typical for quantum mechanical systems in the strong coupling regime, level repulsion occurs also in a polariton system, resulting in the so-called *upper* (UP) and *lower polariton* (LP) branches, represented by the $E^+_{\mathbf{k}}$ and $E^-_{\mathbf{k}}$ energy levels respectively. The dispersion curves are shown in figure 1.2

To establish the desired polariton fields, one has to transform the free Hamiltonian to the basis in which it is diagonal. This can be done by a rotation:

$$\begin{pmatrix} \hat{\psi}^\dagger_{\mathbf{k}} \\ \hat{D}^\dagger_{\mathbf{k}} \end{pmatrix} = \begin{pmatrix} \cos\theta_{\mathbf{k}} & -\sin\theta_{\mathbf{k}} \\ \sin\theta_{\mathbf{k}} & \cos\theta_{\mathbf{k}} \end{pmatrix} \begin{pmatrix} \hat{U}^\dagger_{\mathbf{k}} \\ \hat{L}^\dagger_{\mathbf{k}} \end{pmatrix} \tag{1.9}$$

Where we defined $\hat{U}^\dagger_{\mathbf{k}}$ and $\hat{L}^\dagger_{\mathbf{k}}$ as the creation operators of two new effective particle fields, representing the upper and lower polariton branches. It can be easily checked that this diagonalises $\hat{H}_0$ if:

$$\tan 2\theta_{\mathbf{k}} = \frac{\Omega}{\omega_{\mathbf{k}} - \varepsilon_{\mathbf{k}}} \tag{1.10}$$

The photon and exciton state have been transformed into two new composite particles, the polariton states, and these particles will now mediate the interactions present in the system.
Apart from that, since the upper polariton branch is higher in energy than the lower one, its occupation will be negligible, provided that both the effective temperature and the pumping frequency are smaller than E^+.

Adding Interactions

We have already derived the interactions between two excitons when setting up the exciton field theory (1.6). In addition, the excitons also collide with the photons inside the cavity, corresponding to a Hamiltonian:

$$\hat{H}_{ex-ph} = -\frac{1}{2}\sum_{\{\sigma_i\}}\sum_{\mathbf{k},\mathbf{k}',\mathbf{q}} U_{\{\sigma_i\}}(\mathbf{q})\, \hat{D}^\dagger_{\mathbf{k}'-\mathbf{q},\sigma_4}\hat{D}^\dagger_{\mathbf{k}+\mathbf{q},\sigma_3}\hat{D}_{\mathbf{k},\sigma_2}\hat{\psi}_{\mathbf{k}',\sigma_1} + \hat{\psi}^\dagger_{\mathbf{k}'-\mathbf{q},\sigma_4}\hat{D}^\dagger_{\mathbf{k}+\mathbf{q},\sigma_3}\hat{D}_{\mathbf{k},\sigma_2}\hat{D}_{\mathbf{k}',\sigma_1}$$

$\hat{H}_{ex-ph}$ describes interactions between two excitons with a momentum exchange $\mathbf{q}$, but this time with a decay of one of the excitons to a photon, or the other way around: the interaction of a photon and an exciton resulting in two excitons, also with momentum exchange $\mathbf{q}$. The explicit sum over all spin states $\{\sigma_i\}$ is carried out under the constraint that $\sigma_1 + \sigma_2 = \sigma_3 + \sigma_4$, that is, we assume that the total spin, as well as the total momentum, are conserved quantum numbers in the exciton-photon gas.
After rotating the interaction Hamiltonians to the polariton basis, we derive an effective Hamiltonian that describes an interacting gas of upper and lower polaritons. However, as we pointed out that for low effective temperatures only the lower polariton branch will be significantly occupied, it turns out satisfactory to start this work from an effective field theory that describes the kinematics of an interacting lower-polariton gas. The resulting Hamiltonian that accomplishes this is obtained by transforming to the polariton basis via (1.9) and omitting all terms containing upper-polariton fields:

$$\hat{H}^{LP}_0 = \sum_{\mathbf{k},\sigma}\omega(\mathbf{k})\hat{L}^\dagger_{\mathbf{k},\sigma}\hat{L}_{\mathbf{k},\sigma}$$

$$\hat{H}^{LP}_{\text{int}} = \sum_{\mathbf{k},\mathbf{k}',\mathbf{q}}\left(\frac{1}{2}\sum_{\sigma=\pm}\left(V^{\text{eff}}_1(\mathbf{q})\hat{L}^\dagger_{\mathbf{k}+\mathbf{q},\sigma}\hat{L}^\dagger_{\mathbf{k}'-\mathbf{q},\sigma}\hat{L}_{\mathbf{k}',\sigma}\hat{L}_{\mathbf{k},\sigma}\right) - V^{\text{eff}}_2(\mathbf{q})\hat{L}^\dagger_{\mathbf{k}+\mathbf{q},-}\hat{L}^\dagger_{\mathbf{k}'-\mathbf{q},+}\hat{L}_{\mathbf{k}',-}\hat{L}_{\mathbf{k},+}\right)$$

With $\omega(\mathbf{k}) \equiv E^-(\mathbf{k})$, the lower-polariton dispersion relation that is given by (1.8). The interaction potentials $V^{\text{eff}}_{1,2}(\mathbf{q})$ can be parametrized in function of the former $V_i(\mathbf{q})$ and $U_i(\mathbf{q})$ describing exciton-exciton

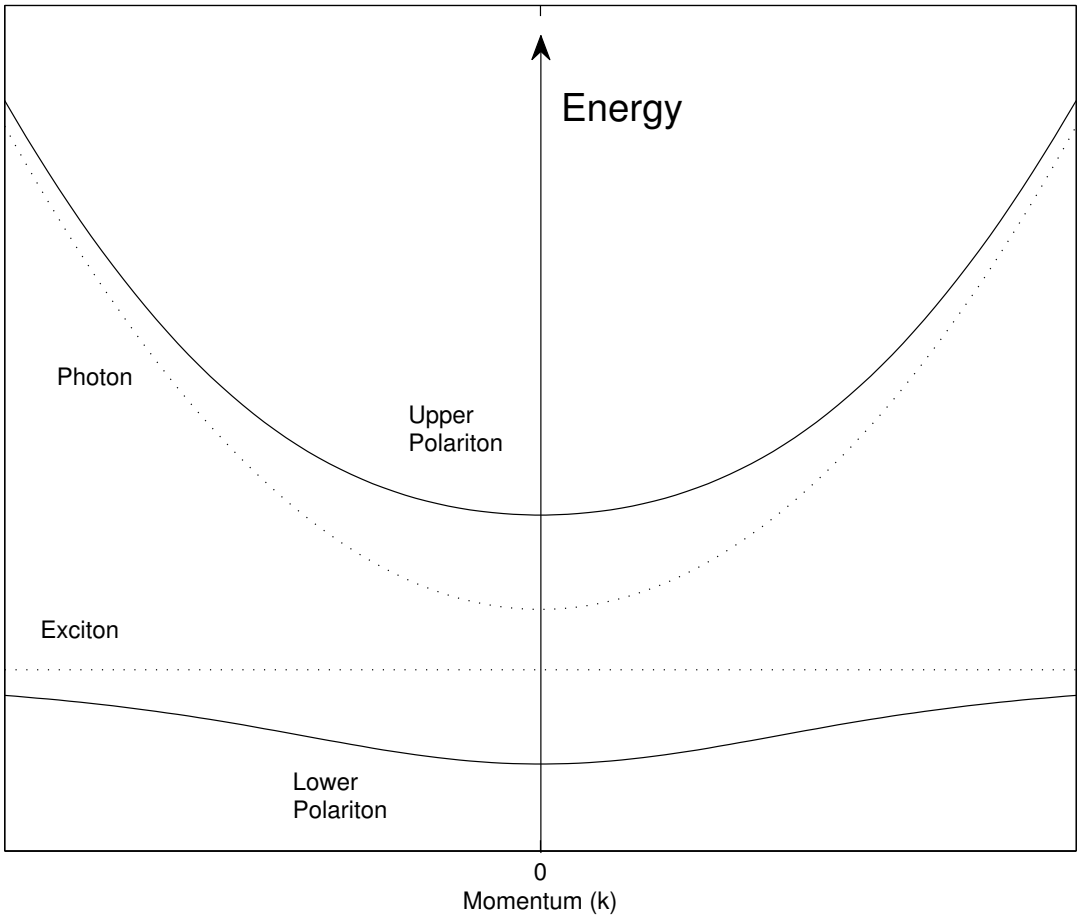

Figure 1.2: The dispersion relation of a polariton system. The original photon and exciton branches have turned into an upper and lower polariton branch because of the strong coupling. A laser beam with energy and momentum close to the lower polariton is used to coherently pump the system.

and exciton-photon interactions. However, as we are working with the lower-polariton Hamiltonian as a starting point for an *effective* field theory, it makes more sense to parametrize $V_{1,2}^{\text{eff}}(\mathbf{q})$ *directly* instead of projecting out these parametrizations from the underlying photon and exciton field theories. The more because they result in complicated functions of both the interaction parameters U_i and V_i, as well as the rotation angle $\theta_{\mathbf{k}}$ and are not really clarifying. We refer the interested reader to [11] where this is elaborated for a one-spin component gas.
Do notice however that the equal-spin lower-polariton interaction is still repulsive and the opposite-spin attractive, since we are still dealing with neutral bosonic particles. Also the composition of molecular-like two opposite-spin-particle bound states is still present, offering us the resonances to tune the interaction strength.

1.3 Polariton Dynamics

After establishing the full Hamiltonian for microcavity exciton-polaritons, the dynamics of the systems can be calculated via the Heisenberg equations of motion. In this way, the time evolution of any operator $\hat{a}$ can be obtained by calculating the commutator with the Hamiltonian of the system:

$$\frac{d}{dt}\hat{a}(t) = i\left[\hat{H}, \hat{a}(t)\right] \tag{1.11}$$

Out of this equation the full dynamics of the polariton system will be derived, but first we need to extend the Hamiltonian, since the microcavity Hamiltonian $\hat{H}_{LP}$ only describes a part of the full polariton system.

1.3.1 Coupling to a Reservoir and Pumping

At this stage we are still considering the polariton system as a closed energy-conserving system of interacting particles, which cannot be a satisfactory theory for obvious reasons. We have to extend our description with the necessary terms that describe the inherent non-equilibrium properties of a polariton system. This can be achieved by discarding the energy conservation of the polariton system *on itself*, and rather consider the polariton system as a *subsystem* of a larger energy-conserving system.

Extending the Hamiltonian

Polaritons are excited by incoming photons from a laser that propagate through the Bragg mirrors surrounding the polariton microcavity. On the other hand, photons that are already inside the microcavity can propagate their way through the Bragg mirrors as well. Due to energy conservation and the hermiticity of the system, these two processes should have the same probability.
The photons coming from the laser outside the polariton cavity are represented by a *photon bath*, a reservoir of photon modes to which the polaritons inside the cavity can couple.
As such the full Hamiltonian that describes energy-conserving system can be formulated as:

$$\hat{H}_{\text{tot}} = \hat{H}_{LP} + \hat{H}_B + \hat{H}_C + \hat{H}_P, \tag{1.12}$$

where $\hat{H}_{LP}$ is the lower-polariton Hamiltonian (1.11).
So we have defined three additional Hamiltonians to describe the complete dynamics of the energy-conserving system:

- $\hat{H}_B$ is the Hamiltonian that describes the bath photons in the reservoir:

$$\hat{H}_B = \sum_{\sigma=\pm}\sum_{\mathbf{q}} \omega_{\mathbf{q}} \hat{b}^\dagger_{\mathbf{q},\sigma}\hat{b}_{\mathbf{q},\sigma}$$

The operators $\hat{b}^\dagger_{\mathbf{q},\sigma}$ and $\hat{b}_{\mathbf{q},\sigma}$ are respectively the creation and annihilation operators of a bath photon with momentum $\mathbf{q}$ and spin σ. The operators satisfy the usual commutation relations for bosonic operators, as outlined in section 1.2.1. The momentum $\mathbf{q}$ of the bath photons is their momentum in *three*-dimensional space outside the microcavity. Therefore it is useful to write this momentum as the sum of a momentum vector parallel to the plane $\mathbf{k}$ and a component perpendicular to the plane q_z: $\mathbf{q} = \mathbf{k} + q_z\mathbf{e}_z$.

- $\hat{H}_C$ is the Hamiltonian that describes the coupling between the reservoir and the microcavity polaritons:

$$\hat{H}_C = \kappa \sum_{\sigma=\pm} \sum_{\mathbf{k},q_z} \left(\hat{b}^\dagger_{\mathbf{k},q_z,\sigma} \hat{L}_{\mathbf{k},\sigma} + \hat{L}^\dagger_{\mathbf{k},\sigma} \hat{b}_{\mathbf{k},q_z,\sigma} \right)$$

  So reservoir photons only interact with polaritons that have the same in-plane momentum $\mathbf{k}$ and spin σ. We therefore assume in-plane momentum and spin conservation by tunneling through the Bragg mirrors. Furthermore we formulated the tunneling probability as neither spin- nor momentum-dependent. Thus we neglected the TE/TM-splitting and possible direct momentum dependence of the Bragg mirrors.

- $\hat{H}_P$ is the Hamiltonian that describes the pumping of the polariton gas:

$$\hat{H}_P = \sum_{\sigma=\pm} \left(F_\sigma \hat{L}_{\mathbf{k}_p,\sigma} e^{-i\omega_p t} + F^*_\sigma \hat{L}^\dagger_{\mathbf{k}_p,\sigma} e^{i\omega_p t} \right) \tag{1.13}$$

  The parameters $F_\pm$ determine the strength of the pumping power of the two spin components. They parametrize all factors of influence: the intensity of the laser, the transmission of photons in the microcavity and the coupling between the photons and the sample to excite excitons. Furthermore we have that constraint that $I_{\text{tot}} = |F_+|^2 + |F_-|^2$, so that the relative difference between the up and down component can be tuned by polarizing the incident laser beam.
  We assume the in-plane momentum $\mathbf{k}_p$ and the laser frequency ω_p to be fixed. Within good approximation only polaritons with the laser momentum are injected in the microcavity. This pumping regime is called *coherent* pumping, since it involves a direct quantum coherence of the polaritons, imposed by the optical coherence of the laser beam.
  Polariton systems can also be pumped *incoherently*. In this regime polaritons are injected at an energy far above the lower-polariton dispersion curve. Scatterings will then thermalize these particles to lower energy and momentum states, causing the original coherence to fade away.

1.3.2 Equations of Motion

Out of a physical system's Hamiltonian the dynamics of the system can be calculated via the *Heisenberg* equations of motion (1.11). Because we have gathered a large number of energy terms for the establishment of the full Hamiltonian (1.12), we will go through this step by step.

The Polariton System

We will start by calculating the time evolution of the interacting polariton gas in the microcavity subsystem. To avoid an overload of notation we will do the derivation for a single-spin polariton fluid. The general derivation however is completely analogous after adding a second spin component and a cross-interaction term.
The bosonic Hamiltonian of interacting lower polaritons can be written as:

$$\hat{H}_{LP} = \sum_{\mathbf{k}} \omega_{\mathbf{k}} \hat{L}^\dagger_{\mathbf{k}} \hat{L}_{\mathbf{k}} + \frac{1}{2} \sum_{\mathbf{k},\mathbf{k}',\mathbf{q}} V(\mathbf{q}) \hat{L}^\dagger_{\mathbf{k}'-\mathbf{q}} \hat{L}^\dagger_{\mathbf{k}+\mathbf{q}} \hat{L}_{\mathbf{k}'} \hat{L}_{\mathbf{k}}, \tag{1.14}$$

where we have used $\omega_{\mathbf{k}}$ as the lower-polariton energy (1.8) with momentum $\mathbf{k}$ and $V(\mathbf{q})$ the amplitude to exchange momentum $\mathbf{q}$ in a collision process.
We approximate that the dispersion relation is quadratic, i.e.:

$$\omega_{\mathbf{k}} \approx \frac{k^2}{2m}$$

This approximation is valid for low-momentum states. Since we have a mixing of a photon and an exciton state, the low-momentum spectrum of the lower polariton is mainly photonic and the higher part more excitonic, with a smooth transition. For small momenta, we can then approximate this spectrum by the photonic one, which is quadratic with an effective pseudomass m.

Since our ultimate goal is to describe the physics of the system in terms of fluid dynamics, it makes sense to work towards a mathematical description in position space instead of momentum space.
We therefore define the operators:

$$\begin{aligned} \hat{\Psi}(\mathbf{r}) &\equiv \frac{1}{\sqrt{V}} \sum_{\mathbf{k}} \hat{L}_{\mathbf{k}} e^{i\mathbf{k}\cdot\mathbf{r}} \\ \hat{\Psi}^\dagger(\mathbf{r}) &\equiv \frac{1}{\sqrt{V}} \sum_{\mathbf{k}} \hat{L}^\dagger_{\mathbf{k}} e^{-i\mathbf{k}\cdot\mathbf{r}} \end{aligned} \tag{1.15}$$

These are the operators respectively annihilating and creating a *localized* particle at position $\mathbf{r}$.
Again we impose the bosonic commutation relations, but this time in position space:

$$\begin{aligned} \left[\hat{\Psi}(\mathbf{r}), \hat{\Psi}(\mathbf{r}')\right] = \left[\hat{\Psi}^\dagger(\mathbf{r}), \hat{\Psi}^\dagger(\mathbf{r}')\right] &= 0 \\ \left[\hat{\Psi}(\mathbf{r}), \hat{\Psi}^\dagger(\mathbf{r}')\right] &= \delta(\mathbf{r}-\mathbf{r}') \end{aligned}$$

Substituting these in the Hamiltonian (1.14) then leads to its formulation in position space:

$$\hat{H}_{LP} = \int d^2r \hat{\Psi}^\dagger(\mathbf{r}) \left(-\frac{1}{2m}\nabla^2\right) \hat{\Psi}(\mathbf{r}) + \frac{1}{2}\int d^2r \int d^2r' \hat{\Psi}^\dagger(\mathbf{r})\hat{\Psi}^\dagger(\mathbf{r}')U(\mathbf{r}-\mathbf{r}')\hat{\Psi}(\mathbf{r}')\hat{\Psi}(\mathbf{r}) \tag{1.16}$$

Now we are ready to calculate the dynamics of the microcavity subsystem by making use of the Heisenberg equation of motion. Taking into account the commutating relations, we then derive:

$$\begin{aligned} i\partial_t \hat{\Psi}(\mathbf{r},t)\Big|_{cavity} &= \left[\hat{\Psi}(\mathbf{r},t), \hat{H}_{LP}\right] \\ &= \left[-\frac{1}{2m}\nabla^2 + \int d^2r'\ \hat{\Psi}^\dagger(\mathbf{r}',t)U(\mathbf{r}-\mathbf{r}')\hat{\Psi}(\mathbf{r},t)\right]\hat{\Psi}(\mathbf{r},t) \end{aligned}$$

As a further approximation, we can assume that there are only local interactions present in the system. This picture is valid if the typical interaction length of $U(\mathbf{r})$ is much shorter than the mean distance between two particles. As a consequence, we can express $U(\mathbf{r})$ as a so-called contact potential with strength g:

$$U(\mathbf{r}-\mathbf{r}') = g\delta(\mathbf{r}-\mathbf{r}'),$$

yielding a simplified equation of motion for $\hat{\Psi}(\mathbf{r},t)$:

$$i\partial_t \hat{\Psi}(\mathbf{r},t)\Big|_{cavity} = \left[-\frac{1}{2m}\nabla^2 + g\hat{\Psi}^\dagger(\mathbf{r},t)\hat{\Psi}(\mathbf{r},t)\right]\hat{\Psi}(\mathbf{r},t)$$

Generalizing the calculation for a binary fluid results in:

$$i\partial_t \hat{\Psi}_\pm(\mathbf{r},t)\Big|_{cavity} = \left[-\frac{1}{2m}\nabla^2 + \alpha_1\hat{\Psi}^\dagger_\pm(\mathbf{r},t)\hat{\Psi}_\pm(\mathbf{r},t) + \alpha_2\hat{\Psi}^\dagger_\mp(\mathbf{r},t)\hat{\Psi}_\mp(\mathbf{r},t)\right]\hat{\Psi}_\pm(\mathbf{r},t) \tag{1.17}$$

Thus the equations of motion that describe the time evolution inside the microcavity are a coupled set of two non-linear differential equations.

Coupling with the Reservoir

Additional dynamics take place because of the coupling of the cavity to the photon reservoir. To solve this, we apply the Heisenberg equations of motion, but now in the system described by the coupling Hamiltonian $\hat{H}_C$. We start by calculating the time evolution of the polariton operator in momentum space and perform the calculation for single-spin polaritons:

$$i\partial_t \hat{L}_{\mathbf{k}}\Big|_{coupling} = \left[\hat{L}_{\mathbf{k}}, \hat{H}_C\right] = \kappa \sum_{q_z} \hat{b}_{\mathbf{k},q_z} \tag{1.18}$$

So in order to solve this equation, the time evolution of the reservoir photons needs to be calculated as well:

$$i\partial_t \hat{b}_{\mathbf{k},q_z} = \left[\hat{b}_{\mathbf{k},q_z}, \hat{H}_B + \hat{H}_{SB}\right] = \omega_{\mathbf{k},q_z} \hat{b}_{\mathbf{k},q_z} + \kappa \hat{L}_{\mathbf{k}}$$

Therefore we find two coupled differential equations to describe the time evolution of the reservoir photons and the microcavity polaritons.
By integrating the latter expression we then find:

$$\hat{b}_{\mathbf{k},q_z}(t) = \hat{b}_{\mathbf{k},q_z}(0) e^{-i\omega_{\mathbf{k},q_z} t} - i\kappa \int_0^t e^{-i\omega_{\mathbf{k},q_z}(t-t')} \hat{L}_{\mathbf{k}}(t') dt' \tag{1.19}$$

Theoretically we have to keep the initial value $\hat{b}(0)$, as it gives rise to quantum fluctuations. For now we will neglect this term by imposing the initial values $\hat{b}_{\mathbf{k},q_z}(0) = 0$, motivated by the fact that we will take a classical limit later on in this work, in which quantum fluctuations are averaged out anyway. Notice however that this is in general *not* allowed, because we *cannot* neglect the commutation relations of this operator. The quantum theory that takes into account the full quantum nature of the problem is described by the *quantum Langevin equation*, for which we refer the interested reader to [20].

Substituting the time evolution of the reservoir photon modes in the equation of motion of the polaritons yields (1.18):

$$i\partial_t \hat{L}_{\mathbf{k}}\Big|_{coupling} = -i \sum_{q_z} \kappa^2 \int_0^t e^{-i\omega_{\mathbf{k},q_z}(t-t')} \hat{L}_{\mathbf{k}}(t') dt' \tag{1.20}$$

From here on, two important appoximations have to made. First of all we assume that the system is *Markovian*, so that there is no memory and all processes take place instantly.
This allows us to write

$$\kappa^2 \sum_{q_z} e^{-i\omega_{\mathbf{k},q_z}(t-t')} \equiv \frac{\gamma_{\mathbf{k}}}{2} \delta(t-t'),$$

where we defined an instant coupling $\gamma_{\mathbf{k}}$ that averages over the couplings with all q_z.
As a second approximation we assume that the couplings to the reservoir are *frequency*-independent. Therefore we have that for all in-plane momenta holds $\gamma_{\mathbf{k}} \equiv \gamma$, a simplification which is certainly valid for the low momentum states that we consider.
Taking into account these simplifications, the approximated time evolution of the polariton operator in the cavity-reservoir coupling system is given by:

$$i\partial_t \hat{L}_{\mathbf{k}}\Big|_{coupling} = -i\frac{\gamma}{2} \hat{L}_{\mathbf{k}} \tag{1.21}$$

Which we can easily solve:

$$\hat{L}_{\mathbf{k}}(t) = \hat{L}_{\mathbf{k}}(0)\, e^{-\frac{\gamma}{2}t}$$

So we have derived that the coupling of the polariton system to a photon reservoir results in a *net loss rate* of polariton particles. This is also what we expected out of physical considerations: the photons

that couple to the excitons to form polaritons can escape through the Bragg mirrors.
The effect of this time evolution can be seen by calculating the time-dependent density operator expectation value in a system with n polaritons in momentum state $\mathbf{k}$:

$$\langle n|\, \hat{L}^\dagger_{\mathbf{k}}(t)\hat{L}_{\mathbf{k}}(t)\,|n\rangle = n\, e^{-\gamma t} \tag{1.22}$$

As such, there is an exponential decay of the polariton density in the microcavity, with a decay rate γ. The typical lifetime of the polaritons is then given by $\tau = 1/\gamma$. In general microcavities the typical lifetime of polaritons is of the order of picoseconds [11]. Transforming the polariton operators to position space via (1.15) and adding again the spin quantum number, then yields the equation of motion:

$$\partial_t \hat{\Psi}_\pm(\mathbf{r},t)\Big|_{coupling} = -\frac{\gamma}{2}\hat{\Psi}_\pm(\mathbf{r},t) \tag{1.23}$$

Notice that we also neglected any spin dependence in the decay rate through the Bragg mirrors. This is also an approximation valid for low momentum states.

The Pump

The equation of motion resulting from the pumping Hamiltonian is found by calculating:

$$i\partial_t \hat{L}_{\mathbf{k},\pm}\Big|_{pump} = \left[\hat{L}_{\mathbf{k},\pm}, \hat{H}_P\right] = F_\pm e^{-i\omega_p t}\,\delta_{\mathbf{k},\mathbf{k}_p}$$

Therefore by puming the polariton gas coherently with a laser, a constant rate of polaritons that take over the laser momentum, energy and spin is injected in the cavity. This balances the previously introduced losses because of photons escaping the microcavity. Notice that under normal circumstances this system balances itself. Indeed, a growing polariton density inside the cavity, automatically results in an increased particle decay rate (1.22).
This result can also be transformed to position space by (1.15) to obtain the equation of motion for the operator $\hat{\Psi}$:

$$i\partial_t \hat{\Psi}_\pm(\mathbf{r},t)\Big|_{pump} = F_\pm(\mathbf{r},t)e^{-i(\omega_p t - \mathbf{k}_p\cdot\mathbf{r})} \tag{1.24}$$

In general the pump $F_\pm$ has a spatial density profile and a time-dependence, but for the purposes of our work, we will approximate the laser beam as static and homogeneous: $F_\pm(\mathbf{r},t) \equiv F_\pm$.

The full dynamics of the polariton operator in position in space is then given by the sum of the dynamics of all considered subsystems. The final result are two non-linear coupled differential equations:

$$\begin{aligned} i\partial_t \hat{\Psi}_\pm(\mathbf{r},t) &= \left[\hat{L}_{\mathbf{k},\pm}, \hat{H}_{tot}\right] \\ &= \left[-\frac{1}{2m}\nabla^2 + \alpha_1\hat{\Psi}^\dagger_\pm(\mathbf{r},t)\hat{\Psi}_\pm(\mathbf{r},t) + \alpha_2\hat{\Psi}^\dagger_\mp(\mathbf{r},t)\hat{\Psi}_\mp(\mathbf{r},t) - i\frac{\gamma}{2}\right]\hat{\Psi}_\pm(\mathbf{r},t) + F_\pm(\mathbf{r},t)e^{-i(\omega_p t - \mathbf{k}_p\cdot\mathbf{r})} \end{aligned}$$

Chapter 2

Polaritons as Quantum Fluids of Light

Now we have presented how polaritons in microcavities can be described by using quantum field theory, it is time to perform the necessary approximations in order to establish a solid toolbox to start calculations from. Our ultimate goal will be to achieve a description of a polariton system in terms of fluid dynamics, since we will show that under the right circumstances this approximation holds perfectly.
First we will clarify the concepts of condensation, starting by explaining shortly the well-known phenomenon Bose-Einstein condensation (BEC), in order to generalize this concept for non-equilibrium quantum systems.

2.1 Polariton Condensation

Due to the coherence properties of polariton systems, they can form condensates similar to Bose-Einstein condensates of cold atoms. The direct relation between these two is a little tricky, since polariton systems are inherently out-of-equilibrium systems. BEC in cold gases involves a phase transition and is a consequence of a spontaneous relaxation process, whereas the coherence in polariton systems is rather a direct manifestation of the locking of the polariton phase to the phase of the incident laser beam.

2.1.1 Bose-Einstein Condensation

The simplest and, moreover, the most extensively studied system in which Bose-Einstein condensation occurs is a non-interacting gas of bosonic particles. For this system, the Bose-Einstein distribution function has the form:

$$n_B(E) = \frac{1}{e^{\frac{1}{k_B T}(E-\mu)} - 1},$$

with T the temperature, μ the chemical potential and T the temperature.
This distribution represents the density of bosonic particles n_B in a certain energy state E. It is clear that this distribution diverges when $E \to \mu$. In these types of systems it can be shown that there is a finite density at which the chemical potential becomes zero. Therefore when the temperature is decreased at fixed density, or density increased at a fixed temperature, there is a point at which the chemical potential reaches the bottom of the density of states. Now, it is clear that under these circumstances the Bose-Einstein distribution diverges at $E = 0$. This critical point determines a phase transition to a *condensed* state, in which there is a *macroscopic* occupation of the zero-energy state.

In more general terms, Bose-Einstein condensation is defined as the appearance of a single particle state with macroscopic occupation. Because of this, one is allowed to describe the condensate by a *single complex wavefunction* Ψ that holds for all the particles in the system. Explicitely formulated, this means that we can write for the many-particle wave function:

$$\psi(\mathbf{r}_1, \ldots, \mathbf{r}_N) \equiv \prod_{i=1}^{N} \Psi(\mathbf{r}_i)$$

Actually the macroscopic occupation of a single particle state allows to replace the corresponding *quantum operator* by its *wave function*, hence neglecting the non-commutativity of the field operators. This approach is appropriate when the occupation of the state is much larger than one.

We have only provided a short summary of the basic principles of Bose-Einstein condensation, inspired by the summary outlined in [9]. We would like to refer the interested reader to the excellent books [14] and [15] for detailed explanations.
The reason why we have explained the basic ideas behind Bose-Einstein condensation, is to make a ground for generalizing this concept in polariton fluids. Moreover, it will be shown that in the appropriate limit, the stable-fuid fluid limit, a polariton system is physically equivalent to a Bose-Einstein, as will be outlined in the coming sections. From time to time we will take this limit to demonstrate that the already established equivalent results for Bose-Einstein condensates can be recovered out of the more general non-equilibrium physics that describes polariton systems.

2.1.2 Coherence by the Pump

Since polariton systems are inherently non-equilibrium systems due to a finite lifetime, the particle losses should be balanced by a constant injection source in order to maintain a stable system. The Bragg mirrors of the cavity are not perfect, and that is why a certain loss rate of photons is inevitable in the experimental set-up. To balance this, a continuous source of photons should be provided to bring the system in balance again. As will be outlined thoroughly during this work, the majority of fascinating physics in polariton systems originates directly from this fundamental non-equilibrium and the experimental possibility to tune the laser momentum and frequency. That is why we offer a detailed explanation of how polariton systems are pumped and how this affects the properties of the polariton gas, based on [10], [9]
In the coherent pumping regime the energy and in-plane momentum of the laserbeam is close to the dispersion curve of the lower-polariton, as is shown in figure 1.2. In this way, a coherent fluid of polaritons can be excited, since they initially take over the momentum and energy from the incident light in a resonant way. The result is a system of polaritons that can be approximated as a macroscopic fluid of particles in the same quantum state, that is, with the same momentum, energy and spin distribution, directly inherited from the laser beam.

Coherence Properties

Initially all excited polaritons take over the energy and in-plane momentum of the laser beam, realizing a coherent condensate of polaritons with a strongly peaked energy-momentum distribution. However, due to excitonic collisions and interactions with for example lattice phonons, the originally peaked energy-momentum distribution will smoothen along the polariton dispersion curve. Therefore we will assume that the typical polariton lifetime is short enough to neglect these thermalization effects and maintain the necessary coherence. In this way the energy-momentum state corresponding to the laser beam will be macroscopically occupied, so that the approximation of a single-state fluid is still valid within high

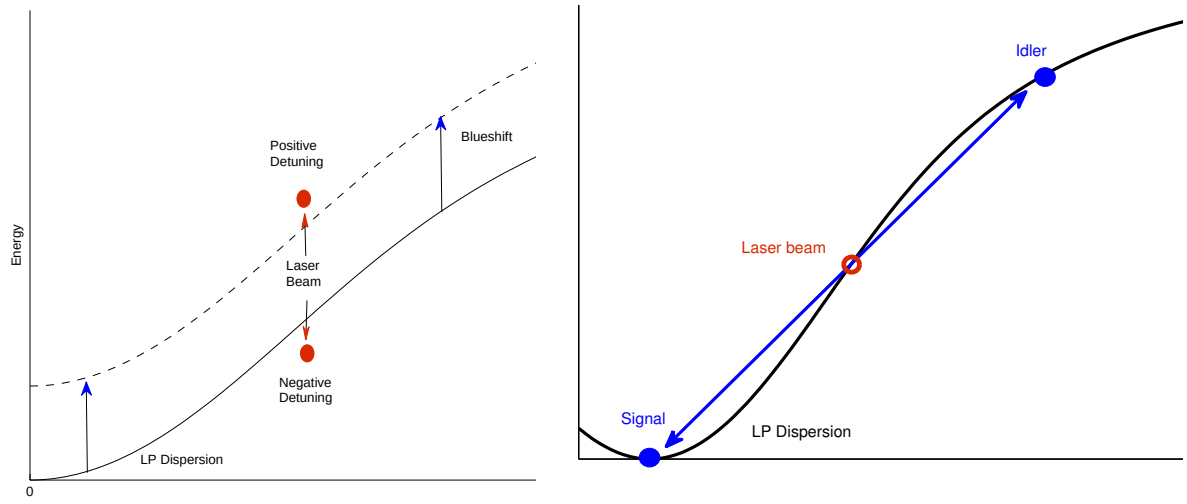

(a) Blueshift of the Spectrum

(b) Parametric Oscillation

Figure 2.1: (a) Due to the increasing interaction energy under pumping, an effective blueshift of the polariton dispersion occurs. If the laser frequency is situated above the spectrum (positive detuning), the dispersion is shifted closer to resonance with the laser beam, resulting in a Kerr bistability. If instead the laser frequency is below the dispersion, the dispersion is pushed out of resonance. (b) At the *magic* angle resonant scattering of the polaritons takes place: the laser beam is unstable and splits resonantly in a low-momentum (signal) and a high-momentum beam (idler).

accuracy. The ansatz of dealing with a single-state fluid is one of the key assumptions during the research presented in this work. The coherence of the fluid allows us to apply *mean field* theory as a valid approximation, as will be pointed out later on.
Although we call the polariton fluid a *condensate*, there is a fundamental difference with an ordinary Bose-Einstein condensate of cold atoms. The presence of a coherent phase in a BEC is a consequence of spontaneous symmetry breaking, involving a second order phase transition, whereas the coherent phase in a polariton fluid is directly *imposed* by the coherent laser beam.

2.1.3 Laser Detuning

The energy-momentum of the laser can be either above or beneath the polariton dispersion curve, corresponding to either *positive* or *negative* detuning. Since the pumping of a polariton fluid naturally results in an upward energy shift due to the increasing interaction energy, these two regimes show a fundamentally different behaviour. During the intense pumping of a fluid with a positive detuning, the energy blueshift pushes up the dispersion curve and brings it closer to resonance with the energy-momentum of the laser. With sufficient laser intensity, the dispersion curve might cross the energy-momentum point of the laser, leaving a fluid with negative detuning. Therefore pumping with positive laser detuning can be unstable, depending on the laser-intensity. This phenomenon, known as the Kerr bistability, is shown in figure 2.1(a) and will be clarified later on by means of mean field theory.
If the condensate is pumped with a negative detuning, the resonance becomes increasingly worse by the blueshift, so that this pumping regime is always stable.

Parametric Scattering

A particularly interesting behaviour is observed when polaritons are injected close to the inflection point of the dispersion curve. At this point a resonant scattering can take place that is both energy and

momentum conserving. The polaritons that originally take over the energy and momentum of the laser will scatter into into a low-momentum state, traditionally called the *signal* state, and a high momentum state, the *idler*. In this way a pump positioned at this angle, sometimes called the *magic* angle, results in three different polariton beams by stimulated scattering. The fluid with the pump wave-vector becomes unstable and polaritons are scattered into the signal and idler beam. This process is called optical parametric oscillation (OPO). Notice that in order for this process to occur, a resonance between the laser energy-momentum and the polariton energy is required. OPO can therefore only take place with a positive laser detuning, as the energy blueshift brings the polariton curve closer to resonace with the laser beam.
In addition, the OPO process can be strongly enhanced by placing a weak laser beam at zero momentum, resulting in an amplification process known as *optical parametrical amplification* (OPA).
The original coherent phase of the polariton fluid gets lost by these stimulated scattering processes, as the only requirement for the phases is that $\phi_{\text{idler}} + \phi_{\text{signal}} = 2\phi_{\text{beam}}$. A graphical image of this process is provvided in figure 2.1(b).

For the purposes of our work, we will assume the laser beam to be far from these resonant processes in order to maintain a coherent phase in the condensate. This approximation is reasonable since we assume small momenta, much smaller than the inflection point of the polariton dispersion. Thus within good approximation a coherent single-state polariton fluid with a coherent phase can be considered.

Incoherent Pumping

Although not relevant in the following of this work, we shall provide a brief description of the principles of non-resonant pumping, for the sake of completeness. In the incoherent pumping scheme the momentum and energy of the incident light is far above the polariton dispersion curve. In this way, a reservoir of polaritons is created that will gradually thermalize along the polariton dispersion curve by collisions. Eventually this will result in the macroscopic occupation of the low momentum states and a non-equilibrium condensate. The principal difference with coherent pumping is that there is no coherent phase present in this condensate, since the earlier coherence fades away by the collisions.
During this relaxation process *spontaneous* coherence effects can occcur under the right circumstances, such as long-range coherence effects and even Bose-Einstein condensation. [11]

2.2 Mean Field Theory

The full polariton quantum field theory established in the previous chapter turns out to be somehow overloaded and impractical to perform realistic calculations of many-particle physics. Furthermore we assume macroscopic coherent systems of many particles, so that we average out the quantum nature of the single polaritons. The general physical formalism that averages the quantum effects from a field theory in a rigorous way is called *mean field theory*.

2.2.1 The Gross-Pitaevskii equation

We have established a description of the full dynamics of a microcavity exciton-polariton system on the level of quantum field theory in (1.25). The way this quantum mechanical description manifests itself on a macroscopical scale is on the level of expectation values of operators. As such, we can calculate the expectation value of the equation of motion of the polariton operator $\hat{\Psi}_{\pm}$. For this we will define:

$$\left\langle \hat{\Psi}_{\pm}(\mathbf{r}, t) \right\rangle \equiv \Psi_{\pm}(\mathbf{r}, t), \tag{2.1}$$

where we have defined the *wave function* $\Psi_\pm(\mathbf{r},t)$ as the expectation value of field operator $\hat{\Psi}_\pm(\mathbf{r},t)$ at position $\mathbf{r}$ and time t.

By taking the expectation value of (1.25) on both sides, we can replace the field operator $\hat{\Psi_\pm}$ everywhere by the wave function $\Psi_\pm$, since taking the expectation value is a linear operation. The only terms in which this is not possible, are the interaction terms, because they consist of products of operators. We can solve this problem by stating that

$$\left\langle \hat{\Psi}^\dagger \hat{\Psi} \hat{\Psi} \right\rangle \longrightarrow \left\langle \hat{\Psi}^\dagger \right\rangle \left\langle \hat{\Psi} \right\rangle \left\langle \hat{\Psi} \right\rangle \tag{2.2}$$

which is called the *mean-field* approximation.
Thus after elaborating this operation, we derive the celebrated Gross-Pitaevskii equation that describes the fluid dynamics of a binary polariton system:

$$\boxed{i\partial_t \Psi_\pm = \left(\omega(-i\nabla) - i\frac{\gamma}{2} + \alpha_1 \left|\Psi_\pm\right|^2 + \alpha_2 \left|\Psi_\mp\right|^2\right)\Psi_\pm + F_\pm(t)} \tag{2.3}$$

Via this equation we have established a hydrodynamical description of a binary polariton fluid, that includes interactions, pumping and decay. This result will be the starting point for the research performed in this work

2.2.2 Internal Energy

The internal energy of the microcavity can be calculated as the expectation value of the microcavity Hamiltonian $\hat{H}_{LP}$. Notice that the internal energy is not necessarily a conserved quantity under time-evolution, since we are integrating over an open subsystem.

$$\begin{aligned}
\mathcal{E} &\equiv \left\langle \hat{H}_{LP} \right\rangle \\
&= \left\langle \int d^2r\ \hat{\Psi}_+^\dagger(\mathbf{r},t)\left[-\frac{1}{2m}\nabla^2 + \frac{\alpha_1}{2}\hat{\Psi}_+^\dagger(\mathbf{r},t)\hat{\Psi}_+(\mathbf{r},t) + \frac{\alpha_2}{2}\hat{\Psi}_-^\dagger(\mathbf{r},t)\hat{\Psi}_-(\mathbf{r},t)\right]\hat{\Psi}_+(\mathbf{r},t)\right\rangle \\
&\quad + \left\langle \left(+ \longleftrightarrow -\right)\right\rangle
\end{aligned}$$

By performing the mean-field approximation for the interaction terms, we then find:

$$\mathcal{E} = \int d^2r \left[\Psi_+^*\left(-\frac{1}{2m}\nabla^2\right)\Psi_+ + \Psi_-^*\left(-\frac{1}{2m}\nabla^2\right)\Psi_- + \frac{\alpha_1}{2}\left(\left|\Psi_+\right|^4 + \left|\Psi_-\right|^4\right) + \alpha_2\left|\Psi_+\right|^2\left|\Psi_-\right|^2\right], \tag{2.4}$$

where we have omitted the explicit writing down of the time- and space-dependence of the wavefunctions. A lot of valuable information can be retrieved out of this expression. First of all we know that the operator $-\frac{1}{2m}\nabla^2$ is the kinetic energy operator and therefore has the dimensionality of an energy. By comparing this to the internal energy, which is also has the dimensionality of an energy, we immediately get that the two-dimensional wave function $\Psi_\pm$ has a dimension of an inverse length scale.
By studying the interaction terms it is then easy to derive that the interaction constants α_i have the dimensionality of an inverse mass. Therefore they can be formulated as $\alpha_i \equiv \frac{1}{m}\tilde{\alpha}_i$, where the $\tilde{\alpha}_i$ are now dimensionless quantities expressed relative to the polariton mass.
When only considering the two interaction terms in the internal energy, we find that we can formulate

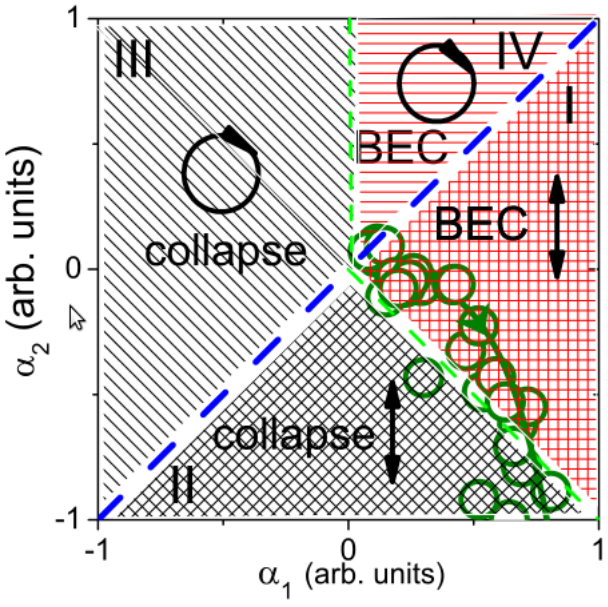

Figure 2.2: A schematic image of the minimum-energy stable fluid phases of a polariton gas in function of α_1 and α_2. The ↻-arrow denotes a circularly polarized spin fluid, meaning that there is only one spin component. The ↕-arrow denotes a linearly polarized fluid, so the two fluids have a finite density. The grey regions are unstable, since there the energy has no lower bound. The circles are the interaction constants that have been measured in [13] and from which this picture is taken.

the interaction energy more suggestively as:

$$\begin{aligned}\mathcal{E}_{\text{int}} &= \int d^2r \left[\frac{1}{4}(\alpha_1+\alpha_2)\left(|\Psi_+|^2+|\Psi_-|^2\right)^2+\frac{1}{4}(\alpha_1-\alpha_2)\left(|\Psi_+|^2-|\Psi_-|^2\right)^2\right] \\ &\equiv \int d^2r \left[\frac{U_1}{2}|N|^4+\frac{U_2}{2}|S|^4\right]\end{aligned}$$

In this way we see clearly that an energy contribution is coming from interactions governed by the fluid density $|N|^2 = |\Psi_+|^2 + |\Psi_-|^2$ with a coupling $U_1 = \frac{1}{2}(\alpha_1+\alpha_2)$, and a spin-related interaction $|S|^2 = \left||\Psi_+|^2 - |\Psi_-|^2\right|$, with a coupling $U_2 = \frac{1}{2}(\alpha_1-\alpha_2)$.

The interaction energy needs to be stable for small density fluctuations. Out of this we can get restrictions to limit the physical range of the interaction constants in a stable system:

$$\begin{aligned}\alpha_1 &> 0 \\ \alpha_1^2 &> \alpha_2^2\end{aligned}$$

The complete derivation of this is outllined in [15] for binary Bose-Einstein condensates, but is identical for polariton systems. On figure 2.2 a schematic image is given of the minimal-energy configurations of binary polariton fluids and the experimentally measured interaction constants.

2.2.3 Validity of the Mean-field Approximation

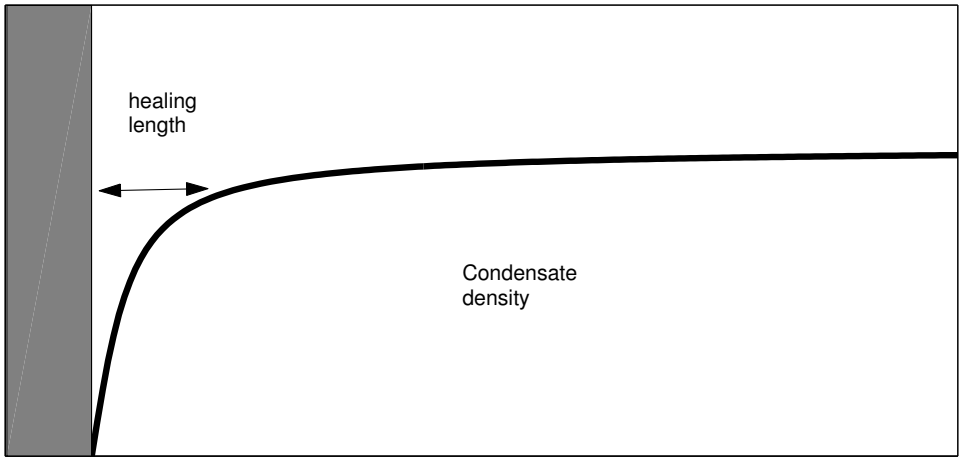

Figure 2.3: A graphical image of the healing length of in condensate: The healing length is the typical length scale necessary to recover the bulk condensate density.

When deriving the Gross-Pitaevskii equation, we were able to substitute the polariton field operator *everywhere* by its quantum expectation value, except in the interaction terms. Therefore the only approximation that we have performed is situated on the level of interactions. Also the validity of this approach needs to be verified by studying the physical regime of interactions in the considered system.
In order to acquire a quantitative measurement to determine the validity, we define the *healing length* of the polariton condensate as the typical length scale it needs to recover to its bulk density in the presence of a defect. For this we have to relate the two typical energy scales that are contained in the Gross-Pitaevskii equation: the kinetic and the interaction energy.
By remembering that the $(-i\nabla)$-operator denotes a wave vector in momentum space, and thus an inverse length scale ξ, we then find:

$$\frac{1}{m\xi^2} = \alpha_1 n_\pm,$$

where $n_\pm = |\Psi_\pm|^2$ is the bulk density of the condensate.
We then find for the healing length $\xi_\pm$:

$$\xi_\pm = \sqrt{\frac{1}{m\alpha_1 n_\pm}} \tag{2.5}$$

The mean-field approximation we performed in the interaction terms (2.2) is now valid for high polariton densities, that is if:

$$n_\pm = \left\langle \hat{\Psi}_\pm^\dagger \hat{\Psi}_\pm \right\rangle \gg \frac{1}{L^2}$$

So if we divide the two-dimensional polariton system in a grid of squares with area L^2, then we need *much more* than one particle in this square to motivate the replacement of the polariton operator by a wave function. This is just the requirement that we need many particles in order to average the quantum fluctuations.
Substituting the healing length as the typical length scale of density fluctuations in the polariton fluid, we then derive the condition $n_\pm \xi_\pm^2 \gg 1$, and this yields:

$$m\,|\alpha_1| \ll 1 \text{ or } |\tilde{\alpha}_1| \ll 1 \tag{2.6}$$

Where we have used the dimensionless coupling $\tilde{\alpha_1}$.
This condition is certainly satisfied for polariton systems because we have that $|\tilde{\alpha}_1| \sim 0.01$ [25]. We

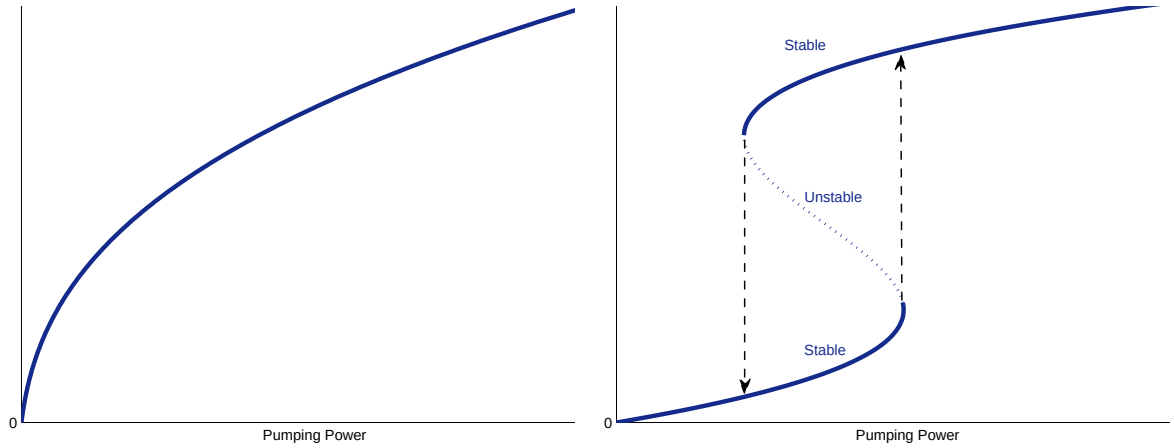

Figure 2.4: The condensate density $|\psi|^2$ as a function of the pumping power I. If $\Delta < \frac{\sqrt{3}}{2}\gamma$ (left) this curve increases smoothly. The increase decreases for higher pumping values, because the system is blueshifted out of resonance. On the other hand, if $\Delta > \frac{\sqrt{3}}{2}\gamma$ (right) a *Kerr bistability* takes place: The blueshift brings the polariton curve in resonance with the laser, resulting in an unstable system. Two stable solution can then be possible, either below or above this state, and a hysteresis curve is the result.

have done the verification by using the self-interaction parameter α_1, as in stable systems we have that $|\alpha_1| > |\alpha_2|$ and we want to have an upper limit.

2.2.4 Steady State Solutions

The time-independent solution of the Gross-Pitaevskii equation can now be determined by substituting a plane-wave *ansatz* for the fluid wavefunctions:

$$\Psi_\pm = \psi_\pm \exp\left\{i\left(\mathbf{k}_p \cdot \mathbf{r} - \omega_p t\right)\right\}, \tag{2.7}$$

where the phase of the fluid is now locked to, but not identical to the phase of the incoming pumping laser.
In doing so, a set of two coupled non-linear equations has to be solved numerically, which in principle can be done. For the purposes of our work however, we are at this stage not interested in the exact steady state solutions. Basically we intend to describe the physics of the first order excitation spectrum and will consider the steady state solutions $\psi_\pm$ as parameters of the system.

Some interesting physics is already contained in this zeroth-order solution. The best way to demonstrate this is to consider a single-spin polariton fluid with Gross-Pitaevskii equation:

$$i\partial_t \Psi = \left(\omega(-i\nabla) - i\frac{\gamma}{2} + g\left|\Psi\right|^2\right)\Psi + F(t) \tag{2.8}$$

Now we can substitute the proposed steady-state ansatz in this equation and its complex conjugate, yielding a system of two equations:

$$\begin{aligned} -F &= \left[\omega(-i\nabla) - \omega_p - i\gamma/2 + g\left|\psi\right|^2\right]\psi \\ -F^* &= \left[\omega(-i\nabla) - \omega_p + i\gamma/2 + g\left|\psi\right|^2\right]\psi^* \end{aligned}$$

Multiplying these two then results in the relation between the laser intensity and the fluid density:

$$|I| = \left[\left(g\left|\psi\right|^2 - \Delta\right)^2 + \frac{\gamma^2}{4}\right]\left|\psi\right|^2, \tag{2.9}$$

where we defined the intensity $|I| = |F|^2$ and the laser detuning $\Delta = \omega_p - \omega(-i\nabla)$.
Two fundamentally different regimes can be distinguished now, depending on the value of Δ. If $\Delta \leq \frac{\sqrt{3}}{2}\gamma$, there is a one-to-one correspondence between the intensity and the fluid density, yielding a smoothly increasing curve.
When $\Delta > \frac{\sqrt{3}}{2}\gamma$ on the other hand, there can be up to three different density solutions for a given intensity. This phenomenon is called a *Kerr bistability*. The reason for this has been explained earlier: due to the increasing interaction energy there is an effective blueshift of the polariton dispersion curve. With positive detuning there can be point where the polariton spectrum is shifted in resonance with the laser beam, after which the spectrum is blueshifted above the laser beam, leaving two possible density solutions.
The plots of the two different pumping regimes are shown in figure 2.4.

Chapter 3

Quasiparticle Excitations

In the previous chapter, we have made a rather severe approximation by neglecting all quantum fluctuations contributing to the physics of the system. A part of this lost information can be recovered by considering fluctuations on the steady state solution. The theory that describes this was first developed by Bogoliubov and it allows to describe the physics of the polariton fluid in terms of quasiparticle excitations on top of the steady state solution. The energy spectrum of these excitations will be derived, giving acces to a wide variety of interesting physics such as the density waves by scattering from a defect and the possibility to give a definition of superfluidity.

3.1 Bogoliubov Theory

The basic principles of Bogoliubov theory will be outlined by considering a polariton fluid consisting of one spin state. In this way the necessary insight can be gathered to obtain the solid basis to generalize the theory eventually for two-spin non-equilibrium fluids. The approach we follow is inspired by [14] and [12].

3.1.1 The Bogoliubov Excitations

In Bogoliubov theory a solution of the single-fluid Gross-Pitaevskii equation (2.8) is postulated, that takes on the form:

$$\Psi(\mathbf{r},t) = \Psi_{SS}(\mathbf{r},t) + \delta\psi(\mathbf{r},t) \equiv e^{i(\mathbf{k}_p\cdot\mathbf{r}-\omega_p t)}\left(\psi + \sum_{\mathbf{k}} u(\mathbf{k})e^{i(\mathbf{k}\cdot\mathbf{r}-\omega(\mathbf{k})t)} + v^*(\mathbf{k})e^{-i(\mathbf{k}\cdot\mathbf{r}-\omega(\mathbf{k})t)}\right) \tag{3.1}$$

So a solution is proposed that consists of the steady-state solution Ψ_{SS}, with a phase locked to the laser beam, and two first-order perturbations $u(\mathbf{k})$ and $v(\mathbf{k})$. The perturbations are expressed in momentum space, with momenta relative to the laser wave vector $\mathbf{k}_p$. In order not to double count momenta and keep a one-to-one correspondence between momenta and coefficients $u(\mathbf{k})$ and $v(\mathbf{k})$, the sum over all momenta $\mathbf{k}$ should be performed in only *half* of the reciprocal space. A good choice of reference frame turns out to direct $\mathbf{k}_p$ along the x-axis and restrict the sum over momenta to $k_x > 0$ with respect to $\mathbf{k}_p$. Therefore we have in the limit of an infinite-sized polariton sample:

$$\frac{1}{V}\sum_{\mathbf{k}} \to \int \frac{d\mathbf{k}}{(2\pi)^2} \equiv \int_0^\infty \frac{dk_x}{2\pi}\int_{-\infty}^{\infty}\frac{dk_y}{2\pi} \equiv \int_0^\infty \frac{kdk}{(2\pi)^2}\int_{-\pi/2}^{\pi/2} d\theta \tag{3.2}$$

In this frame of reference we can interprete the $u(\mathbf{k})$-functions as the coefficients describing waves propagating *upstream* and $v(\mathbf{k})$ as waves propagating *downstream*.

The next step is to plug the Bogoliubov solution in the single-spin Gross-Pitaevskii equation (2.8) and its complex conjugate equation. The zeroth-order terms in $u(\mathbf{k})$ and $v(\mathbf{k})$ satisfy the steady-state solutions we have derived before. The new physics lies in the first-order contributions, which can be split up in two groups: terms oscillating with $e^{-i(\omega t-\mathbf{k}\cdot\mathbf{r})}$ and terms going with $e^{i(\omega t-\mathbf{k}\cdot\mathbf{r})}$, which satisfy:

$$\sum_{\mathbf{k}}\Big(\omega(\mathbf{k})-\mathcal{L}(\mathbf{k})\Big)\begin{pmatrix}u(\mathbf{k})\\v(\mathbf{k})\end{pmatrix}e^{\pm i(\omega t-\mathbf{k}\cdot\mathbf{r})}=0 \tag{3.3}$$

We are interested in the Bogoliubov matrix $\mathcal{L}(\mathbf{k})$, since it contains the physics of the excitations:

$$\mathcal{L}(\mathbf{k})=\begin{pmatrix}-\omega_p+\frac{(\mathbf{k}_p+\mathbf{k})^2}{2m}-i\frac{\gamma}{2}+2g\left|\psi\right|^2 & g\psi^2\\ -g{\psi^*}^2 & \omega_p-\frac{(\mathbf{k}_p-\mathbf{k})^2}{2m}-i\frac{\gamma}{2}-2g\left|\psi\right|^2\end{pmatrix} \tag{3.4}$$

The equation should be satisfied for every value of $\mathbf{k}$ seperately, which only holds if the $\omega(\mathbf{k})$ correspond to the eigenvalues of the Bogoliubov matrix $L(\mathbf{k})$. Thus the eigenvalues of this matrix determine the spectrum of the Bogoliubov excitations $u(\mathbf{k})$ and $v(\mathbf{k})$, which can be obtained by diagonalization:

$$\omega_{\pm}(\mathbf{k})=\mathbf{k}\cdot\mathbf{v}_p-i\frac{\gamma}{2}\pm\sqrt{\varepsilon(\mathbf{k})\left(\varepsilon(\mathbf{k})+2g\left|\psi\right|^2\right)} \tag{3.5}$$

With:

$$\begin{aligned}\varepsilon(\mathbf{k}) &= \frac{k^2}{2m}-\Delta_p\\ \Delta_p &= \omega_p-\left(\frac{k_p^2}{2m}+g\left|\psi\right|^2\right)\end{aligned}$$

This is the spectrum that determines the dispersion relation of the quasiparticle excitations in the fluid. The two different energy solutions correspond to a *particle* and a *antiparticle* branch, in analogy with particle physics. In polariton literature it is more common to note these as the *particle* and the *ghost* branch [24], but these are just different names for the same concepts. Out of the physical ground state, the polariton fluid without density fluctuations, a particle can hop to the particle branch, leaving a hole in the hole branch.

3.1.2 The Quasiparticle Spectrum

The non-equilibrium properties of the fluid allow some peculiar regimes in the dispersion relation of the quasiparticle excitations that are worth investigating. The two parameters that determine the rate of non-equilibrium in the fluid are γ, the decay rate of particles, and Δ_p, the pump detuning. By choosing the right values for these, we should recover the solutions for a fluid in equilibrium, equivalent to a Bose-Einstein condensate. An equilibrium fluid has $\gamma=0$, meaning that there are no particle decays. In addition the oscillation frequency of the fluid is locked to the chemical energy μ instead of the pumping frequency ω_p.
The chemical potential is the energy necessary to add one particle to the fluid, which is in mean-field theory the sum of the mean kinetic and interaction energy per particle in the fluid:

$$\mu=\frac{k_p^2}{2m}+g\left|\psi\right|^2,$$

so that it is readily seen that for an equilibrium fluid holds $\Delta_p=0$.

Again the pump detuning offers us the possibility to explore physical areas that are accessible only in non-equilibrium fluids. To show this we define the dimensionless reduced pump detuning $\Delta'=\Delta_p/(g\left|\psi\right|^2)$. The spectrum can now be classified according to the reduced pump detuning and three different regimes are distinguished, which are plotted on figure 3.1:

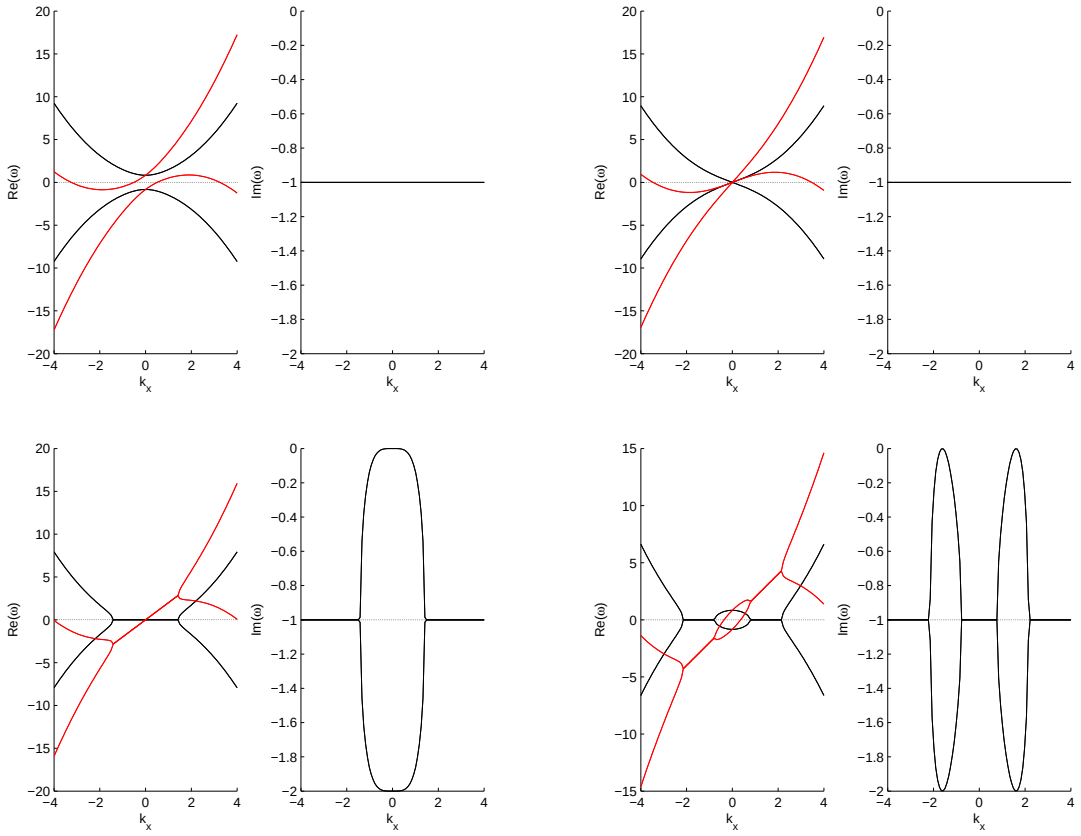

Figure 3.1: The different type spectra of a single-spin polariton fluid with $\gamma' = 1$. The upper two are non-diffusive, left one with negative detuning $\Delta' = -0.3$, the right one with zero detuning $\Delta' = 0$. The lower two are diffusive-like, the left with $\Delta' = 1$ and the right with $\Delta' = 2.3$. The right lines show the tilted spectra for a pumping momentum in reduced units $\mathbf{k}'_p = \mathbf{k}_p / \sqrt{g\,|\psi|^2} = 2$.

- $\Delta' \leq 0$: The only imaginary contribution in the spectrum is the polariton decay rate γ and this comes as a global negative imaginary shift in the polariton spectrum. The spectrum is gapped at $\mathbf{k} = 0$ with an energy splitting of $2\sqrt{|\Delta_p|\left(|\Delta_p| + 2g\,|\psi|^2\right)}$.

- $0 < \Delta' < 2$: In a circular region around $\mathbf{k} = 0$ there is now an additional imaginary energy shift in the spectrum due to the negative argument of the root. The real parts of the two spectral branches stick together in this region. Following the notation of [12] we call these types of spectra *diffusive-like*. Notice that these spectra cannot occur in equilibrium systems, as a finite lifetime is necessary to shift down the imaginary parts of the spectrum sufficiently, in order to maintain a global negative imaginary energy spectrum, assuring a stable system. The Bogoliubov approximation does not hold when $\mathrm{Im}\,(\omega(\mathbf{k})) > 0$ for some wave vector $\mathbf{k}$, as this would correspond to an exponentially growing excitation amplitude.

- $\Delta' > 2$: When Δ' is increased further up to more than twice the interaction energy, a circular region around $\mathbf{k} = 0$ becomes real again. Instead a ring-shaped region for $|\mathbf{k}| > 0$ becomes diffusive-like.

3.2 Excitations in the Binary Polariton Fluid

Now that the principles of Bogoliubov theory have been outlined and the theory has been applied to one-spin polariton fluids, we can generalize the established results for two-spin binary polariton fluids.

3.2.1 Bogoliubov Matrix

For both the spin components seperately we propose a Bogoliubov solution of the form:

$$\Psi_{\pm}(r,t) = e^{i(\mathbf{k}_p\cdot\mathbf{r}-\omega_p t)}\left(\psi_{\pm} + \sum_{\mathbf{k}} u_{\pm}(k)e^{i(\mathbf{k}\cdot\mathbf{r}-\omega(k)t)} + v^*_{\pm}(k)e^{-i(\mathbf{k}\cdot\mathbf{r}-\omega(k)t)}\right) \tag{3.6}$$

The phase of the total wavefunction is thus assumed to be locked again to zeroth order to the phase of the incoming laser beam, as is expected for the steady state solution ψ. Instead of two Bogoliubov coefficients, we now have a total of four.
The spectrum of the system can then be derived by substituting this assumption in the full binary Gross-Pitaevskii equation 2.3, which describes the evolution of the system. Additionally, the solution must also satisfy the complex conjugate of the GP equation. We furthermore assume the amplitudes of the excitations to be small in comparison with the bulk wavefunction ψ, so that we only keep track of terms up to first order in $v(\mathbf{k})$ and $u(\mathbf{k})$. After calculation, we again derive that the Bogoliubov modes have to satisfy:

$$\sum_k \Big(\mathcal{L}(\mathbf{k}) - \omega(\mathbf{k})\Big)\delta\psi(\mathbf{k})e^{\pm i(\omega t-\mathbf{k}\cdot\mathbf{r})} = 0, \tag{3.7}$$

where we defined $\delta\psi(\mathbf{k})$ as the vector containing the Bogoliubov modes arranged as:

$$\delta\psi_{\pm}(\mathbf{k}) = \Big(u_+(\mathbf{k})\ v_+(\mathbf{k})\ u_-(\mathbf{k})\ v_-(\mathbf{k})\Big)^T$$

Couplings between the four different Bogoliubov modes are now present, resulting in a 4×4 Bogoliubov matrix:

$$\mathcal{L}(\mathbf{k}) = \begin{pmatrix} L_{++}(\mathbf{k}) & L_{+-}(\mathbf{k}) \\ L_{-+}(\mathbf{k}) & L_{--}(\mathbf{k}) \end{pmatrix}, \tag{3.8}$$

with:

$$L_{\pm\pm}(\mathbf{k}) = \begin{pmatrix} -\omega_p + \frac{1}{2m}\left(\mathbf{k}_p+\mathbf{k}\right)^2 - i\frac{\gamma}{2} + 2\alpha_1\left|\psi_{\pm}\right|^2 + \alpha_2\left|\psi_{\mp}\right|^2 & \alpha_1\left(\psi_{\pm}\right)^2 \\ -\alpha_1\left(\psi^*_{\pm}\right)^2 & \omega_p - \frac{1}{2m}\left(\mathbf{k}_p-\mathbf{k}\right)^2 - i\frac{\gamma}{2} - 2\alpha_1\left|\psi_{\pm}\right|^2 - \alpha_2\left|\psi_{\mp}\right|^2 \end{pmatrix}$$

$$L_{+-}(\mathbf{k}) = \alpha_2\begin{pmatrix} \psi^*_+\psi_- & \psi_+\psi_- \\ -\psi^*_+\psi^*_- & -\psi_+\psi^*_- \end{pmatrix}$$

$$L_{-+}(\mathbf{k}) = \alpha_2\begin{pmatrix} \psi_+\psi^*_- & \psi_+\psi_- \\ -\psi^*_+\psi^*_- & -\psi^*_+\psi_- \end{pmatrix}$$

The eigenvalues of this matrix describe the spectrum of the quasiparticle excitations in the binary fluid. Notice that in general we will derive four different branches instead of two, that is, if no degeneracy is present in the spectrum.

3.2.2 The Equilibrium Limit

Before starting the diagonalisation process for the entire matrix, it appears useful to study the equilibrium limit of this system, and check whether the results coincides with the known ones for a Bose-Einstein condensate [4]. If we assume an equilibrium system, this is equivalent to considering a system whithout any loss rate, nor any pumping term. As such, we are studying a system with a fixed number of particles.

Basically this means that the general phase of the stationary state is no longer locked by the incident pumping beam, but rather by the chemical potential $\mu_\pm$, fixing the number of particles.
A system which contains two spin fluids that are both populated, has the chemical potentials:

$$\mu_\pm = \alpha_1 |\psi_\pm|^2 + \alpha_2 |\psi_\mp|^2 + \frac{k_0^2}{2m}, \tag{3.9}$$

where k_0, the bulk momentum of the fluid, is introduced instead of the former k_p. Notice that there is a built-in symmetry for $+ \longleftrightarrow -$, as is expected out of physical considerations.
In order to retrieve the spectrum from (3.8), one should substitute $\omega_p \to \mu_\pm$, fixing the number of particles, and $\gamma \to 0$, assuring an infinite lifetime. One derives then a simplified matrices for $L_{\pm\pm}(\mathbf{k})$, revealing an apparent symmetrical structure, whereas the other matrix elements in $\mathcal{L}(\mathbf{k})$ are not affected.

$$L_{\pm\pm}(\mathbf{k}) \to \begin{pmatrix} \frac{k^2}{2m} + \mathbf{k}\cdot\mathbf{v} + \alpha_1 |\psi_\pm|^2 & \alpha_1 (\psi_\pm)^2 \\ -\alpha_1 \left(\psi_\pm^*\right)^2 & -\frac{k^2}{2m} + \frac{1}{m}\mathbf{k}\cdot\mathbf{v} - \alpha_1 |\psi_\pm|^2 \end{pmatrix} \tag{3.10}$$

Because of this internal symmetry, the spectrum of this matrix can be easily calculated by diagonalizing it, and turns out to be the solution of following quadratic equation in $\left(\omega - \frac{1}{m}\mathbf{k}\cdot\mathbf{v}\right)^2$:

$$\left((\omega - \mathbf{k}\cdot\mathbf{v})^2 - \mathcal{E}_+^2\right)\left(\left(\omega - \frac{1}{m}\mathbf{k}\cdot\mathbf{v}\right)^2 - \mathcal{E}_-^2\right) - 4\alpha_2^2\left(\frac{k^2}{2m}\right)^2 |\psi_+|^2 |\psi_-|^2 = 0 \tag{3.11}$$

Where we defined:

$$\mathcal{E}_\pm = \sqrt{\frac{k^2}{2m}\left(\frac{k^2}{2m} + \alpha_1 |\psi_\pm|^2\right)}$$

This time there are two particle and two hole branches in the spectrum of excitations, of which the particle branches are given by:

$$\omega_\pm^p(\mathbf{k}) = \sqrt{\frac{k^2}{2m}} \cdot \sqrt{\frac{k^2}{2m} + \alpha_1\left(|\psi_+|^2 + |\psi_-|^2\right) \pm \sqrt{\alpha_1^2\left(|\psi_+|^2 - |\psi_-|^2\right)^2 + 4\alpha_2^2 |\psi_+|^2 |\psi_-|^2}} + \mathbf{k}\cdot\mathbf{v} \tag{3.12}$$

The hole branches $\omega_\pm^h$ carry a minus sign in front of the root.
To determine the qualitative behaviour of this spectrum, it is interesting to look at the dispersion curve for small k and approximate to the first leading order:

$$\omega_\pm = \sqrt{\frac{k^2}{2m}} \cdot \sqrt{\alpha_1\left(|\psi_+|^2 + |\psi_-|^2\right) \pm \sqrt{\alpha_1^2\left(|\psi_+|^2 - |\psi_-|^2\right)^2 + 4\alpha_2^2 |\psi_+|^2 |\psi_-|^2}} + \mathbf{k}\cdot\mathbf{v} \tag{3.13}$$

For the stable two-component fluid, one readily sees that the spectrum for small $\mathbf{k}$ is linear. Therefore, there is no bandgap present between different branches of the spectrum and it is completely real-valued for every $\mathbf{k}$, provided that $|\alpha_1| > |\alpha_2|$.

3.2.3 General Solutions

The simplifications derived for the stable fluid are expected to complicate when taking into account the finite lifetime of the polaritons and the adaptable phase of the incident laser beam, to which the phase of the stationary state is locked. However, in the appropriate limits, one should always be able to recover the equilibrium results derived in the previous section, and the familiar ones of a single-spin fluid.

It turns out that the complications that arise due to this generalization appear to be able to be absorbed in redefinitions of the variables in (3.11), offering us a recognizable expression after diagonalization of (3.8):

$$\left(\tilde{\omega}^2 - \mathcal{E}_+^2\right)\left(\tilde{\omega}^2 - \mathcal{E}_-^2\right) - 4\alpha_2^2\varepsilon_-\varepsilon_+ |\psi_-|^2 |\psi_+|^2 = 0, \tag{3.14}$$

where we defined the following functions:

$$\begin{aligned}
\tilde{\omega} &= \omega + \frac{i}{2}\gamma - \frac{1}{m}\mathbf{k}\cdot\mathbf{v} \\
\Delta_\pm &= \omega_p - \left(\frac{k_p^2}{2m} + \alpha_1 |\psi_\pm|^2 + \alpha_2 |\psi_\mp|^2\right) \\
\varepsilon_\pm &= \frac{k^2}{2m} - \Delta_\pm \\
\mathcal{E}_\pm &= \sqrt{\varepsilon_\pm\left(\varepsilon_\pm + 2\alpha_1 |\psi_\pm|^2\right)}
\end{aligned}$$

Again we obtain four spectral branches as solutions of the quadratic equation, of which the two positive particle-like solutions are given by:

$$\omega_\pm^p = \frac{1}{m}\mathbf{k}\cdot\mathbf{v} - \frac{i}{2}\gamma + \sqrt{\frac{\mathcal{E}_-^2 + \mathcal{E}_+^2}{2} \pm \sqrt{\frac{\left(\mathcal{E}_-^2 - \mathcal{E}_+^2\right)^2}{4} + 4\alpha_2^2\varepsilon_-\varepsilon_+ |\psi_-|^2 |\psi_+|^2}}, \tag{3.15}$$

with also two ghost branches, obtained by flipping the sign of the root.

It is worthwile checking whether these expressions indeed converge to the already known results in the corresponding limits before continuing:

- In the limit of the decoupled fluid, there is no interaction between the two spin components in the fluid, and therefore the same results as a one component fluid should be found. In order to do so, we should take the limit of $\alpha_2 \to 0$ and $|\psi_+| = |\psi_-|$, and it is easily verified that we retrieve expression (3.5).
- For a stable fluid with infinite lifetime polaritons, we can verify that this expression converges in the limits $\gamma \to 0$ and $\omega_p \to \mu$, with μ described by (3.9). It is easily verfied that in this limit dispersion relation (3.12) holds, as this limit corresponds to $\Delta_\pm \to 0$.

With (3.15) we eventually derived a continuum generalization between two particular cases; the two-component infinite-lifetime polariton fluid, which can as well be considered as a two-component BEC, and the one-component finite-lifetime polariton fluid. As such, it is interesting to determine the intermediate behaviour of this system and discuss the continuous transition between these two limiting cases.

Chapter 4

The Non-equilibrium Spectrum of the Binary Fluid

The dispersion relation for the quasiparticle excitations turns out to take different qualitative behaviours, depending on regions in **k**-space where the spectrum becomes diffusive due to negative arguments of the roots. We have had a glimpse on diffusive-like properties of single-spin fluids, where we derived that the type of spectrum is determined by the ratio of the pump detuning Δ_p to the interaction energy $g\left|\psi\right|^2$. In this chapter we will therefore first of all determine the set of relevant parameters that influence the properties of the binary spectrum, so that we can eventually classify the types of spectra according to specific values of these parameters. The ultimate goal of this chapter is to present a generalized classification of spectra for a two-spin fluid and this forms one of the main parts of the research done for this work.

4.1 Independent Dimensionless Parameters

In order to collect a set of fundamental dimensionless parameters, it is of course useful to begin from a dimensionless equation, which can be done by a rescaling of $\omega \to \omega' = \omega/\left(\alpha_1 \left|\psi_+\right| \left|\psi_-\right|\right)$. In doing so, one fixes the scaling freedom and finds a dimensionless expression for the excitation spectrum, containing all necessary information to start the classification. Notice that we used a rescaling that is also invariant under $+ \longleftrightarrow -$, in order to preserve the global symmetry present in the system.
One can define three independent dimensionless parameters:

$$\begin{aligned} \Gamma &= \frac{1}{\alpha_1 \left|\psi_+\right| \left|\psi_-\right|}\left(\omega_p - \frac{k_p^2}{2m}\right) \\ c &= \frac{\left|\psi_-\right|}{\left|\psi_+\right|} \\ \alpha &= \frac{\alpha_2}{\alpha_1} \end{aligned} \tag{4.1}$$

And they allow us to write down a dimensionless expression for the excitation spectrum after the rescaling:

$$\begin{aligned} \omega'_{\pm} &= \frac{1}{\alpha_1 \left|\psi_+\right| \left|\psi_-\right|}\left(\omega - \frac{1}{m}\mathbf{k}\cdot\mathbf{v} + \frac{i}{2}\gamma\right) \\ &\pm \sqrt{\frac{1}{2}\left(\varepsilon'_+\left(\varepsilon'_+ + \frac{2}{c}\right) + \varepsilon'_-\left(\varepsilon'_- + 2c\right)\right) \pm \sqrt{\frac{1}{4}\left(\varepsilon'_+\left(\varepsilon'_+ + \frac{2}{c}\right) - \varepsilon'_-\left(\varepsilon'_- + 2c\right)\right)^2 + 4\alpha^2\varepsilon'_+\varepsilon'_-}} \end{aligned}$$

Where we defined the rescaled functions:

$$\begin{aligned} \varepsilon'_{\pm} &= z(k) - \Delta'_{\pm} \\ \Delta'_{+} &= \Gamma - \left(\frac{1}{c} + \alpha c\right) \\ \Delta'_{-} &= \Gamma - \left(\frac{\alpha}{c} + c\right) \end{aligned} \tag{4.2}$$

And:

$$z(k) = \frac{1}{\alpha_1 \left|\psi_+\right| \left|\psi_-\right|} \frac{k^2}{2m}$$

The parameters Γ, c and α determine the qualitative behaviour of the spectrum, as they show up in the square roots in the dispersion and determine whether there are diffusive-like regions in $\mathbf{k}$-space.
Notice that there is a conceptual difference between Γ and c on one side, and α on the other. Both Γ and c are parameters directly related to the incoming laser beam, and therefore in principle tunable in an experiment, whereas α is intrinsic to the physics of the polariton system itself. However, one should take care assigning values to α, since they depend on a variety of different processes that can be present. In the following we will assume that only scattering takes places in the system, but this is only an approximation. Remember that the excitons can form bound states of opposite spin, the biexcitons, resulting in a net loss rate of excitons. This effect will be neglected by assuming that the biexciton energy is far above twice the laser frequency, and thus not of importance. If only elastic scattering takes place, the system is energy conserving with respect to interactions and therefore the interaction parameters $\alpha_{1,2}$ need to be real-valued.
One approach could be to determine values for α out of earlier experiments or more detailed theories, which can then be plugged into the equations, as to get a model with only Γ and c dependence. However, on the other hand one might also determine α by making different models depending Γ and c and compare with an experiment where ranges of Γ and c are scanned.
Either way, for the time being we keep α as a free, real-valued parameter and delay the assignment of specific values to a later section.

4.2 Diffusive Regions

In what follows, we will only care about the analytical behaviour of the two square roots in the system, since only they determine the properties of the spectral types in the system, and not the parameters γ and $\mathbf{v}$.
As there are two roots present in the expression describing the dispersion relation, it is obvious that two different imaginary contributions might show up independently in the spectrum. We will deal with both of them sequentially.

4.2.1 Inner Square Root

The imaginary parts showing up in the inner root contribute to both ω_+ and ω_- in the same way, but will get an opposite sign. Regions in k-space with a diffusive spectrum only exist when the following function becomes negative on its domain:

$$\frac{1}{4}\left(\varepsilon'_{+}\left(\varepsilon'_{+} + \frac{2}{c}\right) - \varepsilon'_{-}\left(\varepsilon'_{-} + 2c\right)\right)^2 + 4\varepsilon'_{+}\varepsilon'_{-}\alpha^2 \tag{4.3}$$

After working out this expression and rearranging the terms, we derive that it can be written as a quadratic equation:

$$C_2 z(k)^2 + C_1 z(k) + C_0 \tag{4.4}$$

The coefficients of the polynomial can be written down in function of the dimensionless parameters $\Delta'_{\pm}$:

$$\begin{aligned} C_2 &= \left(\frac{1}{c} - c + \Delta'_- - \Delta'_+\right)^2 + 4\alpha^2 \\ C_1 &= \left(\frac{1}{c} - c + \Delta'_- - \Delta'_+\right)\left(\Delta'^2_+ - \Delta'^2_- + 2\left(c\Delta'_- - \frac{\Delta'_+}{c}\right)\right) - 4\alpha^2\left(\Delta'_+ + \Delta'_-\right) \\ C_0 &= \frac{1}{4}\left(\Delta'^2_+ - \Delta'^2_- + 2\left(c\Delta'_- - \frac{\Delta'_+}{c}\right)\right)^2 + 4\alpha^2\Delta'_-\Delta'_+ \end{aligned}$$

Since $z(k)$ is a positive function in k and $C_2 > 0$, expression (4.4) can only become negative if there is at least one root present in the positive domain. The parametrical region where a diffusive spectrum occurs is therefore bounded by the following curves:

$$\begin{cases} C_1^2 = 4C_0C_2 \\ C_0 = 0 \end{cases} \tag{4.5}$$

After some algebraic manipulations, the former can be expressed as:

$$\left(\Delta'_- - \Delta'_+\right)^2 + 2\left(\frac{1}{c} - c\right)\left(\Delta'_- - \Delta'_+\right) - 4\left(1-\alpha^2\right) = 0,$$

which is a quadratic equation in the variable $\Delta'_- - \Delta'_+$.

4.2.2 Outer Square Root

Also in the the outer root complex contributions might show up, resulting in diffusive regions in the spectrum that are similar to the ones demonstrated for single-polariton fluids. This will happen whenever the following function becomes negative on its domain:

$$\frac{1}{2}\left(\varepsilon'_+\left(\varepsilon'_+ + \frac{2}{c}\right) + \varepsilon'_-\left(\varepsilon'_- + 2c\right)\right) \pm \sqrt{\frac{1}{4}\left(\varepsilon'_+\left(\varepsilon'_+ + \frac{2}{c}\right) - \varepsilon'_-\left(\varepsilon'_- + 2c\right)\right)^2 + 4\varepsilon'_+\varepsilon'_-\alpha^2} < 0$$

Whereas the imaginary contributions coming from the inner root were the same, but opposite in sign for both ω_- and ω_+, this symmetry is clearly gone in this expression. There might be regions where ω_+ is real, while ω_- is diffusive, and in principle both should be considered separately. However, without caring to much about the consequences for now, we can find the boundaries of parametrical regions where qualitative changes appear by squaring this expression to get rid of the inner root.
After rearranging a little, we derive that this relation then can be written as:

$$\left(\varepsilon'_+\varepsilon'_-\right)\left[\varepsilon'_+\varepsilon'_- + 2\left(\frac{\varepsilon'_-}{c} + c\varepsilon'_+\right) + 4\left(1-\alpha^2\right)\right] = 0 \tag{4.6}$$

Due to this factorization, the expression equals zero when:

- $\varepsilon'_{\pm} = z(k) - \Delta'_{\pm} = 0$: This can only occur when the rescaled pumping detuning $\Delta'_{\pm} > 0$ and therefore the two surfaces $\Delta'_{\pm} = 0$ determine a boundary where a qualitative change occur.
- $\varepsilon'_+\varepsilon'_- + 2\left(\varepsilon'_- + c\varepsilon'_+\right) + 4c\left(1-\alpha^2\right) = 0$: After rearranging the terms, we learn that this expression can be written as a quadratic equation as well:

  $$z(k)^2 - \left(\Delta'_+ + \Delta'_- - 2\left(\frac{1}{c} + c\right)\right)z(k) + \Delta'_+\Delta'_- - 2\left(\frac{\Delta'_-}{c} + c\Delta'_+\right) + 4\left(1-\alpha^2\right) = 0 \tag{4.7}$$

  It is easily checked that this equation always has solutions, the question is when they are positive and affect the spectrum. As can be easily deduced out of algebraic relations, the boundary in parameter space is given by:

  $$\Delta'_+\Delta'_- - 2\left(\frac{1}{c}\Delta'_- + c\Delta'_+\right) + 4\left(1-\alpha^2\right) = 0 \tag{4.8}$$

4.2.3 Boundary Surfaces in Parameter Space

Since the variables $\Delta'_{\pm}$ are not really well-defined, in the sense that they are not independent from each other, it is more useful to transform everything back to the original dimensionless variables Γ, c and α, using relations (4.2). Eventually this will allow us to describe boundaries in this parameter space, with different qualitative types of spectra.
After doing the transformation, we derive a number of two-dimensional surfaces in the three-dimensional parameter space, separating volumes with different qualitative behaviour.

- The region where the inner square root is zero in the positive domain, is bounded by the surfaces:

$$\begin{aligned} \left((2-\alpha)^2-1\right)\left(\frac{1}{c}-c\right)^2 &= 4\left(1-\alpha^2\right) \\ \left(\Gamma\left(\frac{1}{c}-c\right)(\alpha-2)+\frac{1}{2}\left(\alpha^2-3\right)\left(c^2-\frac{1}{c^2}\right)\right)^2 &= -4\alpha^2\left(\Gamma-\left(\frac{\alpha}{c}+c\right)\right)\left(\Gamma-\left(\frac{1}{c}+\alpha c\right)\right) \end{aligned} \tag{4.9}$$

  Within these volumes in parameter space the second root is imaginary in a certain region in **k**-space. For these momenta the real parts of ω_+ and ω_- are the same, resulting in a 'sticking' of the branches of the spectrum. The imaginary contributions however are opposite in sign.

- All the surfaces where a qualitative change occur due to a sign flip under the outer root, are given by:

$$\begin{aligned} \Gamma &= \left(\frac{1}{c}+\alpha c\right) \\ \Gamma &= \left(\frac{\alpha}{c}+c\right) \\ 4\alpha^2 &= \left(\Gamma-\frac{\alpha}{c}-3c\right)\left(\Gamma-\frac{3}{c}-\alpha c\right) \end{aligned} \tag{4.10}$$

  By crossing one of these surfaces, there will be a flip in sign under the root for either ω_+ or for ω_-, but not both at the same time in general. Physically this means the appearance of a region in **k**-space where the real part of the spectrum is zero, and only an imaginary contribution is present, so that the spectrum is completely diffusive for these momenta.

4.3 The Different Types of Spectra

Keeping in mind all the reasonings presented in the previous section, a total of six qualitatively different spectral branches can occur, depending on the three dimensionless parameters Γ, c and α.
Due to diffusive regions showing up as a consequence of the outer square root, three different types of spectral branches are possible, these are the same ones that have been discussed in section 3.1.2 and that are shown in figure 3.1. Because we have now four branches, two of these three spectral branches can appear in the spectrum. The three spectra that have at least one gapped mode are shown in figure 4.1 and the three that only have diffusive modes are shown in 4.2.
If there are additional diffusive regions caused by the inner square root, two spectral branches stick together in a certain region in momentum space. The sticking is a result of *avoided crossing* and three other spectral types can be distinguished. These spectra are plotted in figure 4.3.

4.4 Phase Diagram

As mentioned before, there is a conceptual difference between the dimensionless parameter α on one side and Γ and c on the other. It is therefore convenient to assign a certain value to α, as this parameter is in

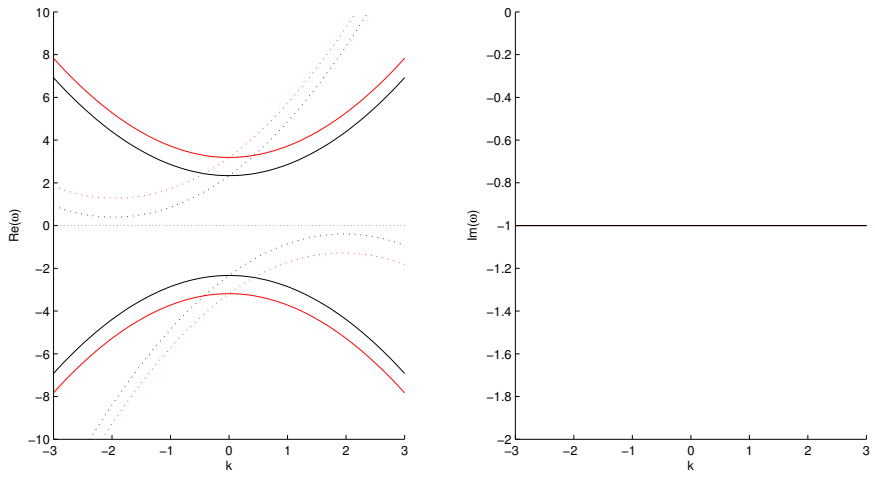

(a) $c = 0.8\ \Gamma = -1$

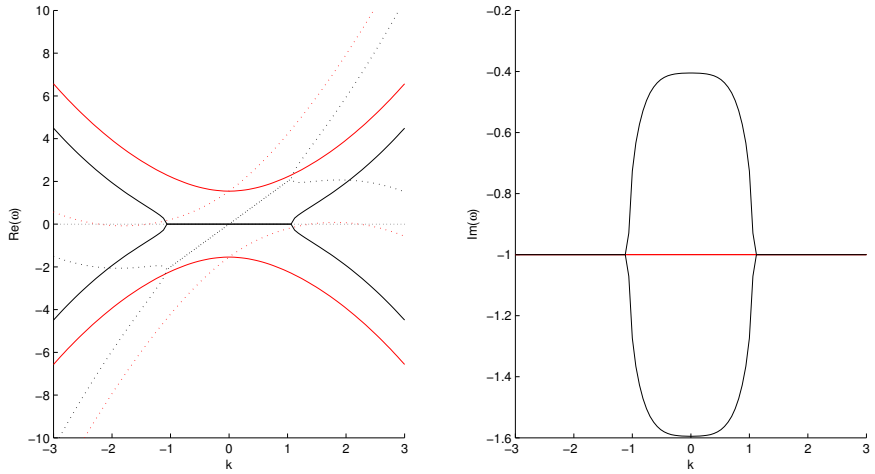

(b) $c = 0.6\ \Gamma = 1$

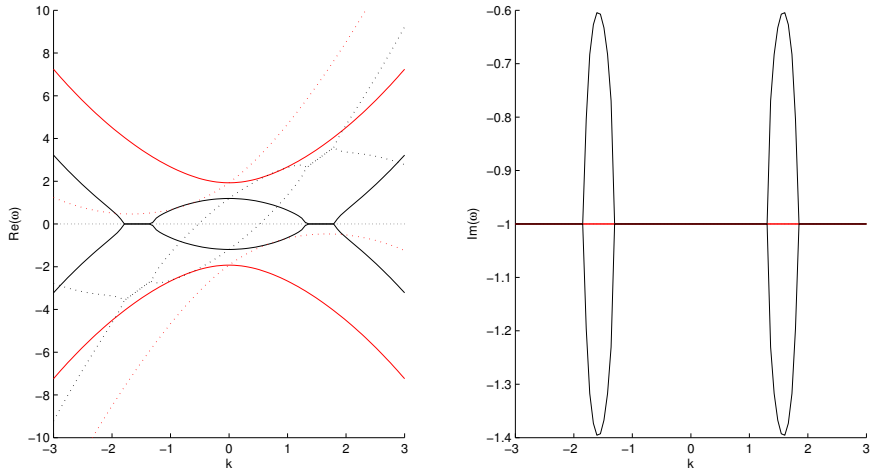

(c) $c = 0.4\ \Gamma = 1.8$

Figure 4.1: The real (left) and imaginary (right) parts of the three spectra with a gapped mode. The interaction strength is $\alpha = -0.1$. The red (black) line are the ω_+ (ω_-) branches. The dotted lines are the tilted spectrum for $k_p = 2\sqrt{\alpha_1 |\psi_+| |\psi_-|}$.

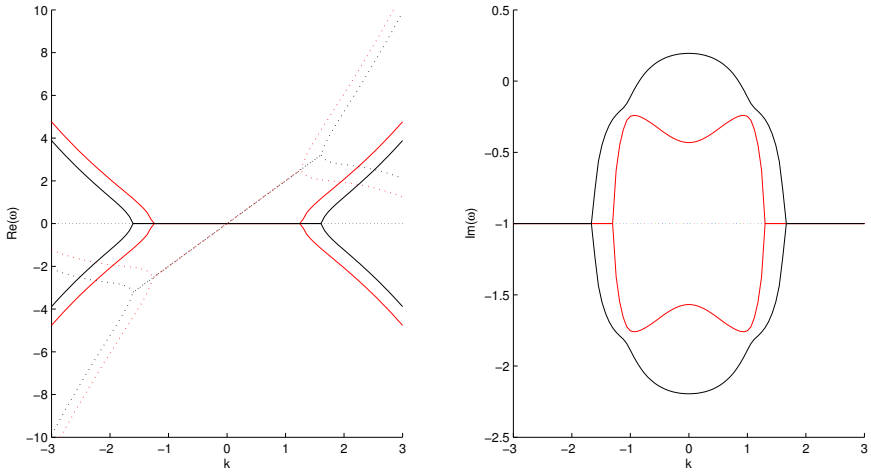

(a) $c = 0.8$ $\Gamma = 2$

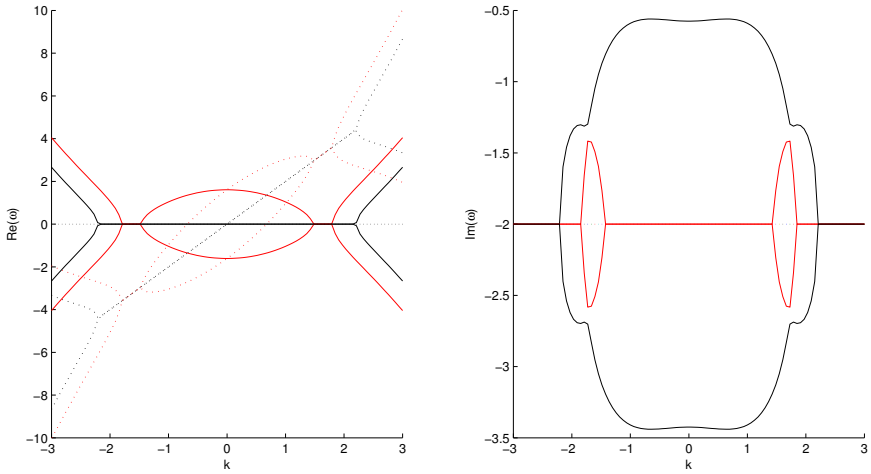

(b) $c = 0.7$ $\Gamma = 3$

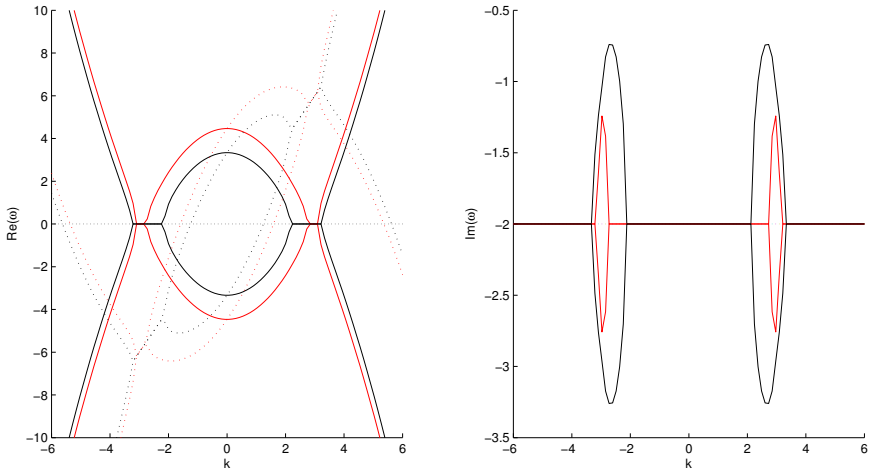

(c) $c = 0.8$ $\Gamma = 6$

Figure 4.2: The real (left) and imaginary (right) parts of the three spectra with a no gapped mode and no sticking. The interaction strength is $\alpha = -0.1$. Same color code as above.

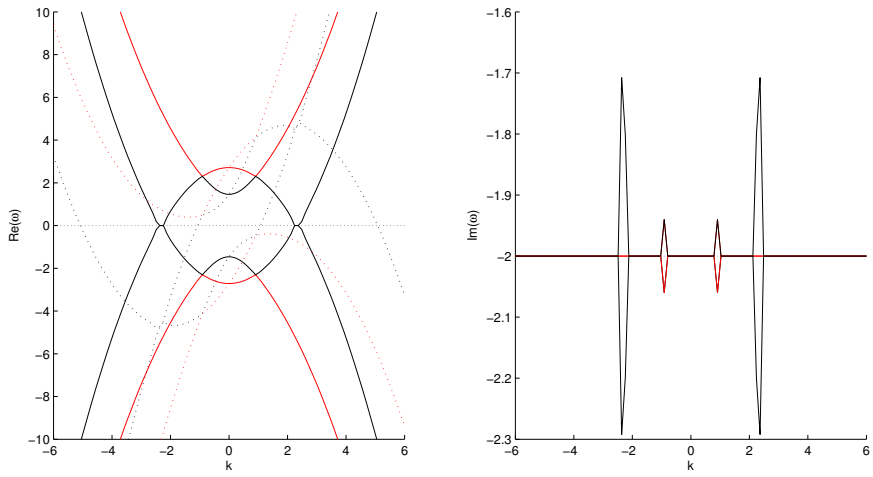

(a) $c = 0.3$ $\Gamma = 3$

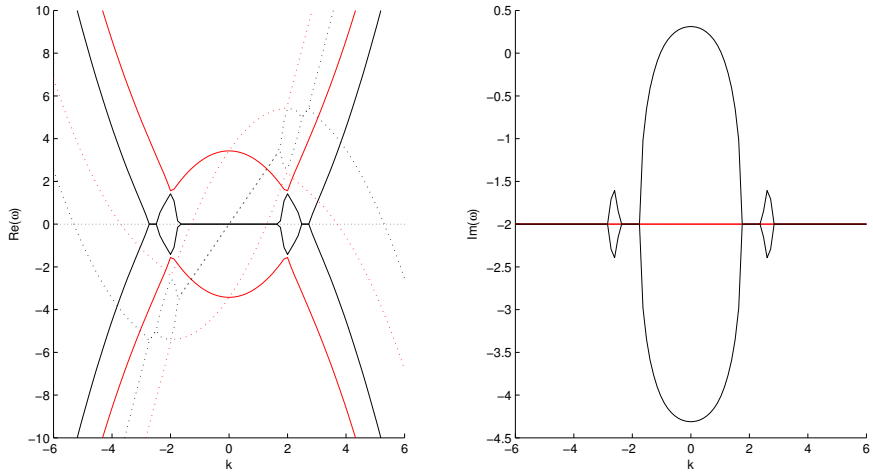

(b) $c = 0.4$ $\Gamma = 4$

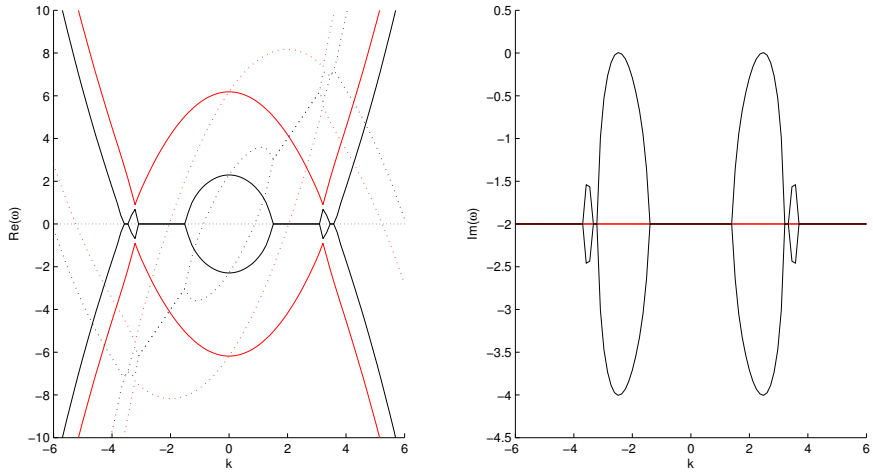

(c) $c = 0.5$ $\Gamma = 7$

Figure 4.3: The real (left) and imaginary (right) parts of the three spectra with sticking of the ω_+ and ω_- branches. The interaction strength is $\alpha = -0.1$. There is an additional sticking that is caused by the inner square root being imaginary. The diffusive contribution of this is too small to see on the scale of the plot for the two lower figures, but they are situated inbetween the two bumps of the outer root. Same color code as above.

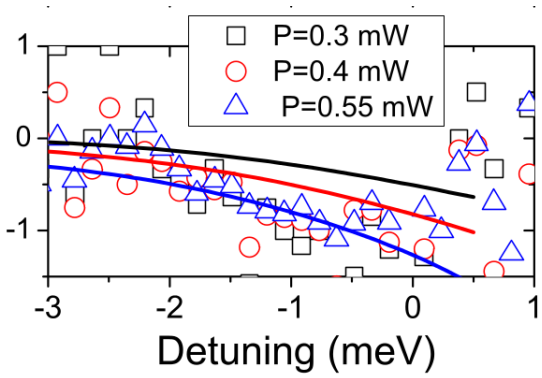

Figure 4.4: The measurements of $\alpha = \alpha_1/\alpha_2$ as a function of the pump detuning for different pumping powers P. [13]

principle determined by the physics of the system, and make a slice of the three-dimensional parameter space for constant α. In this way, we can represent the qualitatively different spectra in a two-dimensional phase diagram for the experimental adaptable parameters Γ and c, showing areas bounded by the curves of section 4.2.3.

Recently experimental measurements have been done [13] to verify the actual value of the ratio of the interaction constants α, of which the results are shown in figure 4.4. It is generally accepted now to approximate the parameter under normal conditions to $\alpha = -0.1$, as is the average outcome of experiments.

We have provided a detailed phase diagram in figure 4.5 that visualises the different regions in parameter space in which the earlier discussed spectral excitation types occur. On this figure different regions that are bounded by a number of parametrical curves in (Γ, c)-space are shown. Each region corresponds to a certain type of excitation spectrum, as is indicated by the schematic of the spectral type. ω_+ and ω_- change indepently by crossing a region, which was also pointed out during the derivation of the curves. The two red lines determine the region where the inner root becomes imaginary, resulting in the sticking of the two dispersions $\omega_\pm$ in a ring-shaped region in $\mathbf{k}$-space.

In addition, the minimum width $\gamma' = \gamma/(\alpha_1 |\psi_+| |\psi|)$ that is needed to have a physical spectrum is drawn. This has been established by determining the minimal imaginary shift that is necessary to assure that all imaginary parts in $\mathbf{k}$-space are negative. This is necessary in order to have excitations that are damped in time, and *not* exponentially increasing, because this is not physical.

The equilibrium point is the point where the two curves $\Delta_\pm = 0$ cross. In this point we have that the laser frequency corresponds to the chemical potentials of both the up-spin and the down-spin fluid. The point where a number of red and blue lines appear to join, is actually deceiving, since they do not cross in reality. It can be show analytically that the mismatch is only of order $\alpha^2 \sim 0.01$, making it impossible to notice on the scale of this plot.

In figure 4.6 a number of additional phase diagrams are shown for α in the range from -1 to 1. In general all contour lines that determine the diffusive regions move to higher Γ for higher α. If $\alpha \geq 1$ it can be shown analytically that there are no solutions for the red contours, so that no sticking of the spectral branches can take place.

On the phase diagram for $\alpha = 0$ we can recover the results for a single-spin polariton fluid. The physics of this system is contained in the subspace obtained by fixing $c = 1$. On this line the different spectral types discussed in 3.1 can be found in function of Γ.

We have provided a generalization of two different limiting cases: the single-spin polariton fluid and the two-spin BEC. By considering a set of three independent dimensionless parameters, we elaborated a

mechanism that allows us to continuously move through parameter space from one limiting case to the other. Thus we have presented a phase diagram in which these two limits can be identified as different subspaces in a higher-dimensional parameter space that connects these formerly separated regions continously.

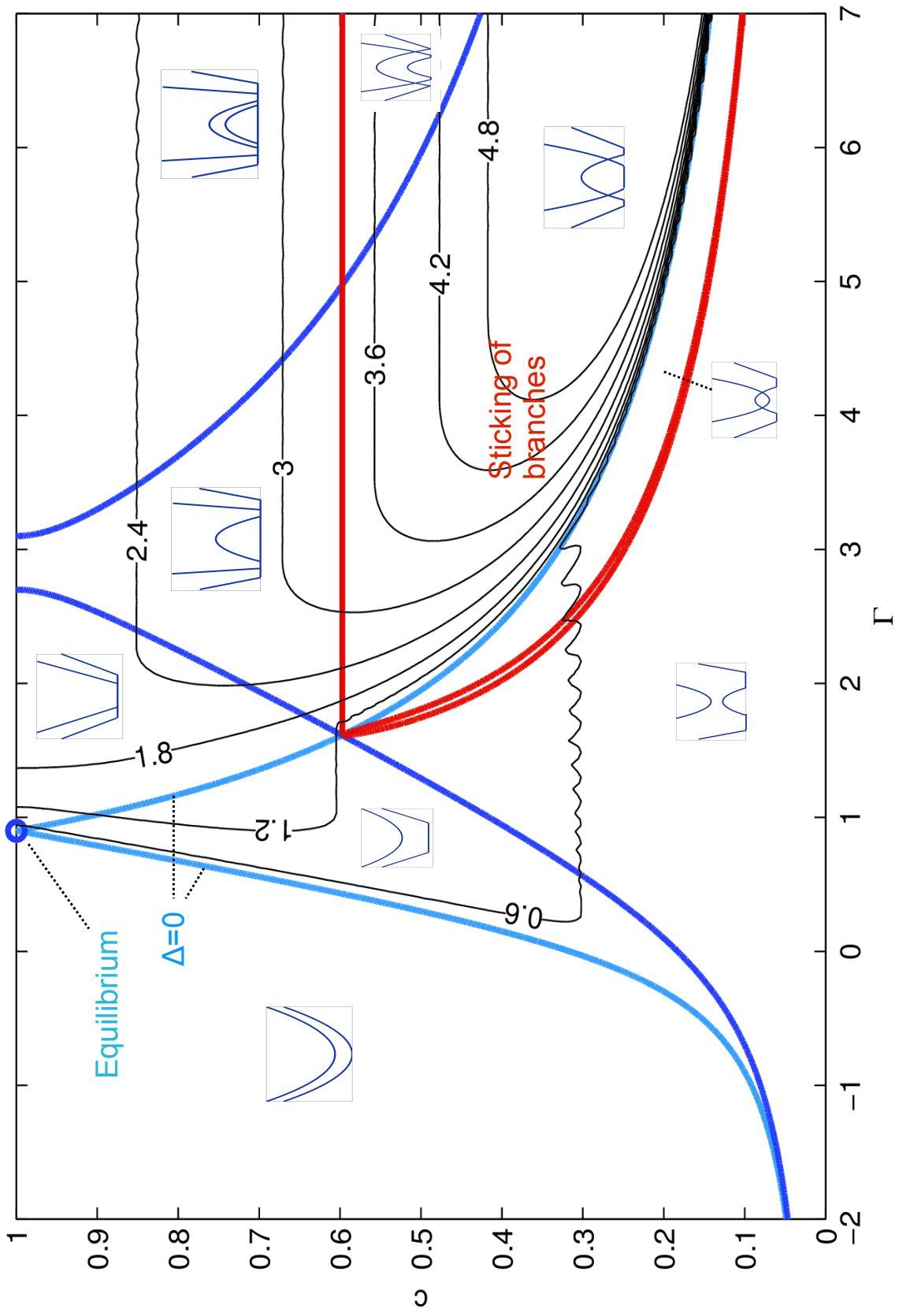

Figure 4.5: The full phase diagram in function of Γ and c, for $\alpha = -0.1$. Blue lines are zeros from the outer square root and red lines from the inner. A schematic image of the spectral type is given in each area. The black lines represent the reduced minimum width, $\gamma / (\alpha_1 |\psi_+| |\psi_-|)$ that is needed to have a stable system, the oscillations are a numerical error.

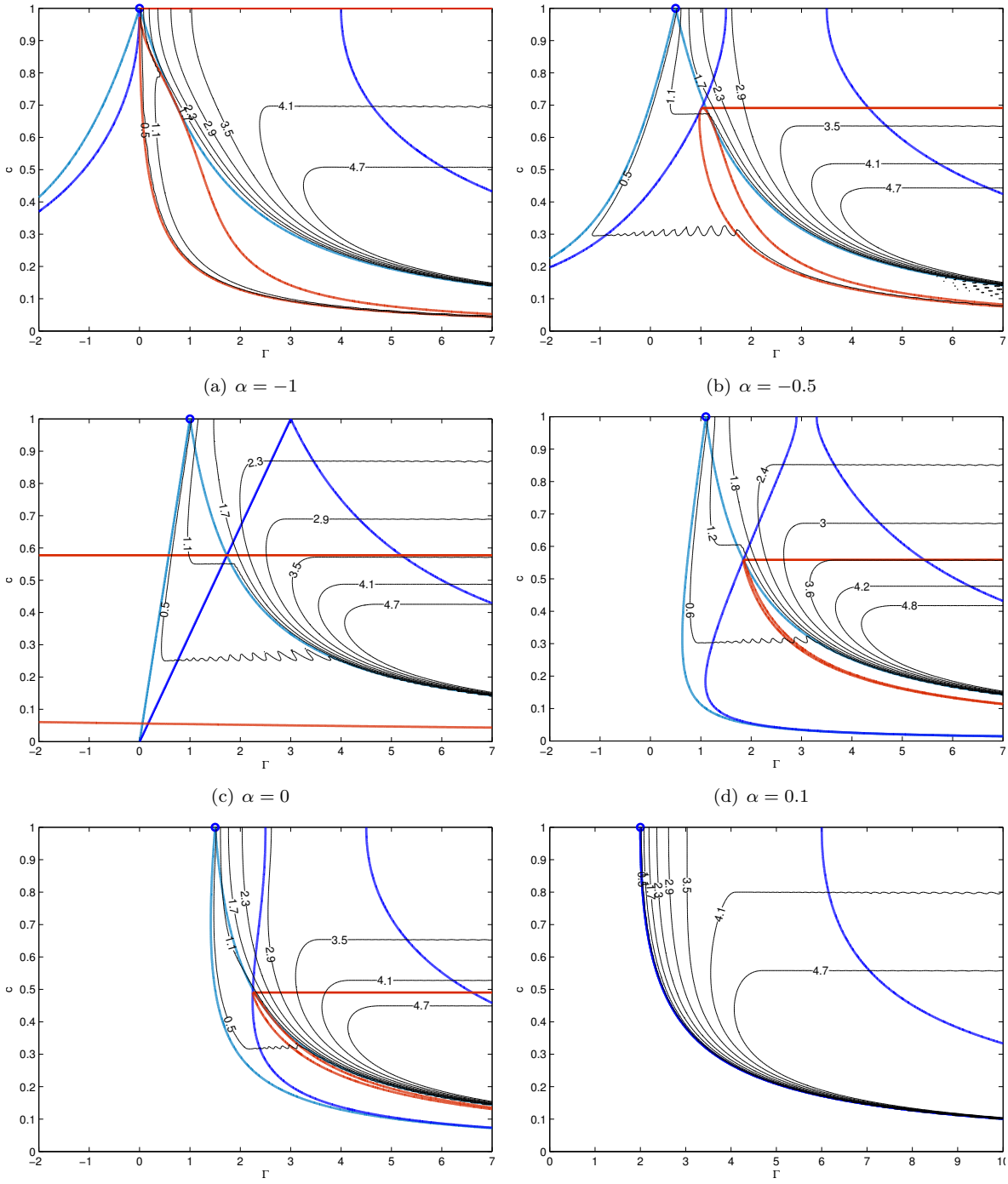

(a) $\alpha = -1$ (b) $\alpha = -0.5$

(c) $\alpha = 0$ (d) $\alpha = 0.1$

(e) $\alpha = 0.5$ (f) $\alpha = 1$

Figure 4.6: Different phase diagrams for α in the range -1 to 1. For increasing α the lines are pushed towards higher Γ-values.It can be shown analytically that there is no additional sticking of the branches when $\alpha \geq 1$, hence the red lines disappear.

Chapter 5

Scattering from a Defect

We have seen that a bulk velocity of the fluid, caused by the pumping wave vector k_p results in a global tilt of the excitation spectrum. When a defect is placed in the polariton fluid, this will affect the density profile of the fluid. These effects will be studied in the following chapter. First of all the defect has to be included in the Gross-Pitaevskii equation to start the necessary calculations. From there on we can study the response of the flowing fluid to a static defect and look at the scattered waves. To conclude this work, the drag force exerted by the defect on the fluid will be calculated and discussed in the context of the previous results.

5.1 The Condensate's Spatial Density Profile

Making use of perturbation theory the response of the condensate density profile can be calculated. For this we will extend the Gross-Pitaevskii equation with a defect potential and study its response to a small perturbation.

5.1.1 The Defect Response

In general when the fluid is affected by a certain potential an extra term has to be included in the Gross-Pitaevskii equation:

$$i\partial_t \Psi_\pm(\mathbf{r},t) = \left(\omega(-i\nabla) - i\frac{\gamma}{2} + \alpha_1 \left|\Psi_\pm(\mathbf{r},t)\right|^2 + \alpha_2 \left|\Psi_\mp(\mathbf{r},t)\right|^2 + V_\pm(\mathbf{r},t)\right)\Psi_\pm(\mathbf{r},t) + F_\pm(\mathbf{r},t), \tag{5.1}$$

where the time- and spatial dependence of the fluid wave function is explicitly written down.
The defect potential we are interested in, is static in time and we assume a *point-like* defect:

$$V_\pm(\mathbf{r}) = g_\pm \delta(\mathbf{r}) \tag{5.2}$$

So the defect is represented by a Dirac-delta function with a coupling strength $g_\pm$, that can be different for the two spin components. Defect potentials are realized in laboratories by placing an additional small laser beam on the polariton sample, which creates exctitons that are not in coherence with the bulk fluid, in a small region in the plane. This can be approximated by a point-like defect if the size of the defect is much smaller than the typical length scale of spatial density fluctuations.

We are now interested in studying the response of the fluid when flowing along such a point-like defect. In order to do so, we assume the defect-fluid interaction to be small and take only into account first order corrections to the steady state. The first order density fluctuations are constructed from the

well-known Bogoliubov modes $u(\mathbf{k})$ and $v(\mathbf{k})$, as defined in (3.6). The defect potential can be expanded in $\mathbf{k}$-space:

$$V_{\pm}(\mathbf{r}) = g_{\pm} \sum_{\mathbf{k}} \left(e^{-i\mathbf{k}\cdot\mathbf{r}} + e^{i\mathbf{k}\cdot\mathbf{r}} \right)$$

Now we substitute the Bogoliubov *ansatz* and the defect potential in the Gross-Pitaevskii equation. To derive the response equation, we only keep track of terms of first order in either $u(\mathbf{k})$, $v(\mathbf{k})$ or $g_{\pm}$.
In this way a new system of linear equations is derived by gathering terms oscillating with the same phase:

$$\sum_{k} \Big(\mathcal{L}(\mathbf{k}) - \omega(\mathbf{k}) \Big) \delta\psi(\mathbf{k}) e^{\pm i(\omega t - \mathbf{k}\cdot\mathbf{r})} = - \sum_{\mathbf{k}} \mathbf{V} e^{\mp i\mathbf{k}\cdot\mathbf{r}}, \tag{5.3}$$

with:

$$\mathbf{V} = \begin{pmatrix} g_+\Psi_+ & -g_+\Psi_+^* & g_-\Psi_- & -g_-\Psi_-^* \end{pmatrix}^T.$$

Since the defect potential is time-independent, we are looking for a static response that is energy-conserving. Therefore we are looking for solutions with $\omega(\mathbf{k}) = 0$. Now the response of the Bogoliubov modes can be related to the defect, so that for every wave vector $\mathbf{k}$ has to hold:

$$\delta\psi(\mathbf{k}) = -\mathcal{L}^{-1}(\mathbf{k})\mathbf{V} \tag{5.4}$$

Out of this equation the momentum distributions of the Bogoliubov modes $u(\mathbf{k})$ and $v(\mathbf{k})$ can be calculated and transformed again to position space by substitution in (3.6). As such the first-order response of the condensate density by scattering from a defect can be calculated. Notice that the defect potential comes in as a driving term in the Bogoliubov equation.

5.1.2 Single-spin Condensates

Since the calculation of the Bogoliubov modes involves the inversion of the Bogoliubov matrix, the complexity of finding exact analytical solutions increases rapidly with the dimensionality of the matrix. For a binary fluid the response is determined by a 4×4-matrix, of which the inverse in general leads to dreadfully long expressions that are far from clarifying. We will therefore start by studying the response of a single-spin fluid, for which analytical solutions can be found that are easy to grasp.
For a single-spin fluid the response equation simplifies to:

$$\begin{pmatrix} u(\mathbf{k}) \\ v(\mathbf{k}) \end{pmatrix} = \begin{pmatrix} -\omega_p + \frac{(\mathbf{k}_p+\mathbf{k})^2}{2m} - i\frac{\gamma}{2} + 2g|\psi|^2 & g\psi^2 \\ -g\psi^{*2} & \omega_p - \frac{(\mathbf{k}_p-\mathbf{k})^2}{2m} - i\frac{\gamma}{2} - 2g|\psi|^2 \end{pmatrix}^{-1} \begin{pmatrix} -g_V\psi \\ g_V\psi^* \end{pmatrix} \tag{5.5}$$

And after evaluation we derive the expressions for the Bogoliubov modes in momentum space:

$$\begin{aligned} u(\mathbf{k}) &= \frac{g_V\psi\Big(\varepsilon(k) - \mathbf{k}\cdot\mathbf{v} + i\gamma/2\Big)}{\varepsilon(k)\Big(\varepsilon(k) + 2g|\psi|^2\Big) - \Big(\mathbf{k}\cdot\mathbf{v} - i\gamma/2\Big)^2} = g_V\psi\,\frac{\varepsilon(k) - \mathbf{k}\cdot\mathbf{v} + i\gamma/2}{\omega_+(\mathbf{k})\,\omega_-(\mathbf{k})} \\ v(\mathbf{k}) &= \frac{g_V\psi^*\Big(\varepsilon(k) + \mathbf{k}\cdot\mathbf{v} - i\gamma/2\Big)}{\varepsilon(k)\Big(\varepsilon(k) + 2g|\psi|^2\Big) - \Big(\mathbf{k}\cdot\mathbf{v} - i\gamma/2\Big)^2} = g_V\psi^*\,\frac{\varepsilon(k) + \mathbf{k}\cdot\mathbf{v} - i\gamma/2}{\omega_+(\mathbf{k})\,\omega_-(\mathbf{k})} \end{aligned}$$

Remember that we defined these functions only for the interval $k_x > 0$, when k_x is lined parallel to the pumping vector k_p. Therefore when $\gamma \to 0$ these functions are strongly peaked around the curve $\omega_-(\mathbf{k}) = 0$ because this corresponds to singularities *inside* the defined domain of the Bogoliubov modes. With a non-zero decay rate γ these functions are smoothened and analytical. Also the value of the pumping detuning Δ_p will have a profound influence on the excitation momentum distribution.

To find the spatial density distribution of the fluid, the Bogoliubov excitations have to be substituted in the proposed Bogoliubov solution (3.1):

$$\begin{aligned}\Psi(\mathbf{r},t) &= e^{i(\mathbf{k}_p\cdot\mathbf{r}-\omega_p t)}\left(\psi+\sum_{\mathbf{k},k_x>0}\left[u(\mathbf{k})e^{-i\mathbf{k}\cdot\mathbf{r}}+v^*(\mathbf{k})e^{i\mathbf{k}\cdot\mathbf{r}}\right]\right)\\ &\equiv e^{i(\mathbf{k}_p\cdot\mathbf{r}-\omega_p t)}\left(\psi+\sum_{\mathbf{k}}\delta\psi(\mathbf{k})e^{-i\mathbf{k}\cdot\mathbf{r}}\right),\end{aligned}$$

where we defined the extended momentum distribution over the full $\mathbf{k}$-space:

$$\delta\psi(\mathbf{k}) = u(\mathbf{k})\,\Theta(k_x>0)+v^*(-\mathbf{k})\,\Theta(k_x<0) \tag{5.6}$$

Up to first order, the density profile of the wavefunction is then given by:

$$\Psi(\mathbf{r},t)\approx|\psi|^2+2\,\mathrm{Im}\left(\psi^*\sum_{\mathbf{k}}\delta\psi(\mathbf{k})e^{-i\mathbf{k}\cdot\mathbf{r}}\right)$$

5.1.3 Density Profiles

The Bogoliubov modes of a binary fluid can be evaluated by inverting the full Bogoliubov matrix numerically. By filling up a grid in $\mathbf{k}$-space with these numerical values, the momentum distribution can be visualized. This grid can then be transformed to position space via a Fourier transform, showing the condensate's density profile by scattering from a defect.

5.2 Superfluidity of a Polariton Fluid

5.2.1 The Landau Criterion

The bulk velocity of a moving fluid leads to an additional energy term $\mathbf{k}_p\cdot\mathbf{r}$ in the energy of the Bogoliubov excitations. This term comes as a global tilting of the spectral branches, as we have shown in the chapter on the spectral branches. When the fluid velocity exceeds a certain velocity, the branches can cross the zero-energy line at non-zero momentum. When this happens energy-conserving scattering is possible and the defect will start to exert a drag force on the fluid.

The Critical Velocity

To define the critical velocity in a fluid, we consider a comoving frame to determine the energy. On top of the condensate we consider a single excitation with momentum $\mathbf{p}$. Therefore the energy of the fluid can be written as:

$$E = E_0+\varepsilon(\mathbf{p})+\mathbf{p}\cdot\mathbf{v}+\frac{1}{2}Mv^2$$

E_0 is the internal energy of the fluid, $\frac{1}{2}Mv^2$ the center of mass energy of a moving fluid with mass M. The energy of an elementary excitation with momentum $\mathbf{p}$ on top of the moving fluid is the sum of its band energy $\varepsilon(\mathbf{p})$ and the dopler shift $\mathbf{p}\cdot\mathbf{v}$, caused by considering a comoving frame.
The central argument is now that excitations will only occur when they are energetically *favorable*, that is when the excitations carry a negative energy:

$$\varepsilon(\mathbf{p})+\mathbf{p}\cdot\mathbf{v}<0$$

Out of this we can derive the celebrated *Landau criterion*, stating that any flow with a velocity v exceeding a certain velocity v_c is unstable and subject to a drag force because of the existence of elementary excitations.
This critical velocity is determined as:

$$v_c = \min_{\mathbf{p}} \frac{\varepsilon(\mathbf{p})}{p} \tag{5.7}$$

This means that any BEC flowing along a defect with velocity $v < v_c$ will not have energy dissipation by excitations, because this is not energetically favorable. The fluid can therefore flow frictionless without exerting a drag force and is called a *superfluid*. If the fluid flows faster than the critical velocity, Bogoliubov modes will get excited with a net drag force as result.

Stable fluids

The Landau criterion is rigorously defined when it comes to stable fluids, but is subject to interpretation for non-equilibrium systems like polaritons. We will therefore start by studying the equilibrium limit before generalizing.
For a single-spin fluid, the equilibrium limit is given by $\Delta_p = \gamma = 0$, yielding a band energy:

$$E(\mathbf{k}) = \sqrt{\frac{k^2}{2m}\left(\frac{k^2}{2m} + 2g\left|\psi\right|^2\right)} \tag{5.8}$$

By applying the Landau criterion, we then find that [14]:

$$v_c = \sqrt{\frac{g\left|\psi\right|^2}{m}} \tag{5.9}$$

So we find that the critical velocity coincides with the speed of sound in the fluid.

Applying the Landau criterion to an equilibrium two-spin fluid then yields the critical velocity [4]:

$$v_c = \sqrt{\frac{1}{2m}}\sqrt{\alpha_1\left(\left|\psi_+\right|^2 + \left|\psi_-\right|^2\right) - \sqrt{\alpha_1^2\left(\left|\psi_+\right|^2 - \left|\psi_-\right|^2\right)^2 + 4\alpha_2^2\left|\psi_+\right|^2\left|\psi_-\right|^2}} \tag{5.10}$$

The reason why the critical velocity is so straightforwardly defined for equilibrium fluids, is the presence of linear modes in the spectral branches. As such the Landau criterion can be conceptually visualized by considering the slope of the dispersion for $\mathbf{k} \to 0$. The kinetic energy $\mathbf{k} \cdot \mathbf{v}$ is represented by a straight line with slope v. The critical velocity is then determined by requiring that the minimum slope of the line is the slope of the dispersion. This image is shown in figure 5.1.

Generalization For Non-equilibrium Fluids

The critical velocity in non-equilibrium fluids is somehow more difficult to interprete for two reasons. First of all there is a finite lifetime of particles which gives an imaginary shift in the excitation spectrum. Because of the fundamtental quantum mechanical uncertainty relation $\Delta E \Delta t \geq \hbar/2$, the excitations are allowed to hop to states that are not energy conserving for a finite time. Therefore the defect will always exert a certain drag force on the fluid because exitations are allowed to exist at any finite bulk velocity.
In addition the Landau criterion needs some reinterpretation because of the freedom of pumping frequency. In an equilibrium fluid the equivalent property was locked to the chemical potential of the system, whereas in an non-equilibrium fluid the pump detuning is an additional experimentally tunable parameter of the system. Therefore new physical regimes are accessible that make it somehow difficult to define a critical velocity.
In spectra with quadratic dispersions, thus without diffusive-like regions, it is still possible to give a

notion to a critical velocity acccording to the Landau criterion. For a one-spin fluid we showed that these correspond to systems with negative pump detuning $\Delta_p < 0$, whereas in binary fluids they correspond to parameterical regions with two gapped spectra. In these systems we can make use of the familiar graphical image to visualize the Landau criterion. The critical velocity is then determined by drawing a line with slope v_p, the bulk fluid momentum, and requiring that v_c is the minimum velocity needed to cross the band dispersion of the excitations. In general this zero-energy point at the critical velocity is not at $\mathbf{k} = 0$, as was the case for equilibrium fluids because of the presence of a linear mode. At the critical velocity there will now be a discontinuous jump in the drag force, since modes are excited which have $\mathbf{k} > 0$. The graphical image of the critical velocity is shown in figure 5.1.
When the spectrum of excitations is diffusive-like the critical velocity is always zero according to the Landau criterion. Indeed, there is always a zero-energy mode having $\mathbf{k} > 0$. Therefore energy-conserving excitations are allowed at any finite bulk velocity, resulting in a finite drag force.

5.3 Supercritical Flow

5.3.1 Cherenkov Radiation

In the stable-fluid limit we have shown that no energy-conserving scattering can take place when the fluid velocity is below the critical velocity. Whenever this velocity is exceeded, however, energy-conserving scattering of Bogoliubov modes appears as the stable solution, giving rise to a finite drag force. These Bogoliubov waves are known as *Cherenkov radiation*, a physical phenomenon that occurs whenever particles exceed the local speed of sound in a medium. Famous examples include the sonic boom of an aircraft crossing the barrier of sound or the blue light observed in nuclear reactors, caused by charged particles moving faster than the speed of light in the medium.

Energy-conserving scattering takes place when one of the spectral branches of the excitations crosses the zero-energy line, corresponding to the constraint $\omega_i(\mathbf{k}) = 0$, where i denotes all branches. In $\mathbf{k}$-space we can draw contours of this constraint to visualize to which Bogoliubov modes scattering is possible for a certain fluid velocity. In the case of a single-fluid Bose-Einstein condensate, we have dispersion (5.8). The constraint $E(\mathbf{p}) = 0$ yields after some analytical calculations:

$$p_x^2 = 2m^2 \left(-c_s^2 + v^2 - \frac{p_y^2}{2m^2} + \left(\left(c_s^2 - v^2 + \frac{p_y^2}{2m^2} \right)^2 - \frac{1}{m^2} \left(c_s^2 p_y^2 + \frac{p_y^4}{(2m)^2} \right) \right)^{1/2} \right),$$

in which the fluid velocity $\mathbf{v}$ is lined along the x-axis.
This relation is a closed curve in the (p_x, p_y)-plane and can be drawn for different fluid velocities v, as is shown in figure 5.2.
When the behaviour of this curve for $\mathbf{p} \to 0$ is studied, we find that:

$$p_x = \pm \sqrt{\frac{1}{(v/c_s)^2 - 1}}\, p_y$$

So the curve is *not* analytic in the point $\mathbf{p} = 0$, because a singularity causes a discontinuous *cusp* in the curve.
Out of this we easily get that the curve makes a jump of an angle 2θ, with:

$$\cos\theta = \frac{c_s}{v} \tag{5.11}$$

Because of the cone-like shape, this is known as a *Mach* cone.

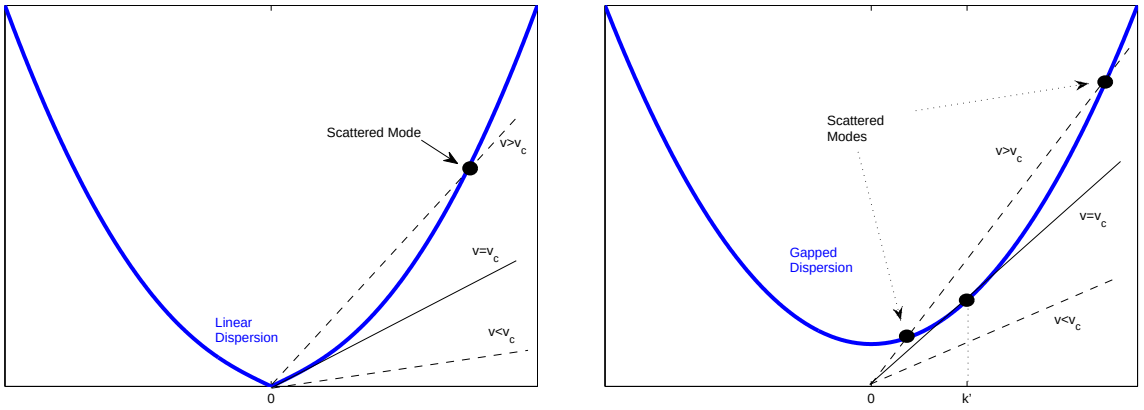

(a) Linear Dispersion

(b) Gapped Dispersion

Figure 5.1: Graphical image of the Landau criterion for a gapped and a linear dispersion of Bogoliubov excitations. The dashed line is the velocity curve vk. For subcritical speeds, below the critical velocity v_c, no modes can be excited, since there is no crossing between dispersion and the velocity curve, and there is a superfluid flow. For supercritical speeds Bogoliubov excitations appear at the momentum modes where the two curves cross each other. For a gapped spectrum there is a finite momentum k' at which modes are excited when $v = v_c$. This will result in a jump in the drag force.

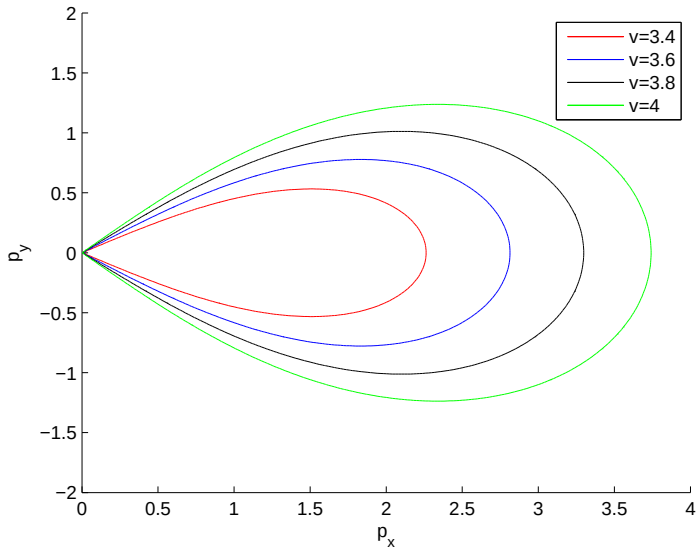

Figure 5.2: Closed zero-energy curves for different supercritical fluid velocities v in a Bose-Einstein condensate with speed of sound $c_s = 1$. There is a singularity in the curves for $\mathbf{p} \to 0$, corresponding to the Mach cone. Only scatterings to modes with angles inside the cone are possible.

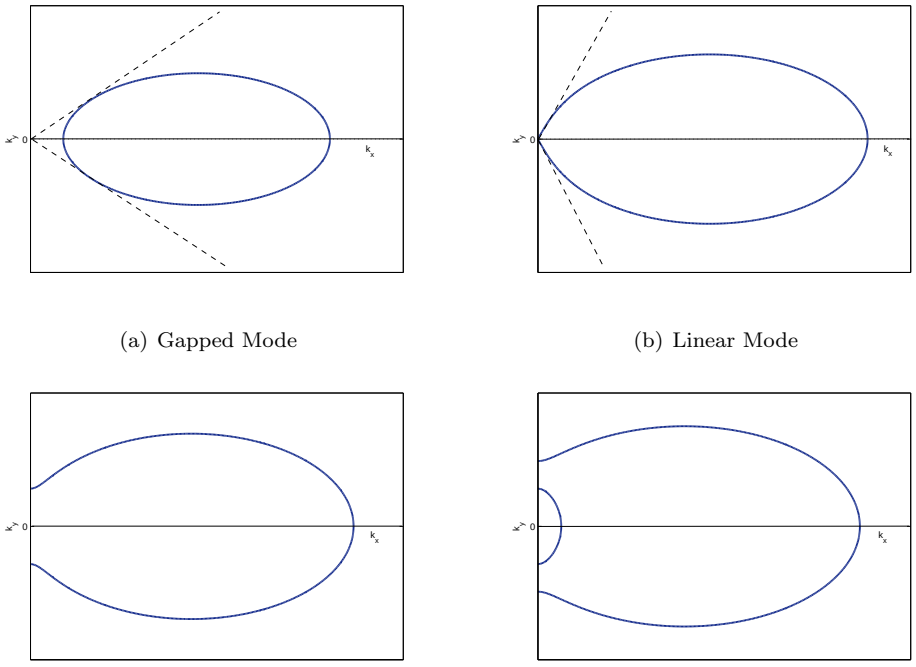

(a) Gapped Mode

(b) Linear Mode

(c) Diffusive Mode, $\Delta < 2g\,|\psi|^2$

(d) Diffusive Mode, $\Delta > 2g\,|\psi|^2$

Figure 5.3: The zero-energy curves for different spectral types in a supercritical flow along the x-axis. The contours represent the momentum states to which energy-conserving scatterings are possible. For non-diffusive modes the Mach cone is drawn, represented by the dashed lines: only scattering to momentum states with angles inside the cone are possible. Momentum states outside the cone cannot get excited. This Mach cone is not present for diffusive-like spectra and therefore scattering is allowed to all angles.

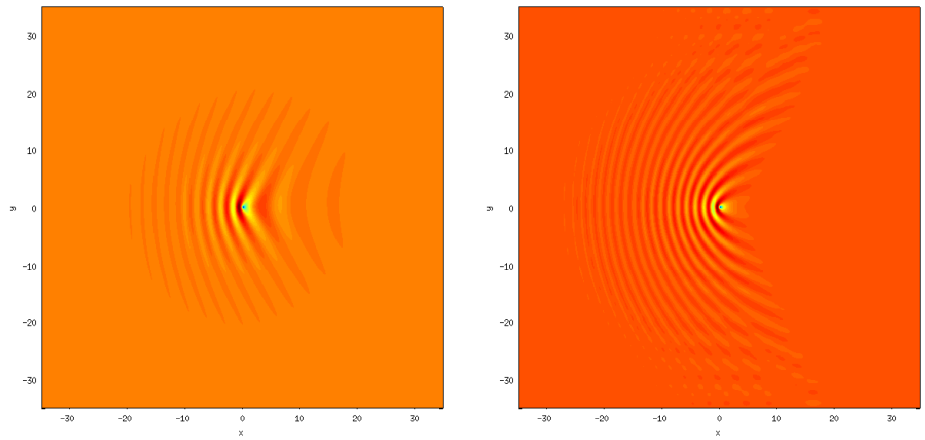

(a) Non-diffusive Mode

(b) Diffusive-like Mode

Figure 5.4: The density profile of a non-diffusive ($\Delta = -0.7g\,|\psi|^2$) and a diffusive-like ($\Delta = g\,|\psi|^2$) mode of a single-spin fluid with supercritical velocity $2c_s$ and $\gamma = 0.3g\,|\psi|^2$. In the non-diffusive fluid scattering takes place only inside the Mach cone, resulting in v-shaped interference pattern because of the missing angle of momenta. In the diffusive-like fluid scattering can take place at all angles, making a more parabolic-like interference pattern.

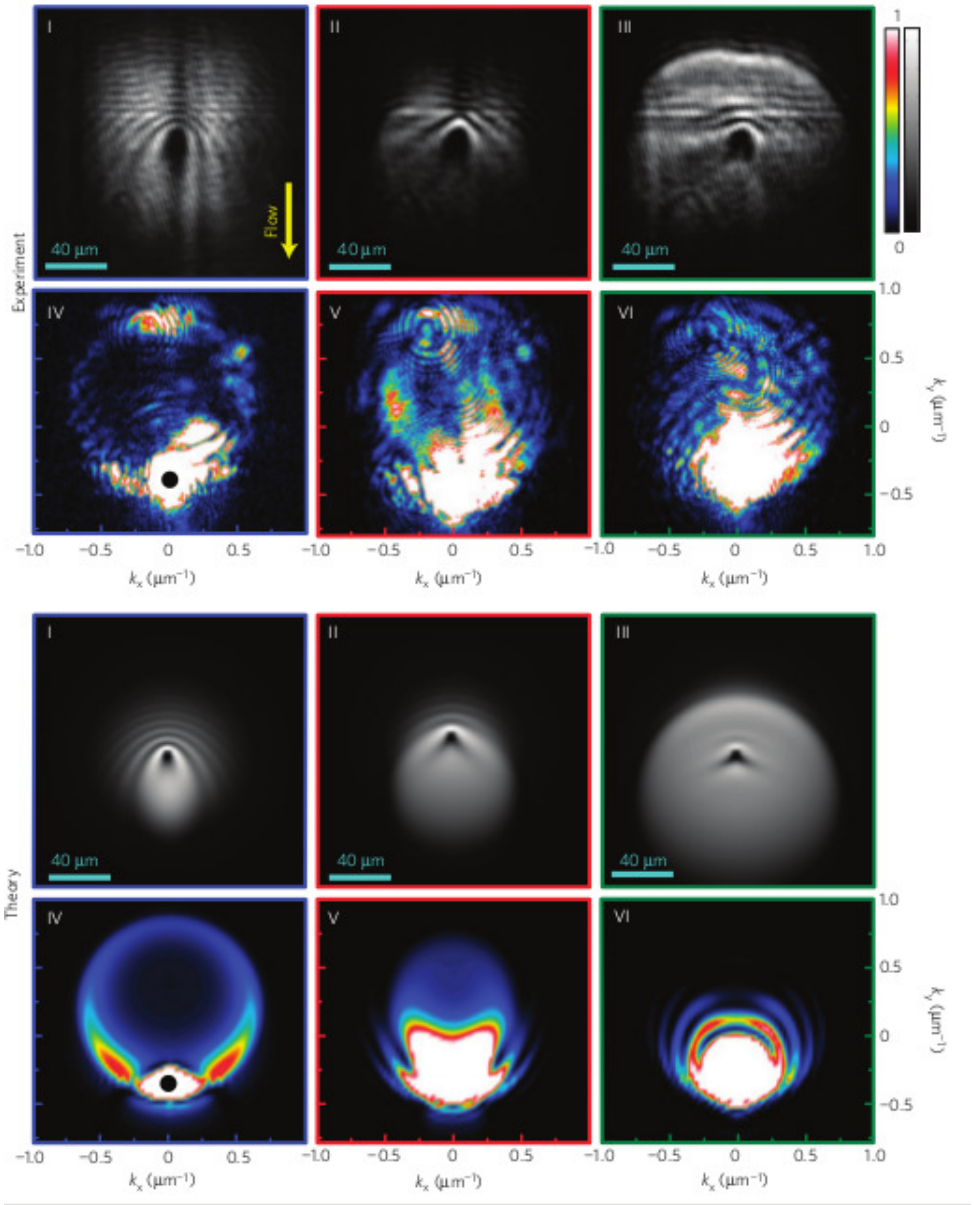

Figure 5.5: Scattering experiments of polariton fluids as carried out by [26] compared to the corresponding calculated density profiles for a supercritical stream of $k_p = 0.521\mu m^{-1}$. The upper six images are the experimental results with the Cerenkov profiles (up) and the momentum space images (down). The six other images are the corresponding numerically calculated images. The pumping power increases from left to right, thus resulting in a *denser* polariton fluid and a *higher* speed of sound. For a low density (left) we are clearly in a supercritical regime, whereas the Cherenkov is more reduced in the right one, meaning that the system flows at a velocity closer to the speed of sound. The wave pattern is more parabolic like, implying that the spectrum is diffusive.

Only scatterings to momentum states inside the Mach cone are possible, as there are no energy-conserving solutions outside this cone. As a consequence the angular distribution of triggered Bogoliubov modes has only contributions *inside* the Mach cone, and components with angles larger than θ are missing in the fourier decomposition. It is easy to notice that a linear spectral branch corresponds to a Mach cone for a supercritical flow. Indeed $\mathbf{p} = 0$ is always a zero-energy solution and with a sufficient tilt in the spectrum caused by the fluid velocity it can be readily seen that a cone-like shape appears as zero-energy solution in momentum space.
For a gapped mode, having $\Delta_p < 0$, a notion of a critical velocity can still be defined. However, we showed that if $v \to v_c$, energy-conserving scattering takes place at a non-zero momentum state, because of a discontinuous transition between the sub- and supercritical flow. As such the Mach cone is now shifted along the p_x-axis to higher momentum states.
For a diffusive-like spectral branch energy-conserving scattering of particles is possible at any finite fluid velocity. The real part of the zero-energy curve in momentum space does not have a single singularity, but rather a region along the p_y-axis for which holds $E(\mathbf{p}) = 0$. Now the angular distribution of scattered modes will look totally different than the distribution of a linear mode, because scattering is possible to *all angles*. See figure 5.3 for schematic drawings of the different zero-energy curves. The finite lifetime of polaritons makes it possible to scatter to energy states that are not necessarily energy-conserving. So the strict constraint of scattering only to momentum states that are situated on the closed zero-energy curves has to be weakened for non-equilibrium fluids. The momentum distribution of the fluid wave was the solution of the response equation (5.4), which involves the inversion of the Bogoliubov matrix:

$$\delta\psi(\mathbf{k}) = -\mathcal{L}^{-1}\mathbf{V} \equiv -\frac{\text{Minor}\,\{\mathcal{L}(\mathbf{k})\}}{\prod_i \omega_i(\mathbf{k})}\mathbf{V},$$

where we used that the inverse of every invertable matrix can be written as its minor matrix, which is analytic in $\mathbf{k}$, divided by its determinant, which is the product of its eigenvalues. Thus we see that resonances occur when the $\omega_i \to 0$ because the Bogoliubov matrix then becomes singular.
By inserting a finite particle lifetime, these resonances are shifted into the complex $\mathbf{k}$-plane, so that the singularities are blurred out. Therefore excitations can scatter to modes that are not necessarily energy-conserving and a richer variety of momentum states is present in the Fourier decomposition, although the distribution is still peaked around the curves $\omega(\mathbf{k}) = 0$. The width of this peak increases with increasing γ, since excitations are then less restricted to scatter with energy conservation, due to a shorter lifetime. Experimental results of images from a polariton scattering experiment [26] are shown in figure 5.5.

For binary fluids, we find that two branches instead of one can cross the zero-energy line independently and make energy-conserving scattering possible. Therefore there can be up to two closed curves in momentum space that determine the constraint $\omega_\pm = 0$.

5.3.2 Calculation of the Drag Force

After clarifying superfluidity by defining a critical velocity and generalizing this concept for non-equilibrium fluids, a quantitative approach for calculating the drag force caused by a point-like defect will be derived. We will start by calculating the drag force for a single-spin fluid, as this alows us to retrieve some analytical results.

Drag Force on a Single-fluid Condensate

In general a force acting on the fluid is the result of the gradient of a certain potential function. Since the fluid has a certain spatial density distribution, the full force acting on the fluid is the sum of all

infinitesimal contributions. Therefore we can write the force acting on the bulk as an integral over space:

$$\mathbf{F} = -\int d\mathbf{r}\,|\Psi(\mathbf{r})|^2\,\nabla V(\mathbf{r}) \tag{5.12}$$

By partially integrating this expression and substituting the defect potential $g_V\delta(\mathbf{r})$, we derive:

$$\begin{aligned}\mathbf{F} &= -V(\mathbf{r})\,|\psi(\mathbf{r})|^2\,|_{\mathbf{r}\to\infty} + \int d\mathbf{r} V(\mathbf{r})\nabla\,|\Psi|^2 \\ &= g_V\int d\mathbf{r}\delta(\mathbf{r})\nabla\,|\Psi|^2 \\ &= g_V\nabla\,|\Psi|^2\,|_{\mathbf{r}=0}\end{aligned}$$

Now we substitute the Bogoliubov ansatz to solve the drag force in momentum space:

$$\mathbf{F} = ig_V\int\frac{d\mathbf{k}}{(2\pi)^2}\mathbf{k}\Big[\psi^*\Big(u(\mathbf{k})-v^*(\mathbf{k})\Big)+\psi\Big(v(\mathbf{k})-u^*(\mathbf{k})\Big)\Big] \tag{5.13}$$

We have seen that the integration domain is restricted to the right half-plane in momentum space, as we defined it in this way to make the Bogoliubov ansatz consistent. It turns out more convenient and more practical to extend these integrals to the full momentum plane. This can be established by using the extended momentum distribution $\delta\psi(\mathbf{k})$, as defined in (5.6).

$$\begin{aligned}F &\equiv ig_V\int\frac{d\mathbf{k}}{(2\pi)^2}\mathbf{k}\Big[\psi^*\delta\psi(\mathbf{k})+\psi\delta\psi^*(-\mathbf{k})\Big] \\ &= 2ig_V^2\,|\psi|^2\int\frac{d\mathbf{k}}{(2\pi)^2}\frac{\mathbf{k}\,\varepsilon(\mathbf{k})}{\omega_+(\mathbf{k})\omega_-(\mathbf{k})}\end{aligned}$$

Written in this form we see that the integrand has poles for $\omega(\mathbf{k})\to 0$, which are the zero-energy curves that we discussed earlier. With this it is clear that the strength of the drag force is governed by the position of the poles in the complex $\mathbf{k}$-plane.

Stable-Fluid Limit

For a stable fluid we have that $\gamma\to 0$, causing a shift of the poles towards the real $\mathbf{k}$-plane. Now the poles of the integrand are determined by the closed zero-energy curves we discussed earlier on.
By elaborating the integrals over the full momentum plane, we find using polar coordinates:

$$\begin{aligned}F &= \frac{ig_V^2\,|\psi|^2}{2\pi^2}\int_0^\infty kdk\int_0^{2\pi}d\theta\;k\cos\theta\;\frac{\varepsilon(k)}{\omega_+(k,\cos\theta)\;\omega_-(k,\cos\theta)} \\ &\equiv -\frac{2ig_V^2\,|\psi|^2}{\pi^2}\int_0^\infty dkk^2\varepsilon(k)\int_0^1\frac{zdz}{\sqrt{1-z^2}}\cdot\frac{1}{\omega_+(k,z)\;\omega_-(k,z)}\end{aligned}$$

Since the integrandum is only a function of $z=\cos\theta$, we transformed to the integration measure $dz = -\sin\theta d\theta = -\sqrt{1-z^2}d\theta$. Furthermore we noted that the integrand is even in z, causing an extra factor 2. Written in these coordinates, the energy of the excitations reduces to:

$$\omega_\pm(k,z) = kvz\pm\sqrt{\varepsilon(k)\left(\varepsilon(k)+2g\,|\psi|^2\right)} \tag{5.14}$$

With $\varepsilon(k)=k^2/(2m)$ for a stable fluid.

Since the poles are now shifted towards the real plane, we can use the Plemelj formula to evaluate the angular integral. In general the theorem states that an integrand with poles appoximating the real axis, can be written symbolically as:

$$\lim_{\varepsilon\to 0}\frac{1}{x-i\varepsilon} = \mathcal{P}\frac{1}{x}+i\pi\delta(x)$$

Where $\mathcal{P}$ denotes the *principal value* of the integrand and $\delta(x)$ is the Dirac delta distribution. Out of symmetry reasons, it follows directly that the principal-value term cancels because the integrand is odd under the transformation $\mathbf{k} \to -\mathbf{k}$ when $\gamma \to 0$. This confirms the physical requirement to maintain a *real* drag force, which we assumed explicitely in (5.12).
The only term contributing to the drag force is therefore the one containing the Dirac-delta distribution. We start by solving the angular integral and noticing that the only pole inside the integration domain of z is contained in $\omega_-(\mathbf{k})$. Therefore the Dirac-delta yields:

$$\delta(\omega_-(\mathbf{k})) = \frac{1}{kv}\delta(z - z_0)$$

With:

$$z_0 = \frac{1}{vk}\sqrt{\varepsilon(k)\left(\varepsilon(k) + 2g\left|\psi\right|^2\right)}$$

So here we have a mathematical constraint that states energy conservation, as only modes having $\omega_-(\mathbf{k}) = 0$ contribute to the drag force.
Substituting all these in the integrand, we find:

$$\begin{aligned} F &= -\frac{2ig_V^2\left|\psi\right|^2}{\pi^2}\int_0^\infty dk k^2 \varepsilon(k) \int_0^1 \frac{z dz}{\sqrt{1-z^2}} \frac{i\pi\delta(z-z_0)}{vk\,\omega_+(k,z)} \\ &= \frac{2g_V^2\left|\psi\right|^2}{\pi v}\int_0^\infty dk\, \frac{z_0(k)}{\sqrt{1-z_0(k)^2}} \cdot \frac{k\,\varepsilon(k)}{\omega_+(k,z_0(k))} \cdot \Theta\left(k < k_{max}\right) \end{aligned}$$

We find that there should be an upper integration boundary k_{max} to assure having a pole inside the integration domain of z. This boundary is determined by requiring that $z \leq 1$ in (5.14):

$$k \leq k_{max} \equiv 2m\sqrt{v^2 - \frac{g\left|\psi\right|^2}{m}} = 2m\sqrt{v^2 - c_s^2}$$

Out of this we immediately derive that if $v < c_s$, with c_s the speed of sound, no solutions can be found for k_{max} and the integral therefore equals exactly *zero*. Here we again encounter the Landau criterion.

Substuting all these and using $\omega_-(k, z_0) = 2kvz_0(k)$, allows us to evaluate the drag force:

$$\begin{aligned} F &= \frac{g_V^2\left|\psi\right|^2}{\pi v^2}\int_0^{k_{max}} dk\, \frac{\varepsilon(k)}{\sqrt{1 - \frac{1}{2mv^2}\left(\frac{k^2}{2m} + 2g\left|\psi\right|^2\right)}} \\ &= \frac{g_V^2\left|\psi\right|^2}{\pi v}\int_0^{k_{max}} dk\, \frac{k^2}{\sqrt{k_{max}^2 - k^2}} \\ &= \frac{g_V^2\left|\psi\right|^2}{\pi v} \cdot \frac{\pi}{4}k_{max}^2 \cdot \Theta\left(k_{max} > 0\right) \\ &= g_V^2\left|\psi\right|^2 m^2 \left(\frac{v^2 - c_s^2}{v}\right)\Theta\left(v > c_s\right) \end{aligned}$$

This result has been derived first in [19] in the context of Bose-Einstein condensation and was used for polariton systems in [12]. A plot of the drag force in function of the fluid velocity is given in figure 5.6.

General Calculation Methods

The analytical calculations performed for a stable single-spin polariton fluid are much more complicated when adding either a finite lifetime, a pump detuning or a second spin component. The finite lifetime results in complex poles and makes the use of the Plemelj formula to evaluate the integrals analytically impossible. In theory it is still feasible to retrieve some semi-analytical results by using the more general

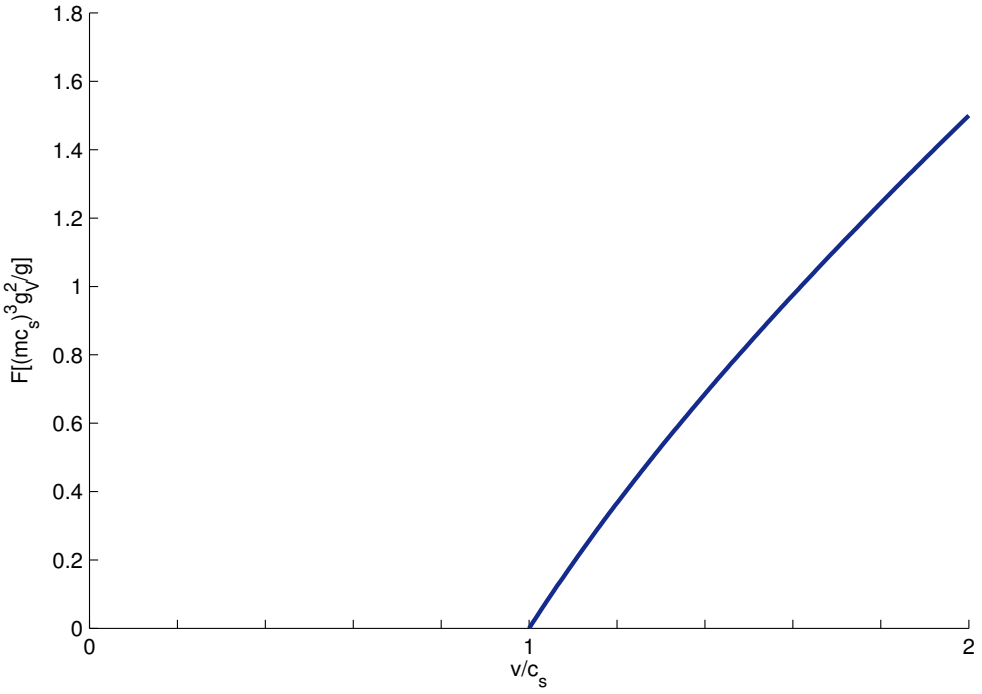

Figure 5.6: The drag force of a Bose-Einstein condensate in function of the fluid velocity. Below the critical velocity the fluid flows frictionless since no excitations are allowed. Above the critcal velocity Bogoliubov excitations result in a net drag force.

residue theorem and choosing appropriate integration contours, but the complexity of calculations increases rapidly. Also adding a non-zero pump detuning limits the possibilities for analytical calculations a lot and causes severe complications.
The most dificult part to overcome, however, is adding the second spin component. For this the evaluation of the inverse of a 4×4-matrix is required and this obviously results in dreadfully long expressions. Furthermore the integrand will now have two poles contributing instead of one, which makes the calculations even longer.

After several attempts to find analytical or semi-analytical results, it turned out more useful to start elaborating a full numerical approach to solve the drag force in general polariton systems. For this we start from (5.13) and extend the equation for a two-component fluid with potential $V_\pm(\mathbf{r}) = g_\pm \delta(\mathbf{r})$:

$$\begin{aligned} \mathbf{F}_\pm &= i g_\pm \int \frac{d\mathbf{k}}{(2\pi)^2} \mathbf{k} \Big[\psi^* \Big(u_\pm(\mathbf{k}) - v_\pm^*(\mathbf{k}) \Big) + \psi \Big(v_\pm(\mathbf{k}) - u_\pm^*(\mathbf{k}) \Big) \Big] \\ &= 2 g_\pm \int \frac{\mathbf{k} d\mathbf{k}}{(2\pi)^2} \, \mathrm{Im} \Big[\psi^* \Big(u_\pm(\mathbf{k}) - v_\pm^*(\mathbf{k}) \Big) \Big] \end{aligned}$$

Now the integral can be discretized by choosing an appropriate grid in $\mathbf{k}$-space and evaluate the integrand on the grid points. The efficiency can be improved by taking into account the $k_y \to -k_y$ mirror symmetry of the integrand, so that only half of the points has to be evaluated explicitely.
As such the expression to be evaluated numerically becomes:

$$F_\pm = \frac{g_\pm}{(2\pi)^2 L_x L_y} \mathrm{Im} \left[\psi_\pm^* \sum_{m=1}^{N_x} \sum_{n=1}^{N_y} \Big(u_\pm \left(k_{x,n}, k_{y,m} \right) - v_\pm^* \left(k_{x,n}, k_{y,m} \right) \Big) \right], \tag{5.15}$$

where we used a lattice of points with $k_x = 0, L_x/(N_x - 1), \ldots, L_x$ and analogously for k_y.
The functions $u_\pm(\mathbf{k})$ can then be evaluated numerically by inverting the bogoliubov matrix $\mathcal{L}(\mathbf{k})$ at these points and using the response equation (5.4).

This method works well in the case of smoothly varying integrands, as the sampled points then provide a good approximation of the Bogoliubov coefficients density profile. However in the limit of small γ, these distributions are strongly peaked around the curves $\omega_i(\mathbf{k}) = 0$ and this results in numerical problems becuase large function values fall inbetween sampled grid points. It is clear that the number of function evaluations scales with $N_x N_y \sim N^2$, so the total calculation time increases with the square of the number of points in one grid dimension.
On the other hand we can estimate the necessary grid spacing in order to have an adequate sampling of the integrand. The decay γ determines the width of the peaks in the Bogoliubov modes and it can be easily verified that the grid spacing has to satisfy $\Delta k \ll \sqrt{\gamma m}$. For small γ this results in numerical problems, since a large density of points is needed to evaluate the peaks correctly, leaving an abundancy of points where the integrand is almost zero. Obviously this causes reduced performance and too long calculation times.
These numerical problems can be reduced profoundly by sampling the grid points in a smarter way, a technique called *importance sampling*. There are numerous methods to achieve this, but the general idea is to center more points around the peaks and less in the regions where the integrand almost equals zero. A simple method that we adapted here is to start by dividing the rectangular grid in a number of smaller subgrids. We start by evaluating the integrand in the center of each subgrid to get a first approximation of the function profile. According to calculated value at the center of the subgrid, we assign a certain number of sampling points to the subgrid, the higher the absolute value of function value, the more points we assign to the subgrid. All these points are then distributed randomly inside the subgrid and evaluated. The mean of all these evaluations is an approximation for the mean function value at the subgrid. To evaluate the full integral, formula (5.15) is applied with the calculated subgrid values.

5.4 Phenomology of a Flowing Polariton Fluid

The scattering physics of binary polariton fluids are now ready to be studied based on the established results of the previous chapter. A wide variety of parameters that can be tuned are present in the model, such as the dimensionless parameters Γ, c and α, the lifetime γ and the potential strengths g_+ and g_-. As it is impossible - and it would be extremely tedious too - to provide a detailed explanation of all these parameters independently, we have elected the most interesting and relevant results after an elaborate and thorough research. In the coming section they are summarized and explained.

In the stable-fluid limit, there is no scattering possible to modes that are not energy conserving. Since we have four spectral branches in our model, there are now two possible modes that can result in scattering when crossing the zero-energy line. The critical velocity was defined according to the Landau criterion as the minimal velocity necessary to have energy-conserving scatterings. At this velocity we saw a sudden increase in the drag force curve due to the excitations that arise. Now, if at a higher velocity a second branch crosses the zero-energy line, an additional sudden increase in the drag force should be visible. This effect is shown in figure 5.7 for a polariton fluid with a gapped spectrum and a small width γ.
In general it is not possible to see this typical behaviour of the drag caused by the crossing of the two branches consecutively. This is because a larger width allows a wider range of scattering modes, so that this effect is blurred out. Furthermore we need a relatively large splitting between the two modes, which can be obtained by increasing α. In a binary Bose-Einstein fluid we can define the speed of sound as

$c_s = \sqrt{\frac{\alpha_1}{m}\left(\left|\psi_+^2\right| + \left|\psi_-^2\right|\right)}$, following the usual definition for single-spin fluïda: $c_s = \sqrt{g\left|\psi\right|^2/m}$. In this way we can normalize the examined fluid velocities in the plots that are shown.

Of great importance for the typical behaviour of the drag force, is the spectral type of the polariton fluid. To demonstrate this, we have provided three schematic images at the end of this chapter in which of the behaviour of the drag force is illustrated for different spectra: a double-gapped, a single-gapped and a full diffusive dispersion. The interaction ratio used is $\alpha = -.1$, so that the regimes can be situated on the phase diagram 4.5. On these images, the curve in the upper square is the drag force exerted on the up-spin component. Two red points are drawn on this curve: one is situated at a low velocity and the other at a high. For these two velocities the corresponding Cherenkov wave profiles and momentum funtions are calculated and shown with color scales. We provided *condensate* density profile: $\left|\psi_+\right|^2 + \left|\psi_-\right|^2$ and a spin profile: $\left|\psi_+\right|^2 - \left|\psi_-\right|^2$. For the two diffusive spectra, we had to make sure that the spectrum is physical by adapting the lifetime γ, thus shifting down all imaginary spectral contributions to negative values.
For the gapped spectrum we see that there is a sudden *jump* in the drag force at the critical velocity, rather than a smooth increase starting from zero, as we have shown for a linear branch (figure 5.6). This was due to the excitation of modes having $k > 0$ at the critical velocity, as was illustrated in figure 5.1.
The Cherenkov waves that result in a supercritical flow are V-shaped because of the Mach cone. Based on physical arguments we have explained that diffusive spectra should have a fundamentally different behaviour than gapped or linear spectra. Indeed, there are excitations to modes that have $k > 0$ at *any* finite fluid velocity in a diffusive spectrum, so that according to the Landau criterion the critical velocity equals zero. This manifests itself in the drag force curve, because for these fluids we typically see an almost linear behaviour. This is also due to the relatively large lifetimes that are necessary to have a physical spectrum.
The Cherenkov waves in diffusive spectra have a more parabolic shape because there is no Mach cone and scattering is not limited to a certain angle. In a double diffusive spectrum, we even see that there is strong scattering to momentum states *perpendicular* to the motion of the fluid. On the images this scattering even resembles a standing wave pattern, but is just an artefact of the numerical fourier transform. Also in momentum space it can be seen that there are two peaks on the axis perpendicular to the fluid velocity, which results in this strong scattering.

On figure 5.8 the effect of a finite lifetime on the drag force curve is demonstrated. Due to an increasing width γ, scattering is allowed to a larger band of excitation modes, so that scattering is possible at any finite fluid velocity. In a gapped mode there is still a notion of a critical velocity, in the sense that there is a sudden jump in the drag force curve. For larger γ this jump gets flattened, eventually resembling a smoothly increasing curve. This is because the peaks in the momentum profile, caused by the zero-energy lines, get spread out for high γ, thus resulting in a smooth profile.

A most remarkable feature that we have noticed, is that the drag force can become *negative* under certain conditions, as is for example shown in figure 5.8 for the diffusive spectrum. This is uttermost strange, since it indicated that the fluid is *driven forward* rather than *slowed down* when flowing along a defect. As such there is no energy *dissipation* caused by friction, but instead there should some mechanism that extracts energy from a source and works as a sort of *engine*.
This exotic process takes place in *both* single-spin and binary fluids and is therefore qualitavely *not* dependent on the spin degree of freedom. We have not found any description of this process in the literature on single-spin polariton fluids, so we believe that we are the first ones to notice.
After some research, we found that the negative drag force only occurs for relatively high positive laser

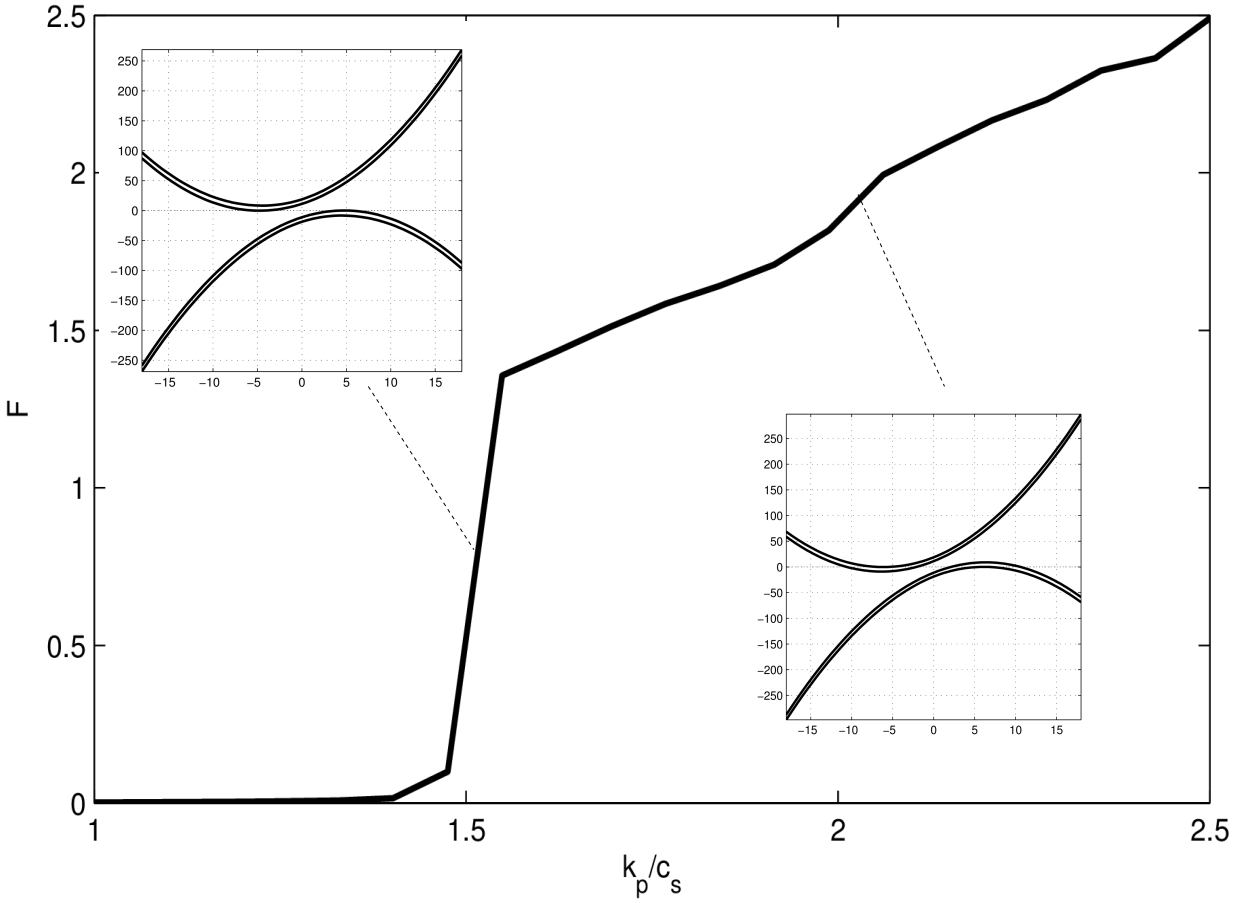

Figure 5.7: The drag force exerted on the positive fluid as a function of the fluid velocity for a double-gapped dispersion, with $\gamma' = .1$, $\alpha = 1$, $c = .1$ and $\Gamma = -1$. There are two branches that cross the zero-energy line consecutively, resulting in two sudden increases of the drag force. There were some numerical issues when this curve was calculated that are due to the small width γ. Still it can be seen that two different points at which the curve makes a sudden increase are present.

detunings, so that it is directly related to the non-equilibrium properties. Furthermore it only takes place for low velocities and it disappears when γ is increased, which is clearly visible on figure 5.8. Therefore we note that this effect occurs when there is *negative* derivative of the drag force curve for $\mathbf{k}_p \longrightarrow 0$.
We can analytically expand the drag force of a single-spin fluid for small $\mathbf{k}_p$, starting from (5.13). Thus we find a linear behaviour:

$$\begin{aligned} F &\sim \gamma k_p \int_0^\infty dk \, \frac{k^3 \left(\frac{k^2}{2m} - \Delta_p\right)}{\left[\left(\frac{k^2}{2m} - \Delta_p\right)\left(\frac{k^2}{2m} - \Delta_p + 2g\left|\psi\right|^2\right) + \frac{\gamma^2}{4}\right]^2} \\ &= \gamma k_p \int_0^\infty dk \, \frac{k^3 \left(\frac{k^2}{2m} - \Delta_p\right)}{\left[\omega_-(\mathbf{k})\Big|_{k_p=0} \omega_+(\mathbf{k})\Big|_{k_p=0}\right]^2} \end{aligned}$$

Indeed, the only way the integrand can become negative is when $\Delta_p > \frac{k^2}{2m}$, so that a positive detuning is necessary.
With a positve detuning, we found that additional imaginary contributions come into the spectral branches. Therefore we required a sufficient width γ, in order to have all imaginary contributions below zero. Imagine now the limiting case in which the imaginary *bulb* of a diffusive branch just touches the zero-energy line in a point k_0. This point k_0 actually corresponds to a full circle of points for which we have exactly that $\omega_+(k_0)\Big|_{\mathbf{k}_p=0} = 0$, which results in a divergent integral for the drag force. Now if we have that $\frac{k_0^2}{2m} < \sqrt{2m\Delta}$, this divergence carries a *negative* sign and we have that $\lim_{k_p \to 0} F = -\infty$. We can easily derive that for a single-spin fluid the maximum imaginary contribution comes at $\frac{k_0^2}{2m} = \Delta - g\left|\psi\right|^2 < \Delta$, so that the drag force indeed diverges. This effect is shown in figure 5.9.
If there is no exact resonance, but the top of the imaginary spectrum is shifted slightly to a negative value, the divergence disappears. Still the drag force is negative for small $\mathbf{k}_p$ because of the large contribution of the integral around k_0. When γ is increased further, the imaginary spectrum gets shifted down further and the resonance disappears completely, making a positive drag force again. This is illustrated in figure 5.8.
Now how can we understand physically what is happening? It seems that there is energy *extracted* out of the positive laser detuning Δ_p. Hence, a mechanism takes place that absorbs energy from the laser beam and converts it into *kinetic* energy through the Bogoliubov excitations. As such we can consider the excitation of Bogoliubov modes as a sort of *engine* that drives the fluid along the defect potential.

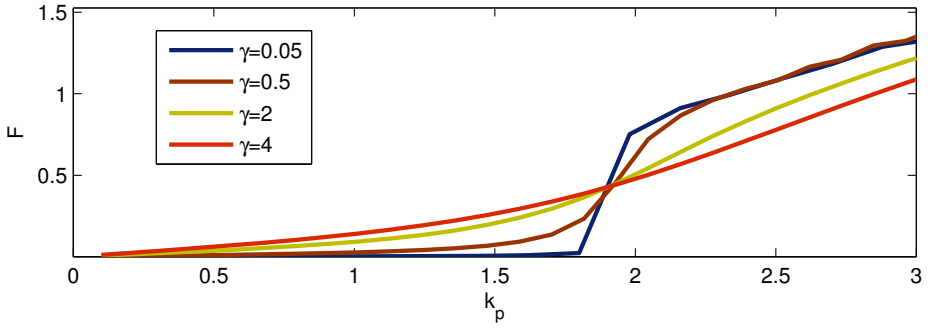

(a) Double Gapped Mode

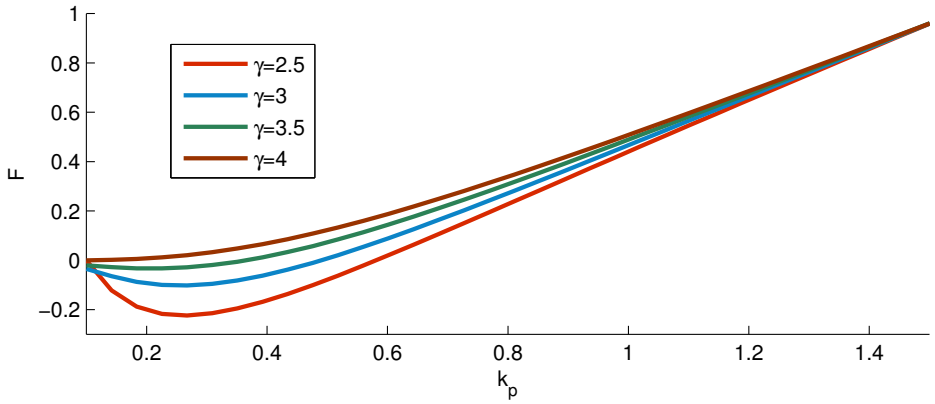

(b) Double Diffusive Mode

Figure 5.8: The drag force curves with different widths γ, for a gapped and a diffusive spectrum. For a gapped spectrum, the drag force exerted on the fluid increases with γ for subcritical speeds, whereas it decreases for supercritical velocities. In a diffusive spectrum, yhe drag force can become negative for low fluid velocities, an effect that disappears if γ is increased.

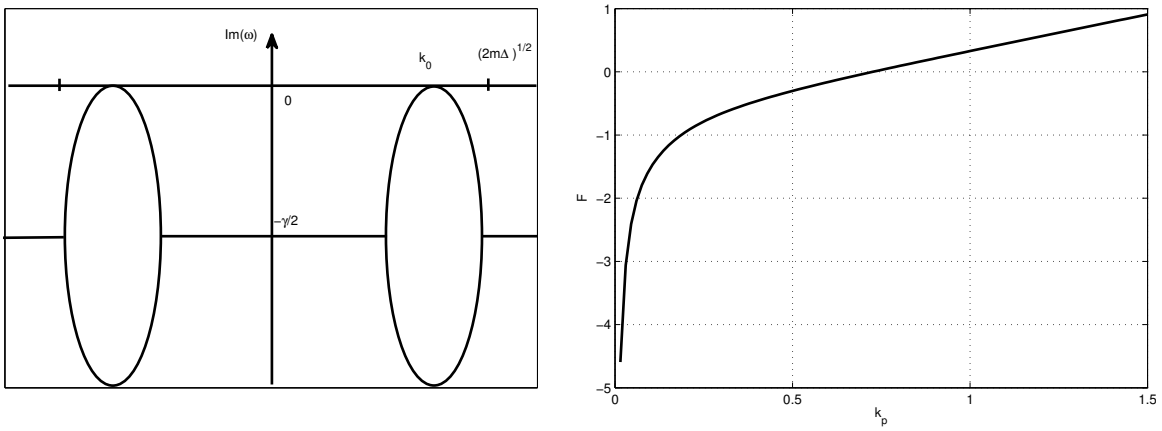

Figure 5.9: The limiting case: the imaginary spectrum just touches the zero-energy line in a point k_0, as is illustrated in the left panel. This corresponds to a circle in the $\mathbf{k}$-plane where both the real and the imaginary spectrum are *exactly* zero. Because of this the drag force diverges to negative values for $k_p \to 0$. This is shown in the right panel for $\Delta_p = 3.5g\,|\psi|^2$ and $\gamma = 2g\,|\psi|^2$.

Double Gapped

C=0.8
Γ=-1
γ=1

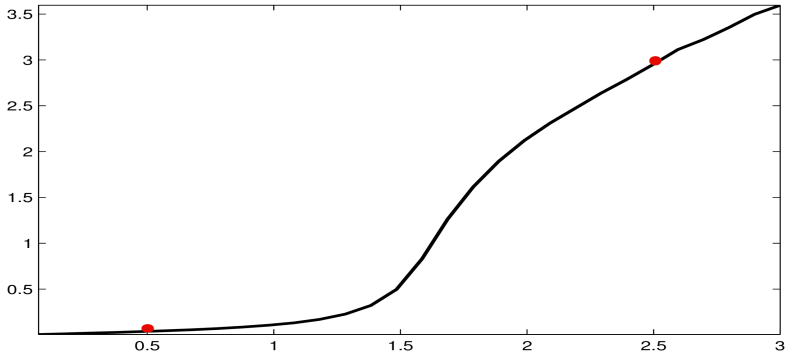

Density

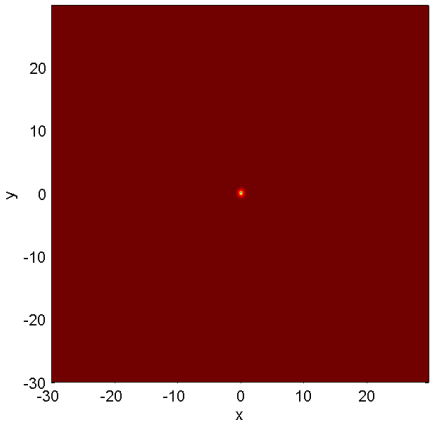

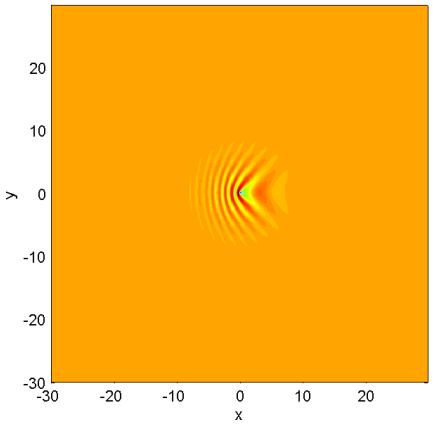

Spin

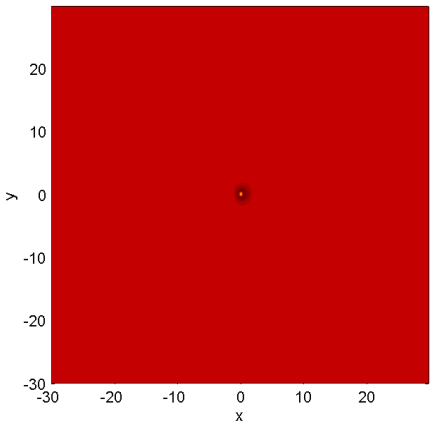

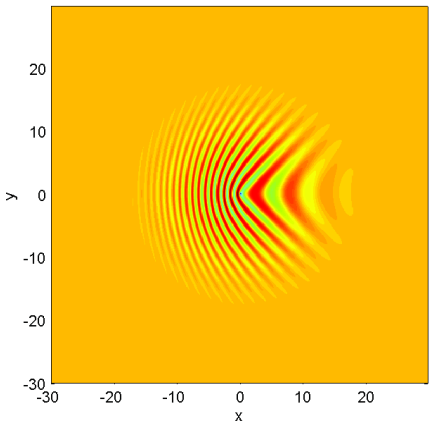

Momentum Space

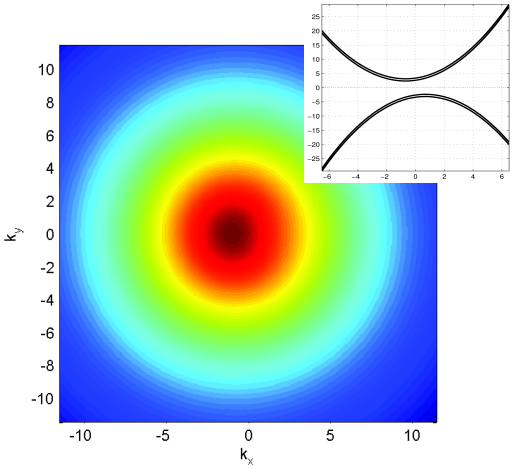

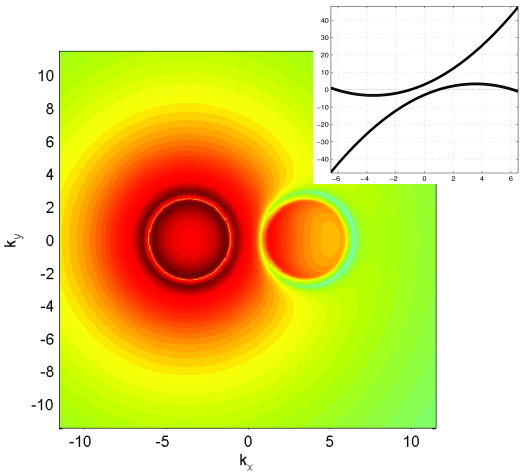

Single Gapped

C=0.2
Γ=2
γ=1

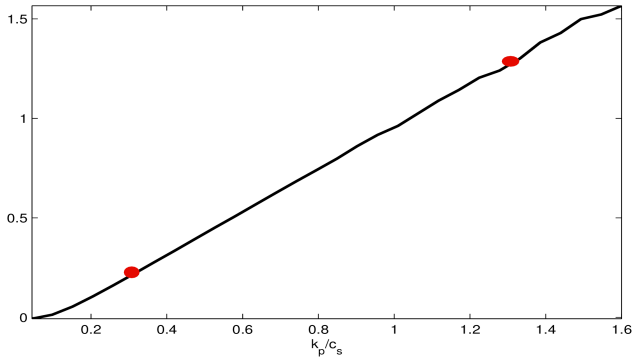

Density

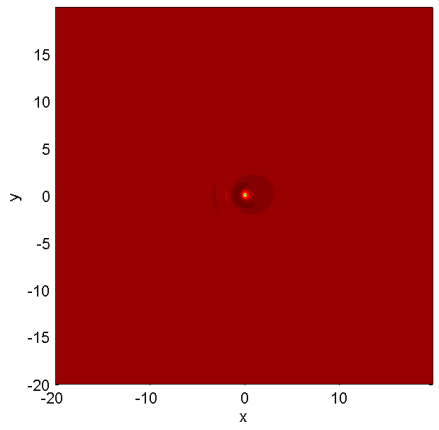

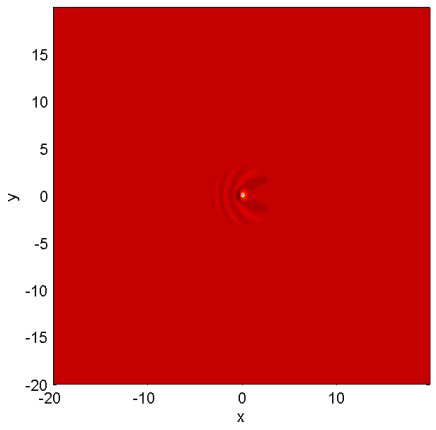

Spin

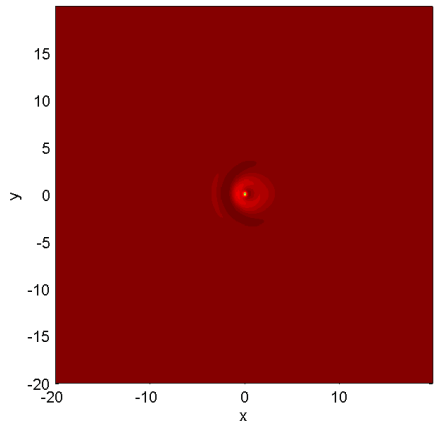

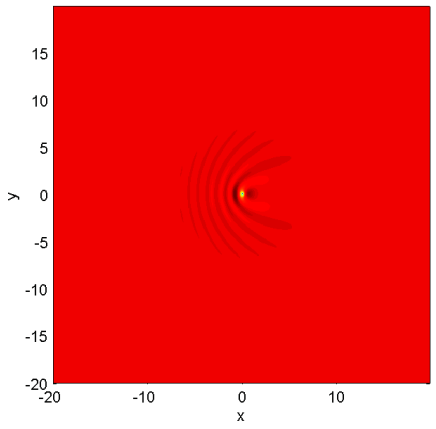

Momentum Space

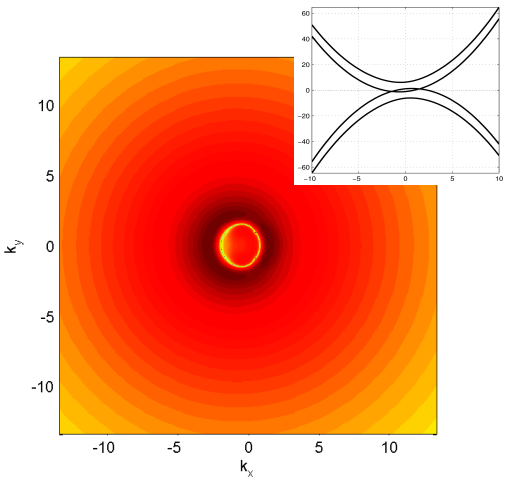

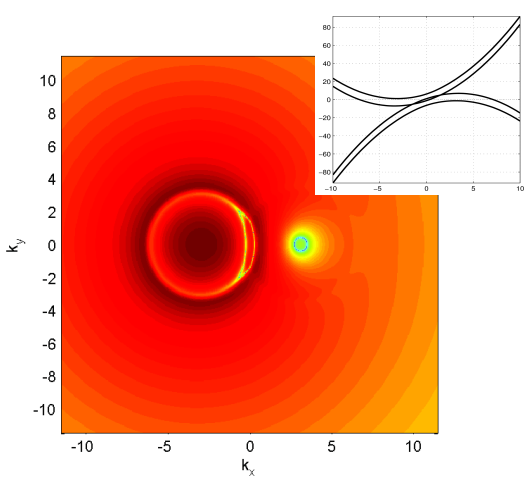

Diffusive

c=0.7
Γ=3
γ=2.5

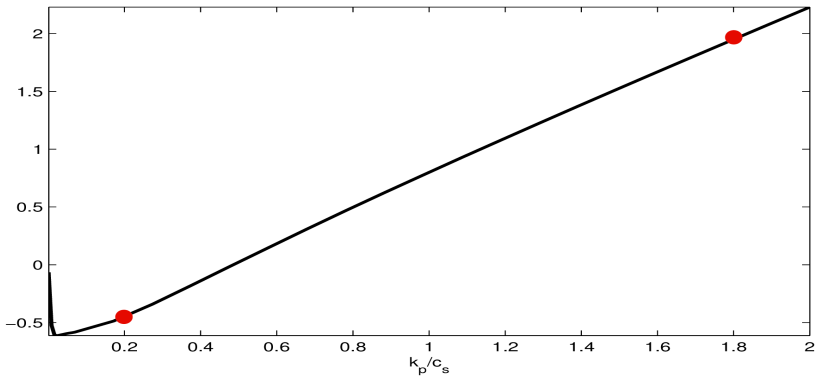

Density

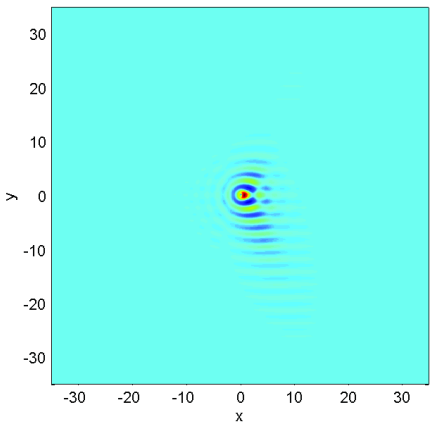

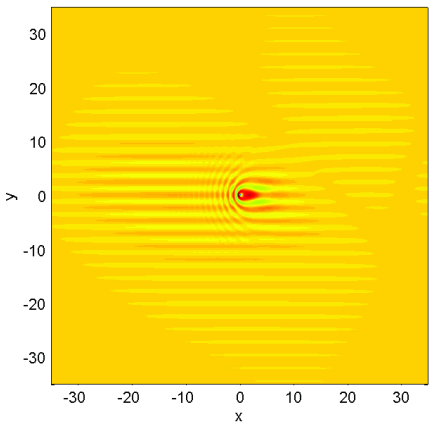

Spin

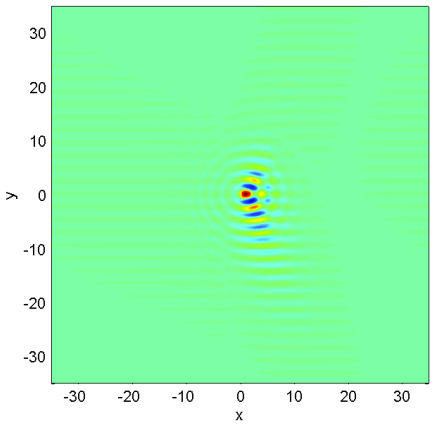

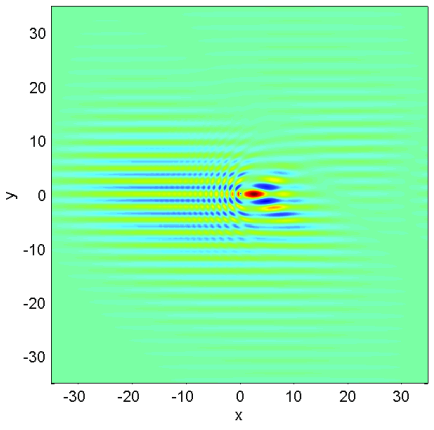

Momentum Space

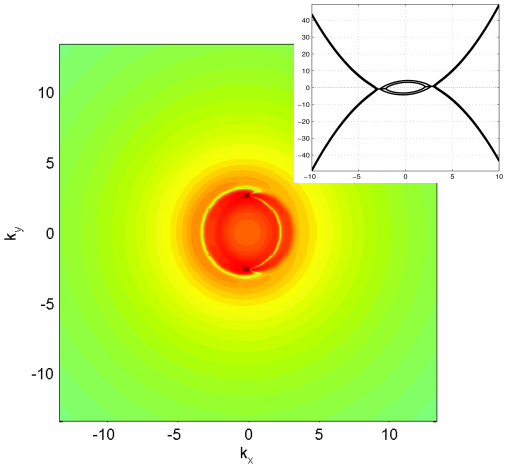

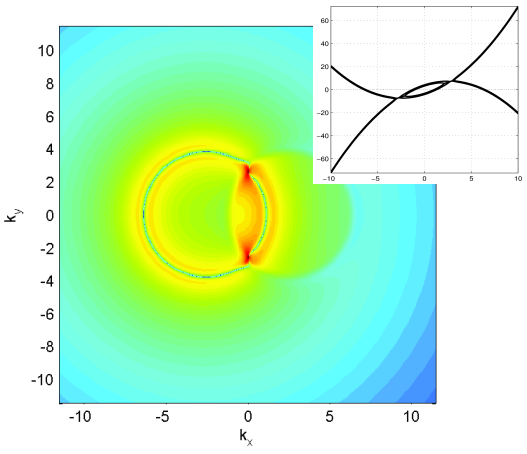

Chapter 6

Conclusions

In this work we have studied the physics of binary polariton fluids by combining the physics of single-spin polariton fluids and binary Bose-Einstein condensates. First we have derived the full Gross-Pitaevskii equation, which describes the polariton physics in terms of fluid dynamics. From there on we have derived the spectrum of Bogoliubov excitations and classified the spectra according to three seperate dimensionless parameters: Γ, the reduced energy difference between the pumping energy and the polariton dispersion, c, the ratio of spin-up and spin-down densities, and α, the ratio of the self-interaction and the cross-interaction.
Ultimately the scattering physics of a flowing polariton fluid has been examined by studying the excitation properties of Bogoliubov modes. The notion of a critical velocity has been generalized in terms of non-equilibrium fluids and different methods to calculate the drag force exerted on the fluid have been presented.
A summary of the main results in this work:

- Via a phase diagram in function of the reduced parameters Γ and c the different excitation spectra that can occur in a fluid can be classified in terms of parametrical regions. In this way, we have presented a method that combines the physics of both a binary Bose-Einstein condensate and a single-spin polariton fluid. We can move continuously through parameter space from one of the limiting cases to the other.

- The effect of the excitation spectra on the behaviour of the drag force has been studied extensively. Gapped and linear spectra give rise to a Mach cone and thus a V-shaped diffraction pattern, whereas diffusive spectra allow scattering to all angles and have more parabolic-like diffraction patterns. This manifests itself in the drag force: for gapped and linear spectra, there is a sudden increase in the drag force at a critical velocity, whereas diffusive spectra have a rather smoothly increasing curve.

- The lifetime of the particles has a strong effect on the scattering physics. The shorter the lifetime, the higher the bandwidth γ and the more the peaked momentum profiles get smoothened. This was a consequence of the fact that scattering is allowed to non-energy conserving modes for a finite particle lifetime. As a consequence of increasing lifetime, the drag force curve becomes smoother and any discontinuities are flattened out.

- A negative drag force can occur with positive pump detuning. A mechanism has been presented by which the system transfers energy from the positive detuning in the excitation of Bogoliubov modes, so that the fluid is driven forward along the defect.

Bibliography

[1] J.J. Hopfield, *Theory of the contribution of excitons to the complex dielectric constant of crystals*, Phys. Rev. 112 (1958), pp. 15551567.

[2] S.I. Pekar, *The theory of electromagnetic waves in a crystal in which excitons are produced*, Sov. Phys. JETP 6 (1958), p. 785.

[3] C. Weisbuch et Al., *Room-temperature cavity polaritons in a semiconductor microcavity*, Physial Review B, vol 49 nr. 23

[4] L.Yu. Kravchenko, *Critical Velocities in Two-Component Superfluid Bose Gases*, 17 October 2007, J Low Temp Phys (2008) 150:612-617

[5] C. Ciutti and Iacopo Carusotto, *Quantum Fluid Effects and Parametric Instabilities in Microcavities*, 13 July 2005, Wiley-VCH

[6] C Ciuti, P Schwendimann and A Quattropani, *Theory of polariton parametric interactions in semiconductor microcavities*, 3 September 2003, stacks.iop.org/SST/18/S279

[7] P. Le Jeune, X. Marie, T. Amand, F. Romstad, F. Perez, J. Barrau, and M. Brousseau *Spin-dependent exciton-exciton interactions in quantum wells*, 15 August 1998, Physkcal Review B, Volume 58, Nr 8

[8] , Y.G. Rubo, *Mean-field Description of Multicomponent Exciton-polariton Superfluids*, 28 September 2012, arXiv:1209.6538v1

[9] J. Keeling and Natalia G. Berloff, *Exciton-polariton Condensation*, 17 December 2010, Contemporary Physics Vol 52, No. 2, March-April 2011, 131-151

[10] I. Carusotto, *Quantum Fluids of Light*, 19 May 2012, arXiv:1205.6500

[11] J. Keeling, F. M. Marchetti, M. H. Szymanska, P.B. Littlewood, *Collective Coherence in Planar Semiconductor Microcavities*, arXiv:cond-mat/0702166

[12] A.C. Berceanu, E. Cancellieri, F.M. Marchetti, *Drag in a Resonantly Driven Polariton Fluid*, arXiv:1205.3610

[13] M. Vladimirova, S. Cronenberger, D. Scalbert, *Polariton-polariton Interaction Constants in Microcavities*, Physical Review B 82, 075301 (2010)

[14] L. P. Pitaevskii, S. Stringari, *Bose-Einstein Condensation*, Oxford University Press, 03/04/2003

[15] C.J. Pethick and H. Smith, *Bose-Einstein Condensation in Dilute Gases*, October 20, 2008, 978-0521846516

[16] Caroline Aarssen, *Superfluïditeit van een ééndimensionale polaritonkwantumvloeistof*, Masterproef UA, Juni 2012

[17] E. Hanamura, H. Haug, *Condensation Effects of excitons*, 1977, Phys. Rep. 33 209

[18] J. J. Hopfield, *Theory of the Contribution of Excitons to the Complex Dielectric Constant of Crystals.* Physical Review, vol. 112, nr. 5, pg. 1555-1567(1958)

[19] G. E. Astrakharchik and L. P. Pitaevskii, *Motion of a heavy impurity through a Bose-Einstein condensate*, PHYSICAL REVIEW A 70, 013608 (2004)

[20] G.W. Ford, M. Kac, *On the Quantum Langevin Equation*, Journal of Statistical Physics, vol 46, 1987

[21] Giovanna Panzarini and Lucio Claudio Andreani, *Exciton-light coupling in single and coupled semiconductor microcavities: Polariton dispersion and polarization splitting*, Physical Review B, vol 59 nr7, 1999

[22] Y.G. Rubo,*Mean-field description of multicomponent exciton-polariton superfluids*, arXiv:1209.6538, 2012

[23] D. Sanvitto, F. M. Marchetti *Persistent currents and quantised vortices in a polariton superfluid*

[24] Joanna M Zajac and Wolfgang Langbein*Parametric scattering of microcavity polaritons into ghost branches*, . arXiv:1210.1455 , 2013

[25] Michiel Wouters, *Notes for Speech Polaritons Lausanne*

[26] A. Amo et al.,*Superfluidity of polaritons in semiconductor microcavities*, Nature Physics 5, 805 - 810 (2009)